Award Number: W81XWH-12-2-0038

TITLE: Prevention of Blast-Related Injuries

PRINCIPAL INVESTIGATOR: Albert I. King

CONTRACTING ORGANIZATION: Wayne State University
Detroit, MI 48201

REPORT DATE: July 2016

TYPE OF REPORT: Annual

PREPARED FOR: U.S. Army Medical Research and Materiel Command
Fort Detrick, Maryland 21702-5012

REPORT DOCUMENTATION PAGE

Form Approved
OMB No. 0704-0188

1. REPORT DATE	**2. REPORT TYPE**	**3. DATES COVERED**
July 2016	Annual	15Jun2015 - 14Jun2016

4. TITLE AND SUBTITLE
Prevention of Blast-Related Injuries

5a. CONTRACT NUMBER

5b. GRANT NUMBER
W81XWH-12-2-0038

5c. PROGRAM ELEMENT NUMBER

6. AUTHOR(S)
Albert King, John Cavanaugh, King Yang, Liying Zhang, Xin Jin

E-Mail: king@rrb.eng.wayne.edu

5d. PROJECT NUMBER

5e. TASK NUMBER

5f. WORK UNIT NUMBER

7. PERFORMING ORGANIZATION NAME(S) AND ADDRESS(ES)
Wayne State University
5700 Cass Ave., Suite 4900
Detroit, MI 48202-3692

8. PERFORMING ORGANIZATION REPORT

9. SPONSORING / MONITORING DAGENCY NAME(S) AND ADDRESS(ES)
U.S. Army Medical Research and Materiel Command
Fort Detrick, Maryland 21702-5012

10. SPONSOR/MONITOR'S ACRONYM(S)

11. SPONSOR/MONITOR'S REPORT NUMBER(S)

12. DISTRIBUTION / AVAILABILITY STATEMENT
Approved for Public Release; Distribution Unlimited

13. SUPPLEMENTARY NOTES

14. ABSTRACT

This report covers work done on blast testing of live anesthetized swine and on unembalmed cadavers. A detailed histological study of blast-exposed swine brain showed that there was damage to both the axons and the neuron cell bodies in the form β-APP immunoreactivity and other tests, suggesting that the mechanism of injury may be different from that of blunt impact. We have also developed computer models of the swine and human brain and are in the process of validating them against the acquired experimental data. It is proposed that future research concentrate on seeking injury mechanisms to brain cells caused by a pressure wave.

15. SUBJECT TERMS
Keywords: Blast-related brain injury, Open field testing of swine and PMHS, Computer modeling of swine and human brain, brain injury mechanisms

16. SECURITY CLASSIFICATION OF:			**17. LIMITATION OF ABSTRACT**	**18. NUMBER OF PAGES**	**19a. NAME OF RESPONSIBLE PERSON** USAMRMC
a. REPORT	**b. ABSTRACT**	**c. THIS PAGE**			**19b. TELEPHONE NUMBER** *(include area code)*
U	U	U	UU	130	

TABLE OF CONTENTS

	Page No.
Introduction	4
Statement of Work	4
Task I Report	4
1. Blast Testing of Instrumented Swine	4
2. Blast Testing of Noninstrumented Swine	8
3. Brain Histology to Assess Brain Injury in Blast Exposed Swine	9
Task II Report	13
Task III Report	14
1. Comparison of biomechanical responses predicted by the swine head model against experimental measurements	14
2. Investigation of the over predicted intracranial pressure ICP) at the frontal lobe	22
3. Analysis of sensor location sensitivity on model predicted ICP	25
4. Conclusions	28
Task IV Report	29
1. Methods	29
2. Results	30
3. Discussion	33
Additional Studies	34
Discussion	35
Conclusions	36
Publications and Presentations	36
Appendices	39

**

INTRODUCTION

This research project is designed to determine the cause of mild traumatic brain injury due to blast overpressure and, if possible, the human tolerance to blast overpressure. It consists of an experimental portion in which 12 swine and 6 post-mortem human subjects (PMHS) are to be exposed to blast. The experimental effort is supplemented by a computer modeling section which can extend the results of the tests to blast scenarios not easily achievable experimentally. In the second report, we reported on the results of our experimental research and of our modeling effort, In this report, we report the completion of our swine testing and results of our histological findings in the swine brains. We were only able to do one more cadaver test due to specimen unavailability and thus need an extension of the award to complete this task as well as the cadaver head modeling task that depends on the data to be collected. We will submit a final report upon completion of the tasks associated with cadaver testing.

STATEMENT OF WORK

The Statement of Work (SOW) for this project is as follows:

I. Perform open field blast testing on 6 anesthetized minipigs to obtain biomechanical data and on 12 anesthetized minipigs to obtain pathohistological data
II. Perform open field blast testing on 6 unembalmed post-mortem human subjects (PMHS) also known as cadavers to obtain biomechanical data
III. Develop and validate a computer model of the pig brain simulating the effects of a blast over-pressure
IV. Develop and validate a computer model of the human brain simulating the effects of a blast over-pressure

TASK I REPORT

Task I - Perform open field blast testing on 6 anesthetized minipigs to obtain biomechanical data and on 12 anesthetized minipigs to obtain pathohistological data (Original Proposal)

In this task, there were three separate work items:
1. Blast testing of instrumented swine
2. Blast testing of noninstrumented swine
3. Brain histology to assess brain injury in blast exposed swine

1. Blast Testing of Instrumented Swine

a) Summary of Test Methodology

We have completed open field blast testing of anesthetized swine to obtain biomechanical data of brain response due to blast overpressure. The target incident overpressures (IOP) were nominally 150 kPa (low), 300 kPa (medium) and 450 kPa (high). The range for the nominal low level blasts (150 kPa) was between 148 kPa to 161 kPa; while that for the nominal medium level blasts (300 kPa) was between 218 kPa to 341 kPa; and that for the nominal high level blasts (450 kPa) was between 341 kPa to 552 kPa. Within each group, the pig head was oriented to the blast wave in one of three different directions: front and rear, or side. A detailed analysis was conducted on the mechanical data from frontal blasts. All the data were grouped into three incident overpressure levels according to recorded incident pressure by the pencil transducer located next to the head of the swine.

(b) Frontal blast data analysis: We have completed analysis of the frontal blast data and have submitted a manuscript to a peer-reviewed journal. This manuscript can be found in Appendix I and is currently under review. We have also presented our findings on the mechanical response of the swine brain to blast at the following conferences:

Invited presentation BMES annual conference, Tampa, Florida "Free Field Blast Induced Mechanical Response, Axonal Injury and Glial Changes in Swine Brain." October 2015.

Poster presentation: The 2015 Military Health System Research Symposium (MHSRS). "Biomechanical Response of swine exposed to open-field blasts." August 2015.

(c) Analysis of data for side and rear blasts:

Data from side and rear blasts were checked for outliers and re-analyzed. Questionable data collected from damaged sensors were removed. Peak ICP pressures from side and rear blasts at each location of the brain are shown in Figure 1 for side blasts and in Figure 2 for rear blasts. Compared with frontal blasts, data collected from the side and rear are less consistent. However, the peak pressure values in side and rear blasts were lower than those in frontal blasts. The large variation in peak pressures at the same location could be partly due to the decreased functionality of sensors after being subjected to high level frontal blasts. Additionally, the placement of pressure sensors was changed between 2013 and 2014. Distributions of peak linear accelerations and peak angular velocities for side and rear blasts are shown Figures 3 and 4 respectively.

(d) Computation of accelerations and velocities at the head center of gravity.

Linear acceleration and angular velocity of the head at its center of gravity (c.g.) were computed from the measured data. The relative distance between the sensor location and the head c.g. was based on the swine brain injury model that was developed under Task II.

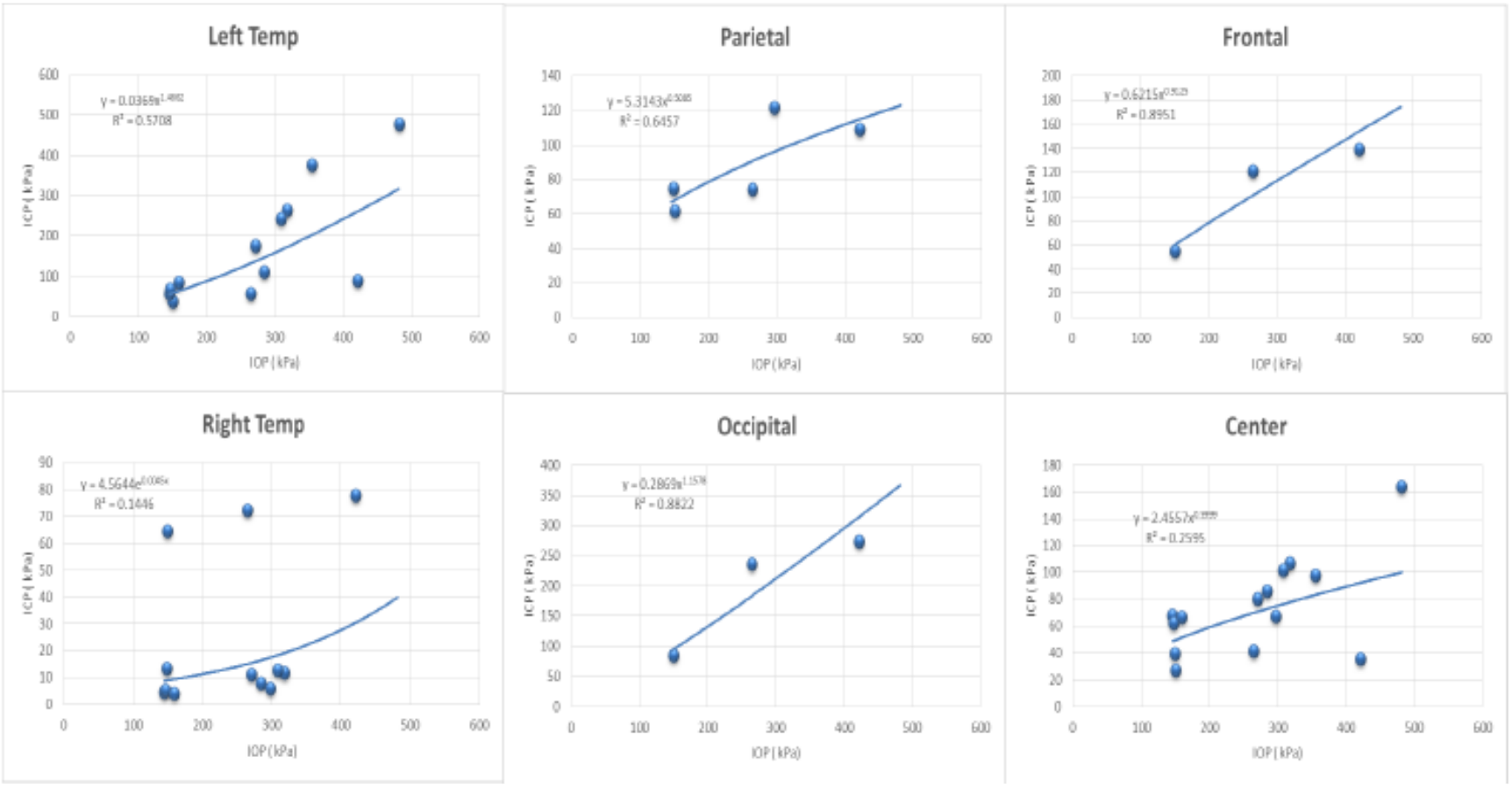

Figure 1. Side blast data – Intracranial pressure (ICP) vs. incident overpressure (IOP) for various regions of the brain

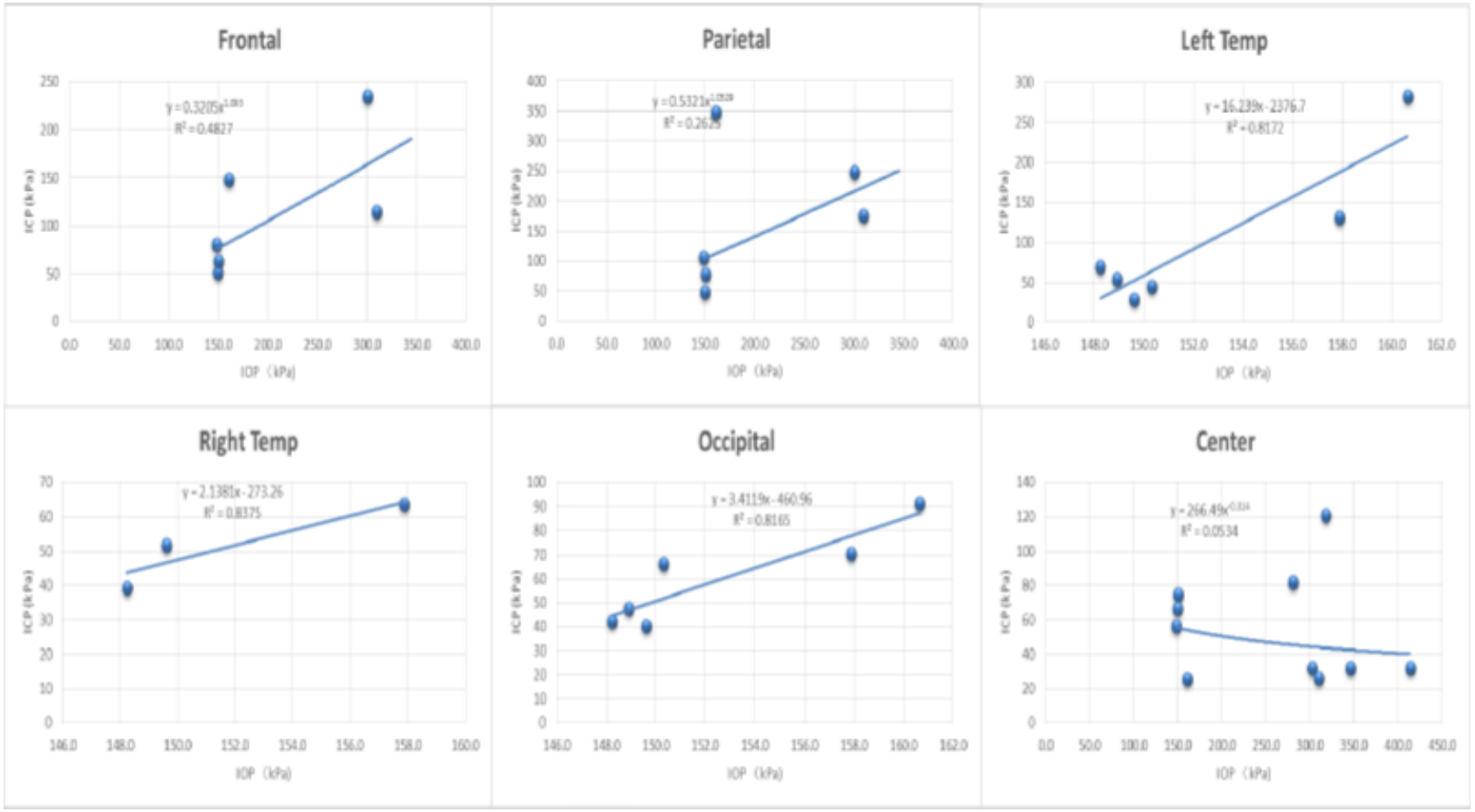

Figure 2. Rear blast data – Intracranial pressure (ICP) vs. incident overpressure (IOP) for various regions of the brain

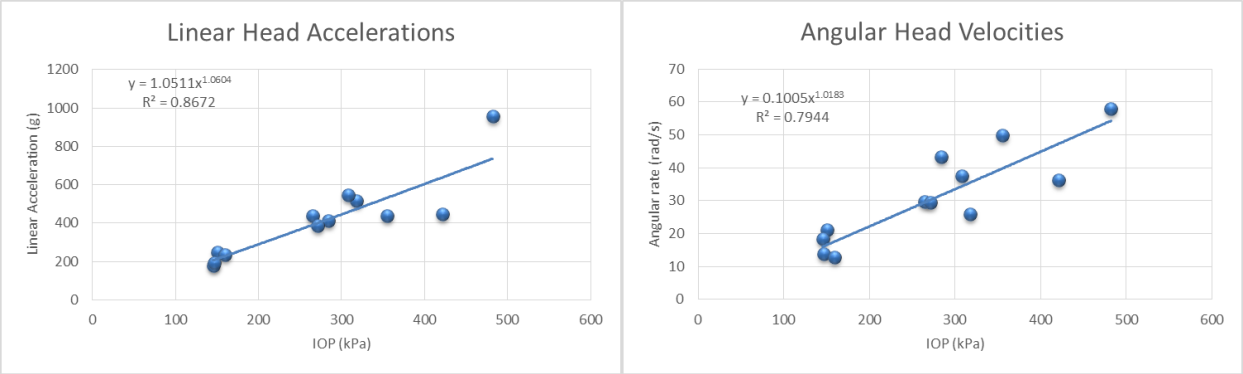

Figure 3. Head motion in side blasts.

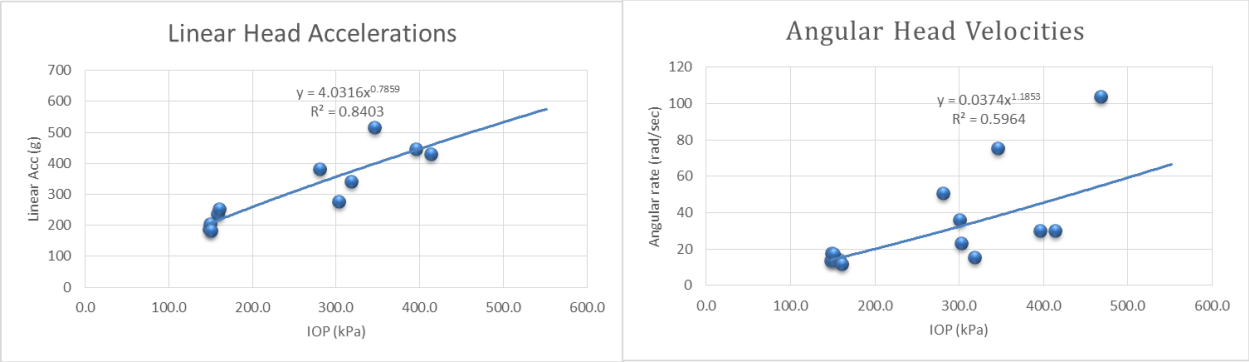

Figure 4. Head motion in rear blasts.

2. Blast Testing of Non-Instrumented Swine

The noninstrumented swine were exposed to a single blast to assess the injuries sustained. Thus, the test methodology was as follows:

The animal was anesthetized at Wayne State University and transported in an ambulance to the test site on the day of the experiment, arriving at about 8 am, after a 90- to120-minute drive from Detroit, MI to Port Clinton, OH. Anesthesia levels were maintained until it was ready for testing. The wait was due to the time needed to prepare the instrumented swine or cadaver which was to be tested alongside the non-instrumented swine. So for the first test of the day, there were generally two test subjects exposed to the same blast. After the non-instrumented swine was exposed to blast, it was taken back into the ambulance and driven back to Wayne State University for observation and blood draw. It was sacrificed on the third day and the brain was removed and preserved for histological study.

We completed the experimental protocol by testing of 12 swine at two pressure levels – seven at 300 kPa and five at 400 kPa, nominally. The protocol also included 5 sham

animals which underwent the entire test protocol but were not exposed to blast. That is, the sham animals were anesthetized, transported by ambulance to Ohio where they waited for about 2 hours, put in the sling used to test blast animals for about 45 minutes, returned to the ambulance and driven back to Wayne State University for observation and blood draw. They were sacrificed on the third day and the brain was removed and preserved for histological study.

3 Brain histology to assess brain injury in blast exposed swine

During the period from July 1st to 2015 to June 30th 2016, considerable progress has been made in various aspects of processing brain samples.

A) By July 1st, 2015, a total of 17 non-instrumented swine were tested as part of the histological assessment of blast induced injury changes in the brain. The final samples in various groups were, Sham =5; Medium Pressure =7, High Pressure= 5. From this period, the focus of the histology was on processing brain tissue from all sham, mild and high pressure blast groups.

We completed processing 6 blocks from the anterior lobe of each brain. This resulted in a total of 102 blocks with 30 blocks from 5 sham swine, 42 blocks from 7 medium pressure (222-332 kPa) exposed swine and 30 blocks from 5 high pressure (290-403 kPa) exposed swine. The process of cutting each brain into 5 mm blocks and their further sectioning was previously explained. 48 sections from each block were collected resulting in a total of 4896 sections thus far from 6 blocks/animal from all the 17 animals (Table 1). We completed staining representative sections from each block by various markers of injury. Axonal injury was assessed by incubating sections in antibody solutions against neuroflilament light chain (NF-L), neurofilament medium chain (NF-M) and against beta amyloid precursor protein (β-APP). Astrocytic and microglial expression changes were assessed by incubating sections in antibody solutions against glial fibrillary acidic protein (GFAP) and ionized calcium-binding adapter molecule 1 (IBA-1), respectively.

Serum harvested at the stated time points (pre blast or sham test, 6, 24, 48 and 72 hours after blast or sham test) was also being assessed for temporal changes in neurofilament heavy chain (NF-H), GFAP and interleukin 6 (IL-6).

Table 1 - Details of the number of anterior blocks and representative sections collected so far			
group	Anterior blocks/animal	# of blocks/group	# sections per animal/group
Sham (n=5)	6/animal	30	288/1440
Medium pressure (n=7)	6/animal	42	288/2016
High pressure (n=5)	6/animal	30	288/1440

We further completed the quantification of β-APP, GFAP and IBA-1 stained sections by methods explained previously. Sections stained by NF-L and NF-M were observed for qualitative changes. Furthermore, we also completed an ELISA analysis of serum samples from all the 17 swine. The serum samples were collected before sham or blast and at 6, 24, 48 and 72 hours after blast or sham procedures were tested for changes in the expression of phosphorylated neurofilament heavy chain (pNF-H Elisa Kit, Encor Biotechnology, Gainesville, FL), glial fibrillary acidic protein (GFAP; cat#NS830, EMD Millipore, Billerica, MA) and interleukin-6 (IL-6; cat# ESIL6, Life Technologies, Carlsbad, CA). Of the three biomarkers analyzed, there was some evidence of higher GFAP in severe blast group than the sham group ($p = .08$). No apparent difference in GFAP was found between sham and medium pressure group. No significant changes were observed with regard to pNF-H and IL-6 serum levels. A manuscript (Appendix-2) with histology and biomarker data was submitted to the journal PLOS ONE and is awaiting a decision after a revised submission.

B) As part of our continuing efforts to complete processing the remainder of the cortical regions encompassing parietal, temporal and occipital lobes including the associated sub-cortical structures such as hippocampus, thalamus and hypothalamus posterior aspects we completed coronal sectioning and staining 15 of the 17 samples. These blocks were designated as blocks 7-10 (Table 2). The brainstem was separated into a left and right half by a midline (pyramidal tracts) cut. Then each left brainstem half was further cut into three 5 mm sagittal blocs designated as midline, 5 mm lateral and 10 mm lateral that encompass the superior colliculus, pyramidal tract, cerebellum and other associated structures (Table 3). So far sections from the coronal and sagittal blocks of 14 animals have been probed to assess blast induced neurotrauma. Axonal injury changes have been assessed by beta amyloid precursor protein (β-APP) and neurofilament light chain (NF-L) immunocytochemistry. Inflammatory response has been assessed by glial fibrillary acidic protein (GFAP) and microglial (Iba1)

immunocytochemistry for changes in the expression of astrocytes and microglia respectively.

The posterior aspect of the brain is being studied at this time. Figure 5 shows four 5-mm thick sections of the posterior brain. Septal nucleus, anterior commissure, thalamus, 3rd ventricle, hypothalamus, hippocampus, and midbrain structures could be seen. These blocks will be used to obtain 35-40 µm coronal sections which will ultimately be used to stain for various injury markers.

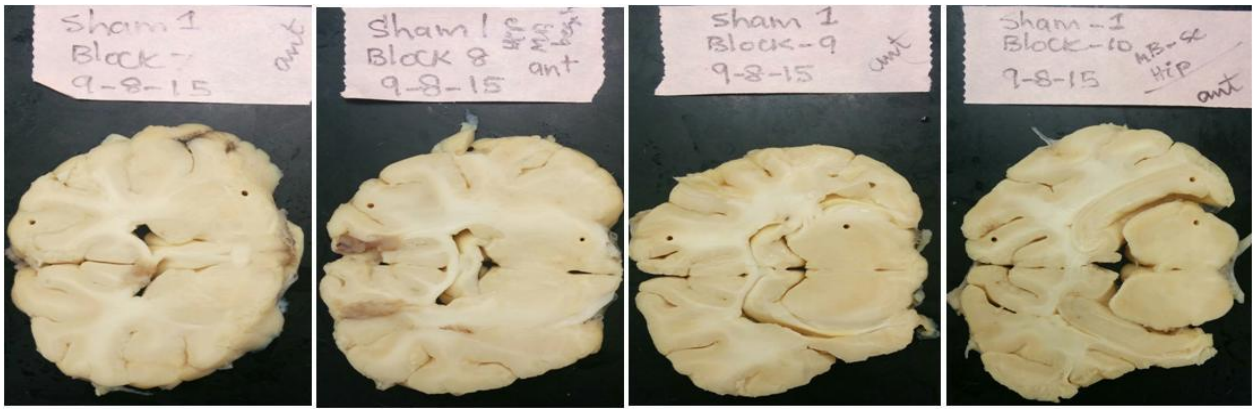

Figure 5. Coronal sections of the posterior brain being prepped for histological studies.

Table 2- Details of the number of posterior blocks and representative sections collected so far

group	Posterior blocks/animal	# of blocks/group	# sections per animal/group
Sham (n=5)	4/animal	20	192/960
Medium pressure (n=7)	4/animal	28	192/1344
High pressure (n=3)	4/animal	12	192/576

Images of three 5 mm thick sagittal blocks encompassing the brainstem are shown in Figure 6. These sagittal blocks will be cut into 30-40 µm sagittal sections which will ultimately be used to stain for various injury markers.

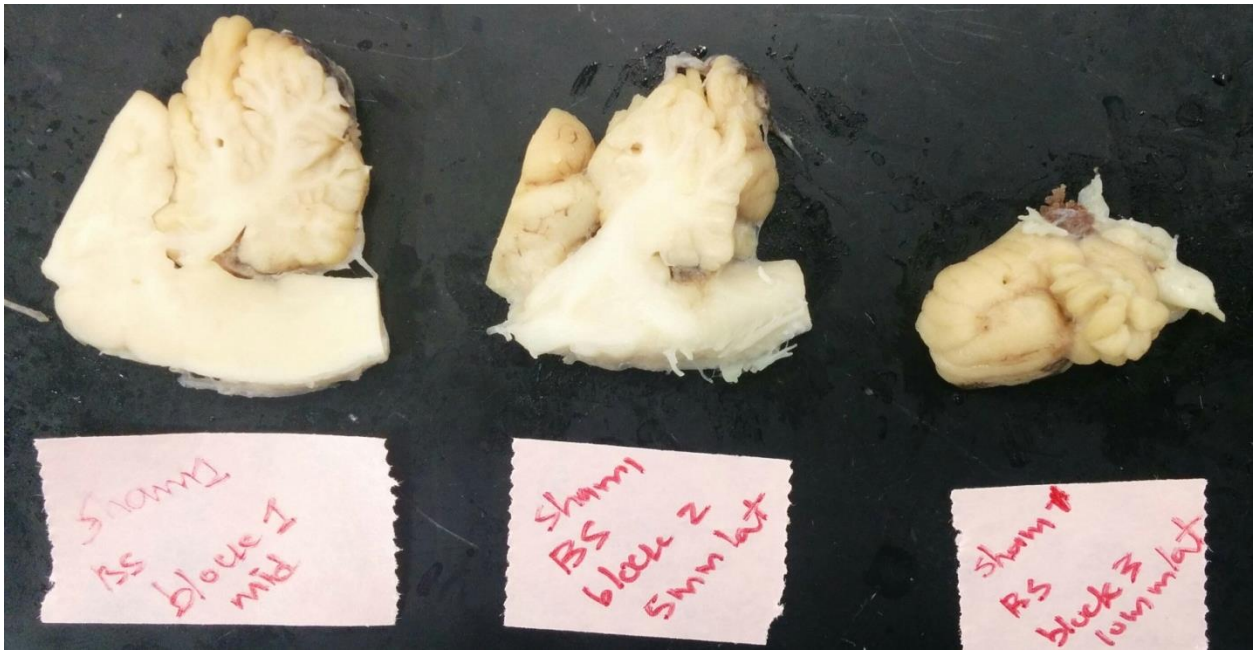

Figure 6. Sagittal sections of the brain stem being prepped for histological studies.

Table 3- Details of the number of sagittal blocks and representative sections collected so far			
group	Posterior blocks/animal	# of blocks/group	# sections per animal/group
Sham (n=5)	3/animal	15	96/480
Medium pressure (n=7)	3/animal	21	96/672
High pressure (n=3)	3/animal	9	96/288

Key findings:

1. Open field blast induces marked axonal injury changes as evidenced prominently by β-APP immunohistochemistry in the cortex and sub cortical white matter tracts of frontal lobe.
2. Open field blast induces profound changes in the number of astrocytes and microglia in the medium pressure blast group.
3. Presence of GFAP almost exclusively in the white matter tracts may support an ongoing axonal injury.

4. Evidence suggestive of higher serum GFAP levels in the high pressure blast group lends credence to astroglial changes as shown by histology.

5. GFAP may be considered as one of the key serum markers of blast induced injury changes considering a) high astrocyte counts in blast sections; b) close association of GFAP staining in the white matter tracts suggesting putative injury changes in the white matter tracts; c) evidence of higher GFAP levels in the serum in the high pressure group.

Our immediate objectives:

- Complete the quantification of the APP, GFAP and Iba1 from the posterior aspects of the brain. Once completed, these data will offer insights into the extent of the injury in various lobes of the brain including brainstem.
- This data will be incorporated into another manuscript which will be submitted for publication in a high quality journal.
- We will continue with cleaved caspase, Fluoro-Jade C, H&E and Prussian blue staining encompassing all the regions of the brain.

TASK II REPORT

Task II – Perform open field blast testing on 6 unembalmed post-mortem human subjects (PMHS) also known as cadavers to obtain biomechanical data

During this reporting period, we received several calls for potentially available specimens. However, they were not accepted due to various reasons, such as failure of blood examination, over long post mortem time, and conflict of schedule among testing groups. Eventually, we were able to obtain one male specimen from University of Michigan, suitable for our use. Relevant biological data on the specimen are provided in Table 4.

Table 4. PMHS Data

PMHS ID	Sex	Age	Height	Weight	COD
UM 34930	Male	87	70''	140 lb	Mylodislastic Leukemia

PMHS Preparation

The protocol for PMHS preparation, sensor usage, and sensor locations was kept the same as in previous tests.

Blast testing of PMHS

The third PMHS blast tests were conducted on 9/24/15, the seventh day after his death, at ARES, Inc. in Port Clinton, OH. A total of 9 tests were conducted on the cadaver.

Data from test 4 (lateral low level blast) was not recorded due to a failure of the triggering system. Similar to the second cadaver test, perfusion of artificial cerebrospinal fluid (aCSF) was performed prior to each blast to maintain physiological conditions within the skull.

Intracranial pressure and accelerometer data were filtered at CFC 6000 and angular rate data were filtered at CFC 3000. All plots are provided in the Appendix 3.

Plans for the next reporting period

No conclusions can be reached with the data from three specimens. We will continue to analyze the data and collect more test data so that we can arrive at some conclusions.

We have obtained approval from the Army (ACURO) for using the Wayne State University body donation program as a specimen source. Currently, we are waiting for available bodies from all approved sources.

TASK III REPORT

Task III - Develop and validate a computer model of the pig brain simulating the effects of a blast over-pressure

In this reporting period, the major work focused on the following tasks:

1. Comparison of biomechanical responses predicted by the swine head model against experimental measurements
2. Investigation of the over predicted intracranial pressure (ICP) at the frontal lobe
3. Analysis of sensor location sensitivity on model predicted ICP

1. Comparison of biomechanical responses predicted by the swine head model against experimental measurements:

Details related to the development of the finite element (FE) model of pig head and FE modeling of blast waves using multi-material arbitrary Lagrangian-Eulerian (MMALE) methods have been discussed in previous yearly reports. In this reporting period, the focus was on comparing the model predicted incident pressure (air pressure) and ICP (brain pressure) values against experimental measurements.

The previously developed swine head model was integrated with a three-dimensional (3D) mesh of the air domain and the interaction of the shock wave with the swine head model was achieved through a fluid/solid coupling algorithm. The *CONSTRAINED_LAGRANGE_IN_SOLID formulation available in LS-DYNA was used to model the coupling between the shock wave and the simulated pig head. Figure 7a schematically shows the experimental boundary conditions, as described in the experimental studies (Task I) while Figure 7b shows the modeling set-up to simulate the blast.

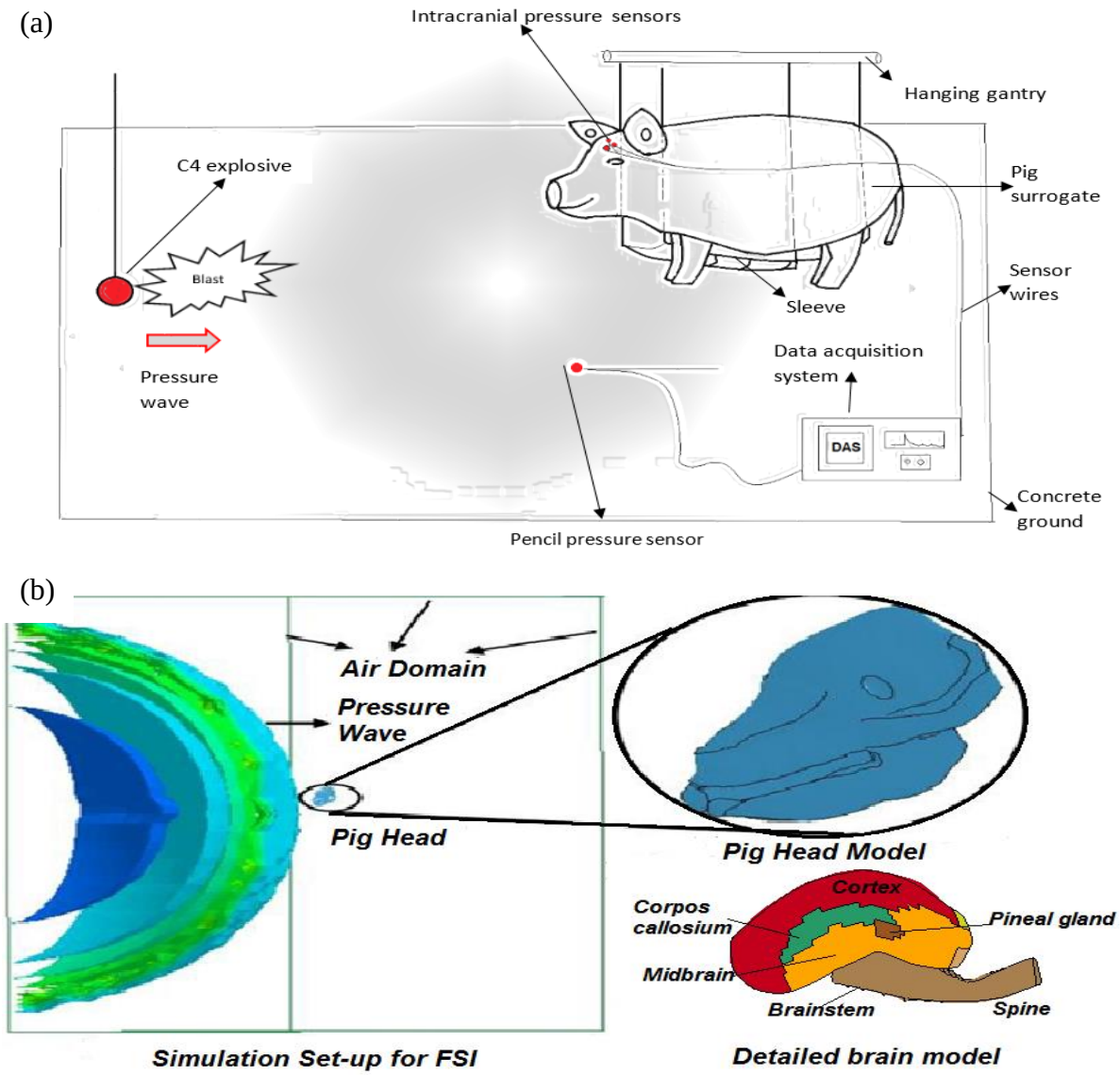

Figure 7. Schematic descriptions of the experimental setup (a) and simulation setup (b). The geometric locations where intracranial pressure sensors were installed in the experiments were identified in the FE model (Figure 8). Four elements surrounding the pressure sensor locations were averaged to calculate the model-predicted intracranial responses for comparison with experimental data.

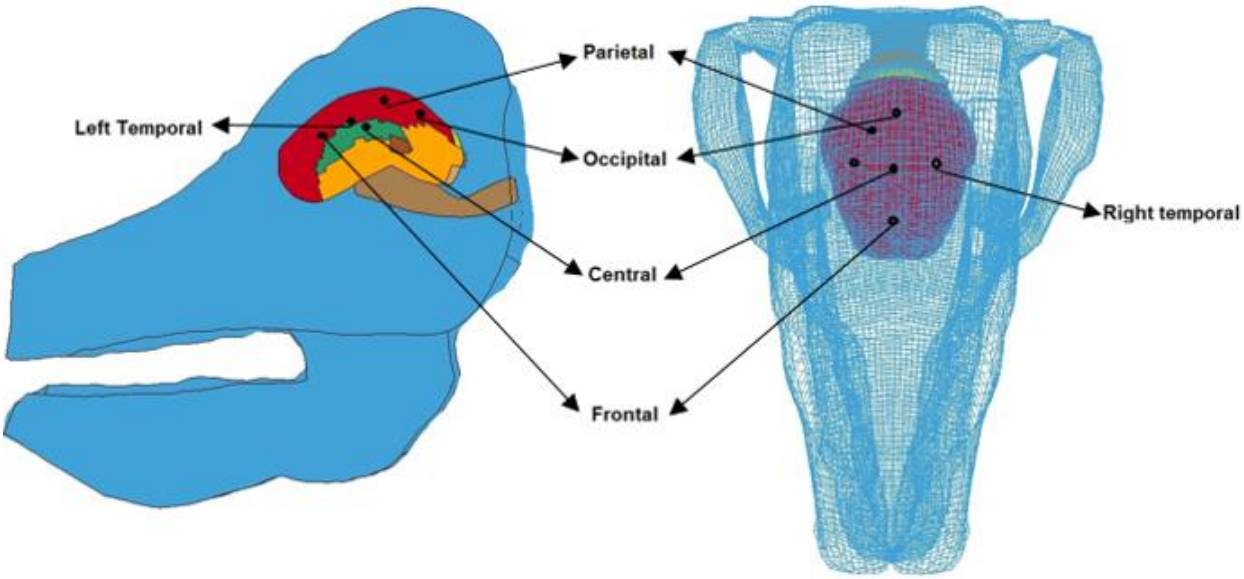

Figure 8. Locations of pressure sensor installation inside the pig brain and the corresponding elements in the numerical model.

In previous reports, the pressure-time histories predicted by the MMALE simulations were validated against theoretical Conwep calculations at the prescribed ranges. In this reporting period, a brief comparison of the incident pressure measured in the experiments and from the simulation was also conducted to ensure that the surrogate experienced a similar incident pressure during numerical simulations. The incident pressure-time histories for the simulations as well as those measured from the pencil air pressure sensor during the experiments are shown in Figure 9. The incident pressure in numerical studies for the high (Figure 9 (a)), medium (Figure 9 (b)), and low (Figure 9 (c)) pressure levels matched well against the experimentally measured pressures at the same pressure levels, respectively.

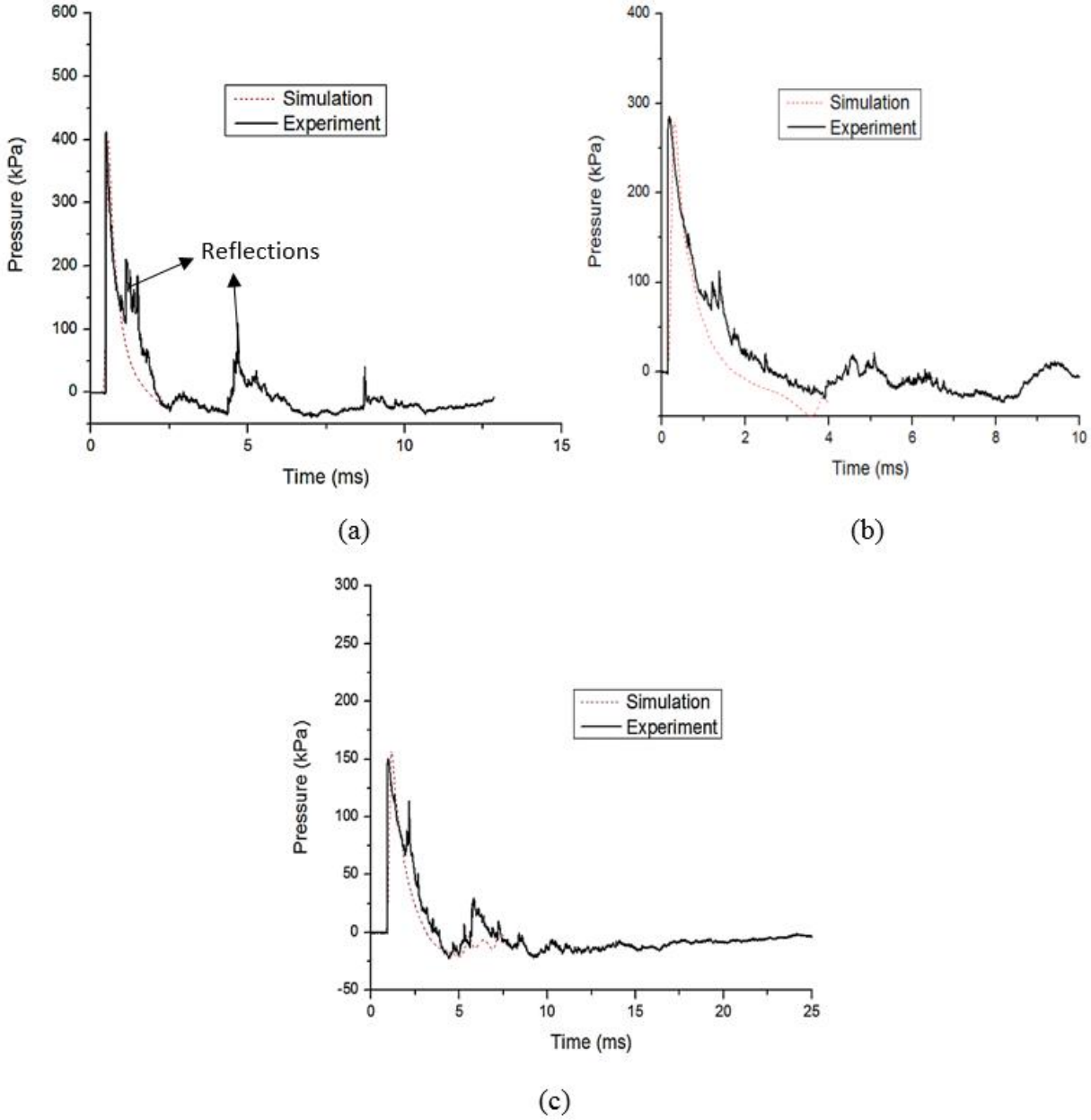

Figure 9. Comparison of model predicted and experimentally measured incident pressure for (a) high level (400 kPa), (b) medium level (275kPa), and (c), low level (150 kPa) of blasts.

There were some small reflections present in the experimental data as shown in Figure 9 while the simulation results did not have any of these reflections because surrounding infrastructures, such as the ground and the metal frames were not explicitly modeled. Table 1 compares the average peak incident pressures measured experimentally and that calculated from the simulations. All differences were less than 2.2%.

Table 4. Comparison of the experimentally measured and model predicted incident pressures at the three preset pressure levels

Peak incident over pressure (kPa)			
Pressure Level	Experiment (Mean ± SE)	Simulation	% Difference
Low	150.2±0.9	150	0.1
Medium	278.2±13.9	280	-0.6
High	409.2±18.9	400	2.2

The model predicted peak incident over pressures and ICPs at the frontal, central, occipital, right temporal, left temporal, and left parietal locations are shown in Figures 10(a), (b), and (c) for the three different pressure levels using the same sampling rate as that used in the experiments. In all simulations, the incident pressure exhibited a typical Friedlander waveform. Also, the peak ICP at the frontal location was always higher than the peak incident pressure for all simulations. Contrary to other theoretical solutions, the ICP at the occipital location did not become negative. This is probably due to the technical difficulties when inserting the occipital sensor into the pig brain, because of the relatively thick skull and neck at the posterior region of a pig head. As a result, this sensor was located within the occipital lobe but not at the posterior edge of the occipital lobe.

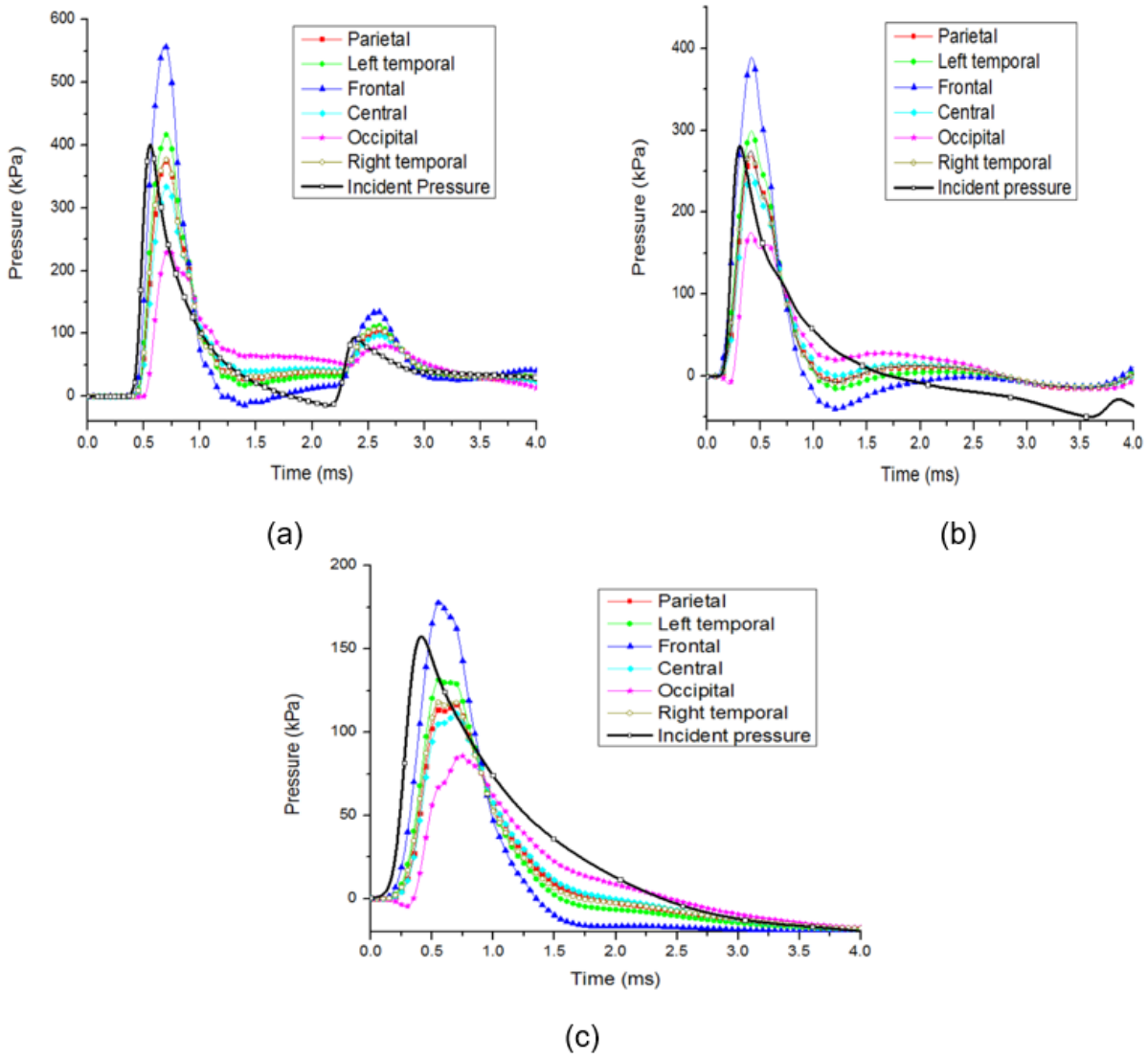

Figure 10. Model-predicted ICPs at different sensor locations for (a) the high level (400 kPa), (b) medium level (275kPa), and (c) low level (150 kPa) blasts.

The model-predicted ICP-time histories were further compared with experimental measurements. The ICP-time histories at the central, frontal, right temporal, left temporal, parietal, and occipital locations taken from two experiments subjected to the medium level of blast were compared with model-predicted ICPs. As can be seen in Figure 11, the differences in the respective peak values between experimental and model predicted results were relatively small except for that measured at the frontal location.

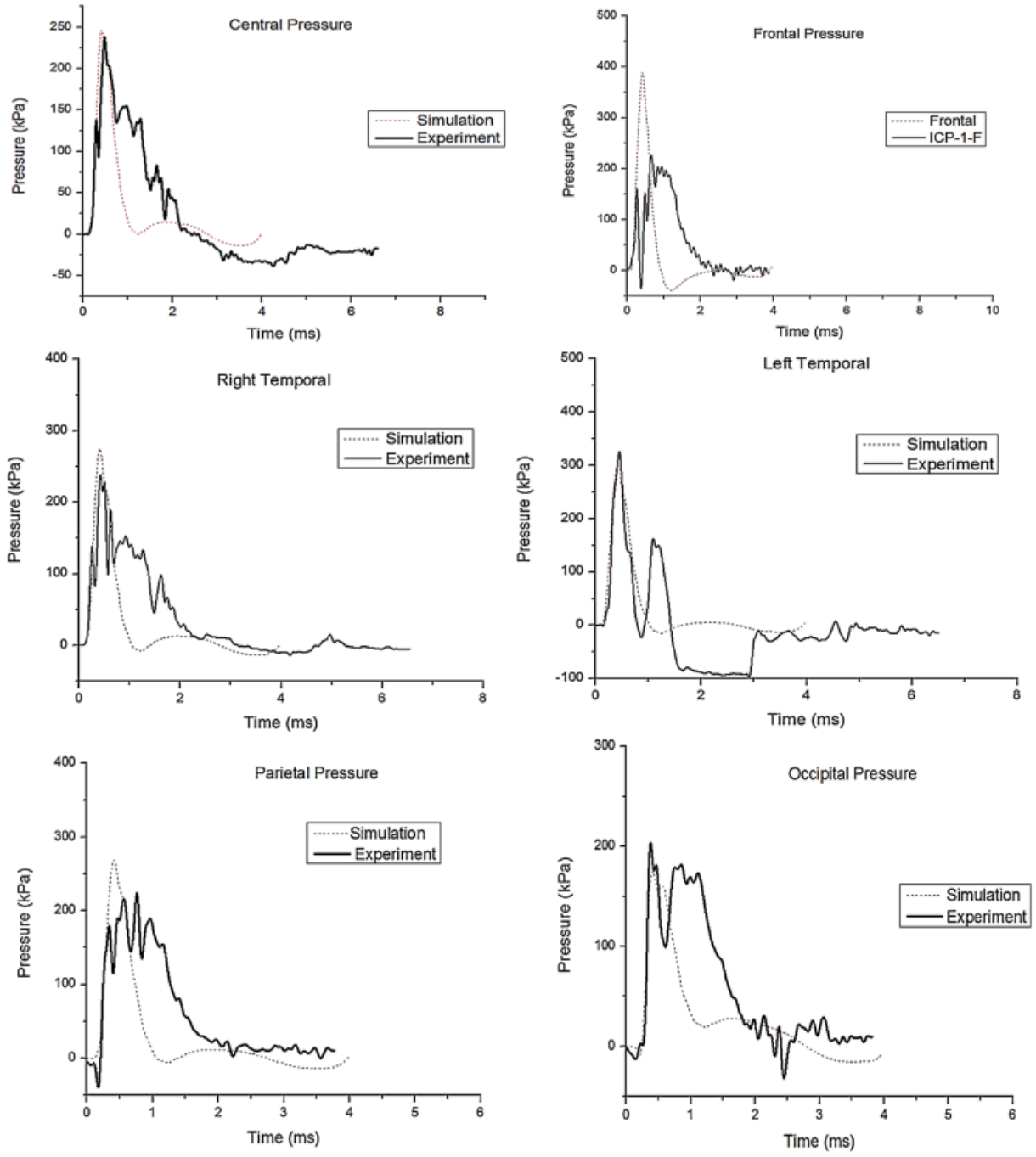

Figure11. Comparison of model-predicted and experimentally measured ICP-time histories for the medium level (275kPa) blast

Although not shown, similar model-predicted and experimentally measured pressure time histories were obtained for the high as well as low levels of incident over pressure. Additionally, the peak model-predicted and all experimentally measured peak ICPs at

the frontal, parietal, central, right temporal, left temporal, and occipital locations for all three incident pressure levels are shown in Figure 12.

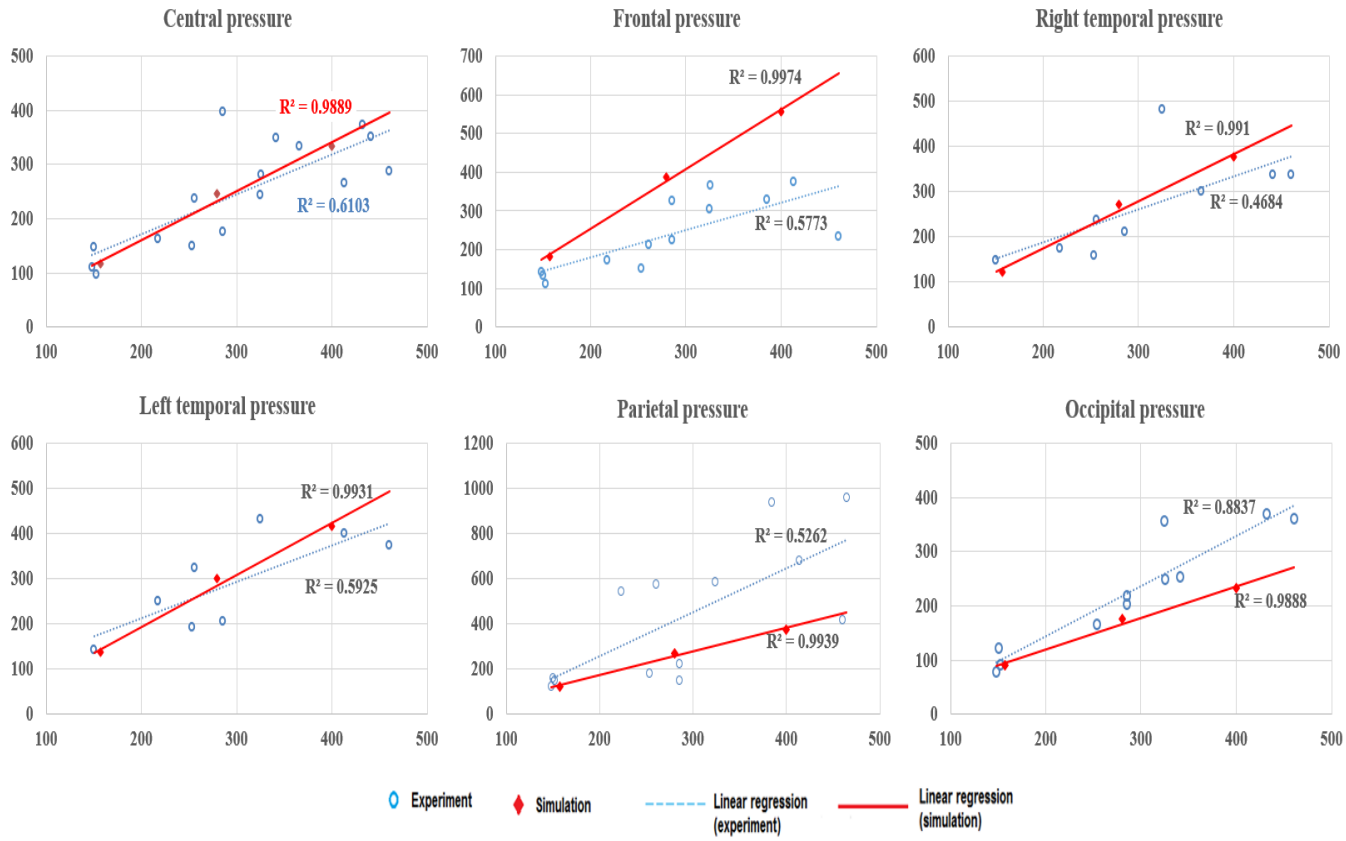

Figure 12. The ordinate - peak model predicted ICPs (diamond shaped) and experimentally measured ICPs (empty circle) versus the incident over pressure (the abscissa) at different brain locations. All units are in kPa.

The model over predicted the frontal ICP while the ICPs at other locations seemed to have a reasonable agreement with the test data. It was also observed that all simulated ICPs had a linear relationship with respect to the incident pressure with an R^2 value greater than 0.98. Quantitative comparisons between the experimentally measured and model predicted peak ICPs are shown in Table 4. Considering the large variations +seen in experimentally obtained ICPs, it is believed that the model predicted ICPs agreed reasonably well with experimental data.

Intracranial pressure showed an increasing trend with respect to the incident over pressure in both the experimental data and the simulation results, as shown in Figure 12. The model-predicted ICP results were highly linear with all coefficient of determination (R^2) greater than 0.98. This result is as expected due to the use of a linear viscoelastic material for the brain and an elastic material for the skull. In reality,

the response of the brain tissue is non-linear, strain rate dependent, and directionally variant in nature. Unfortunately, the constitutive material model representing such behaviors is not available in the explicit code of LS-DYNA. Moreover, the experiments have their own limitations of accuracy, such as, inadequate sealing of the skull after sensor insertion. The simulation results are based on theoretical equations for certain boundary conditions while the experimental results may have additional artifacts due to reflective boundary conditions. These reasons may explain the lack of reproducibility issues as seen in the experimental peak values shown in Figure 12.

2. Investigation of the over-predicted intracranial pressure (ICP) at the frontal lobe

The simulation results showed that the model over predicted the peak ICP at the frontal location by 46%, 65%, and 79% for the low, medium, and high incident pressure levels, respectively. As the blast wave travels through the brain from the frontal to occipital region, the peak pressure magnitude continues to decrease. The low experimentally measured frontal ICP can be due to the reasons listed below.

Anatomically speaking, multiple frontal sinus chambers are located within the frontal region of a pig's skull where the skull bones are the thinnest compared to other regions (Figure 13). The thin nature of the skull may reduce the efficacy of resealing the skull after pressure sensor installation. Additionally, there is a significant downward slope present when the pig is positioned with the pig head facing forward. This downward slope and the frontal sinuses in conjunction with potential incomplete sealing of the skull may act to lower the peak experimentally obtained pressure when compared to an intact skull.

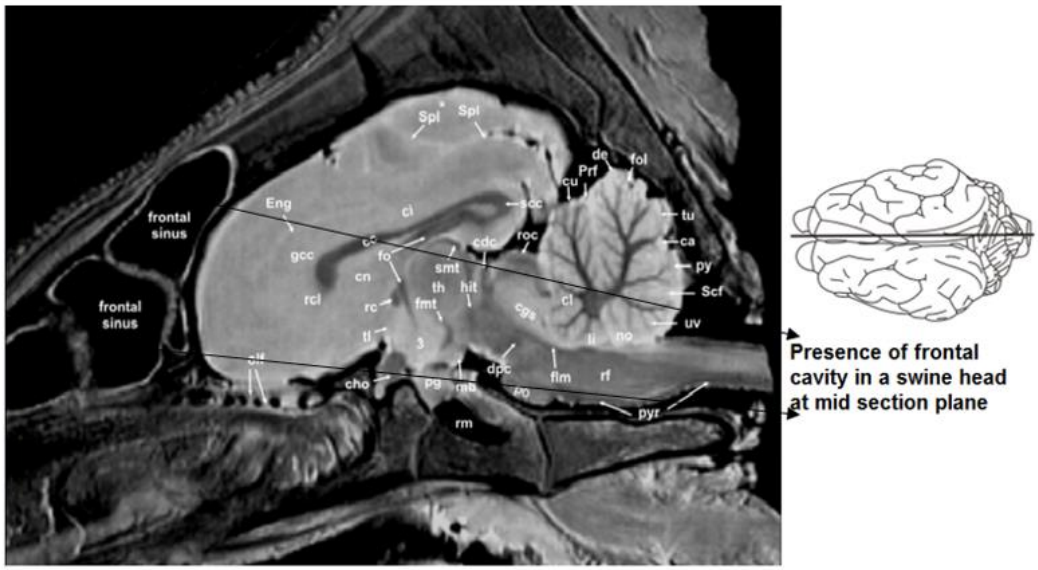

Figure 13. A lateral view of pig brain showing frontal sinuses (Reproduced from Schmidt, 2015).

Theoretically speaking, the pressure in an air filled (or occasionally fluid filled) cavity is lower than that of the ICP when no such cavity exists. Additionally, the integrity of the skull needs to be compromised in order to install the ICP pressure sensor. As a result of this needed experimental procedure, the measured ICP may be affected by two potential mechanisms. First, an air passageway is created between the brain and frontal sinuses. Although careful sealing of the skull is ensured, no attempt was made to seal the boundary between the brain and sinus chambers. Second, the fluid filled sinuses after sensor installation may entrap some air bubbles within the chambers. Both mechanisms could serve to lower the measured ICP.

To validate the existence of frontal sinus cavities in the pigs we used, a post-experiment pig head was harvested. The scalp and the surrounding soft tissues were carefully removed. A diamond saw was then used to cut the skull along the mid sagittal plane as shown in Figure 14. The presence of a sinus cavity can be clearly identified, right on top of the frontal sensor location.

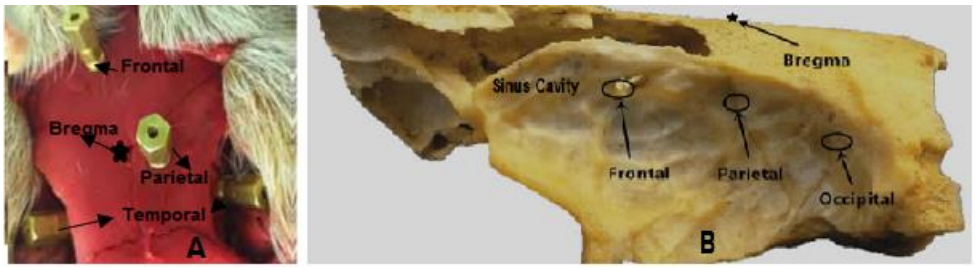

Figure 14. (A) A snapshot showing the locations of two installed mounts for pressure transducer installation, and (B) A sectional view of a skull which shows the frontal sinus cavity along with corresponding frontal sensor location.

A series of parametric studies was conducted with different assumed boundary conditions at the central region of the pig head. Three cases were considered: (1) both the skull and brain were intact; (2) the skull had a small opening while the brain was intact; and (3) the brain had a small hole on the surface while the skull was intact. Case 2 was intended to study the effect of an unsealed hole in the skull at the sensor location at the nasal cavity location. Case 3 was used to simulate a trapped air bubble between the skull and brain. The sketches of Cases 2 and 3 are shown in Figure 15. The holes were simulated by removing some of the elements in the skull or brain. The model-predicted peak pressures at the frontal sensor location of the brain for all three cases are plotted in Figure 16.

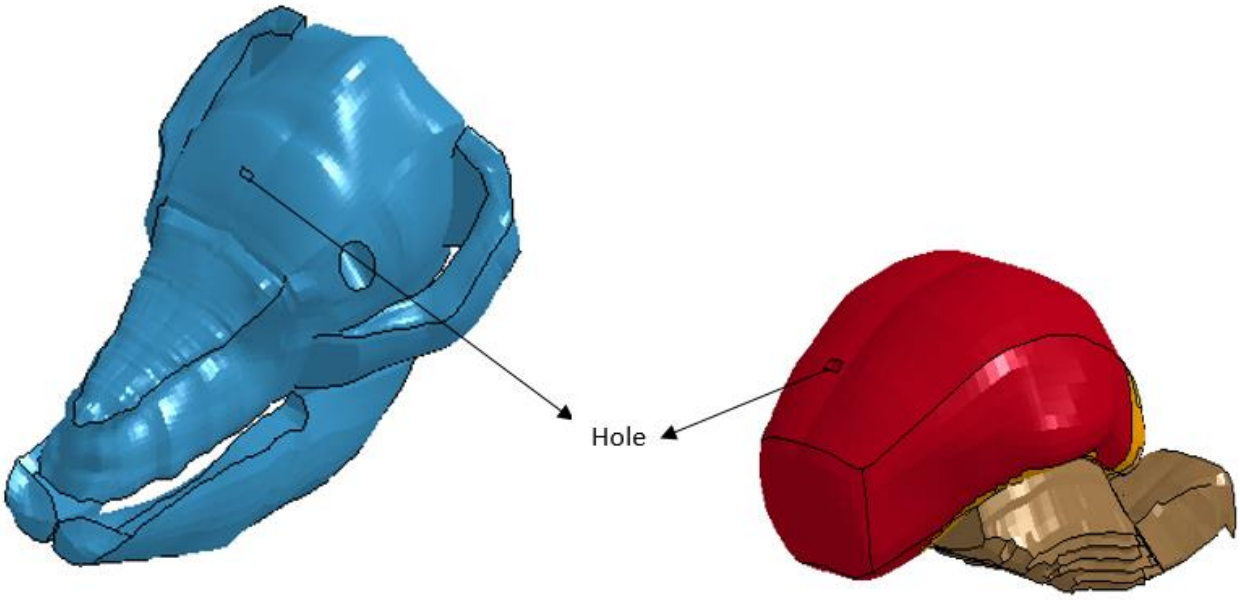

Figure 15. Simulations with openings on the skull and brain: (left) the skull has a small opening while the brain is intact; (right) the brain has a small hole on the surface while the skull is intact.

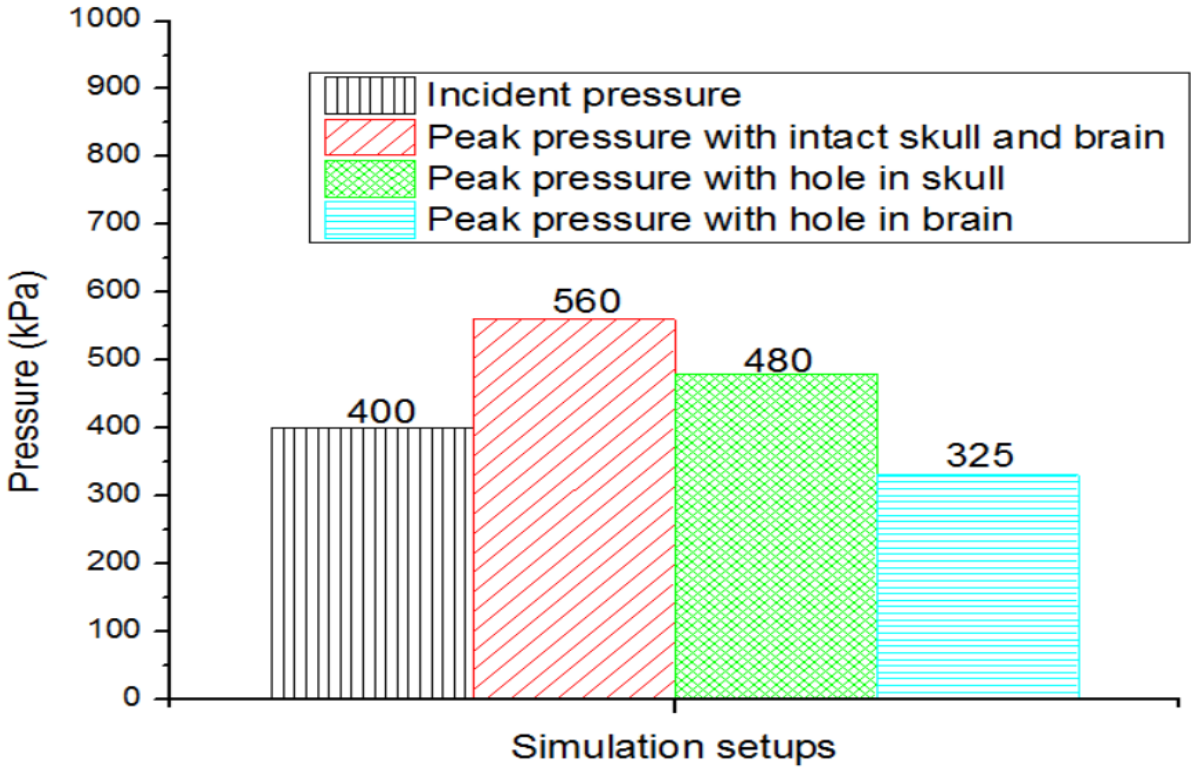

Figure 16. Comparison of model-predicted ICPs in all three cases: 1) both the skull and brain are intact; (2) the skull has a small opening while and brain is intact; and (3) the brain has a small hole on the surface while the skull is intact.

It can be seen that in Case 1, the peak ICP at the central brain is higher than the peak incident pressure by about 25%. An opening on the skull slightly decreased the ICP, and a significant pressure drop could be observed when a bubble existed on the surface of the brain. The low experimentally measured pressure is likely due to the presence of entrapped air bubbles or a direct air passageway from the brain to the atmosphere.

Upon reviewing Figure 11, it is seen that there are reflections in the experimental data that could not be simulated. These reflections are more than likely from the surrounding structures that were captured by the sensors. The model predicted very well the rising portion of the Friedlander wave as well as the peak value along with the initial decay in the curve. However, due to reflections in the later stage of the decay curve, the simulation curve partially deviated from the experimental curve. The corresponding reflections in the incident wave as well as the reflections inside the two hemispheres of the brain also affected the shape of ICP curve as shown in Figure 11. Similar to the incident pressure curve, the ICP curves at various locations inside the brain matched the initial rise and peak values except at the frontal location, but the later portion of the curve deviated from the experimental data. The reason for the mismatch between the experimentally measured and simulation-predicted duration is unknown, although it is suspected that this phenomenon may be related to the reflections captured by the sensor. More research is needed in order to better understand the reasons for this mismatch.

It is worth noting that sensor location plays a major role in ICP response. For example, the sensor at the occipital location did not show any negative pressure or countercoup scenario during the experiment. One of the reasons is because of the technical difficulties in surgically inserting the sensor into the rearmost location of the brain near the skull, due to the thick neck and skull at the posterior end of the pig's head.

3. Analysis of sensor location sensitivity on model predicted ICP:

Additional computational studies were conducted to determine the effect of varying sensor locations. In these cases, the pressure sensors were moved to a very frontal location (near the front - approximately 10 mm anterior to the frontal sensor location in the experiments) and a very posterior location (rear end - approximately 10 mm posterior to the occipital sensor location in the experiments) as shown in Figure 17. The model-predicted ICPs demonstrated the coup and countercoup phenomena (Figure 18), just like those seen in blunt impact conditions, within the first 2 ms after the shock wave reached the pig head. The ICP time history curves for all three blast levels at both extreme locations (A' and B') are shown in Figure 19. Further, a brief comparison was made between sensor locations between A and A' and between B and B' are shown in Figures 20 and 21, respectively. From these figures, it is clear that a higher peak pressure is found at a frontal location near the brain-skull interface (corresponding to A' position) compared to the original location (A). On the other hand,

the pressure at a far rear end location (B') is lower than the original sensor location (B). The higher pressure at the front end close to the skull was due to the impedance mismatch between the two materials. These results suggest that there is a greater possibility of injury in the region close to the skull-brain interface at the frontal location as higher intracranial pressures were correlated with elevated levels of bio-markers that are supposed to indicate blast-induced neurotrauma (BINT), as stated by Cernak et al. (2011). Also, the lower negative pressure at a rearmost position (corresponding to the B' position) shows a countercoup phenomenon at the rear end of the brain.

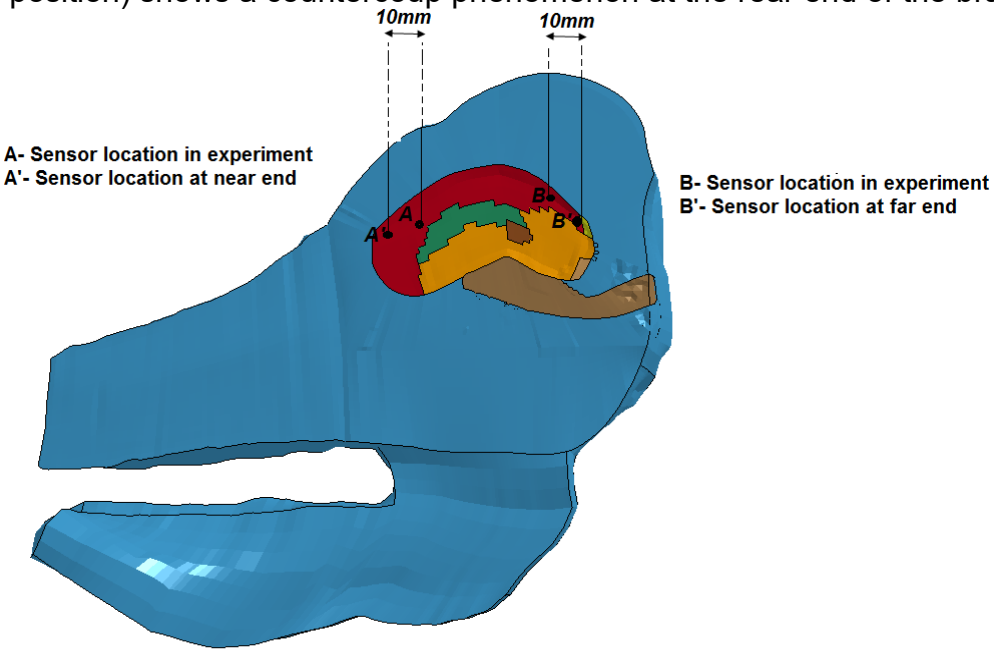

Figure 17. Additional sensor locations selected to study the coup and countercoup phenomenon.

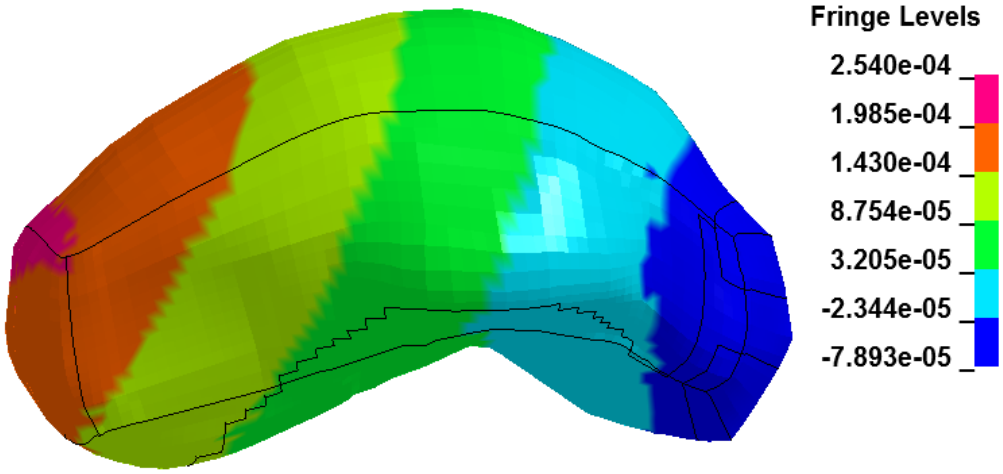

Figure 18. Coup and countercoup phenomenon at the 400 kPa incident pressure level (the fringe units are in GPa).

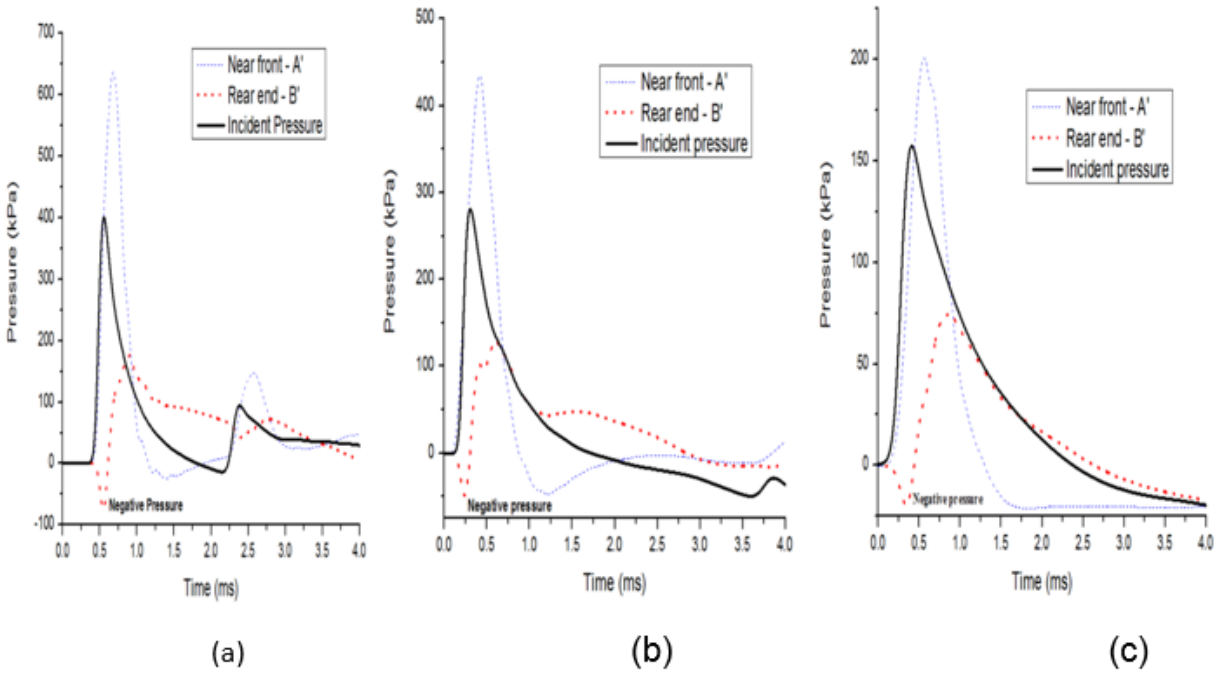

Figure 19. Intracranial pressures at the far front and rear ends of the brain at the high incident pressure level (a), medium incident pressure level (b), and low incident pressure level (c).

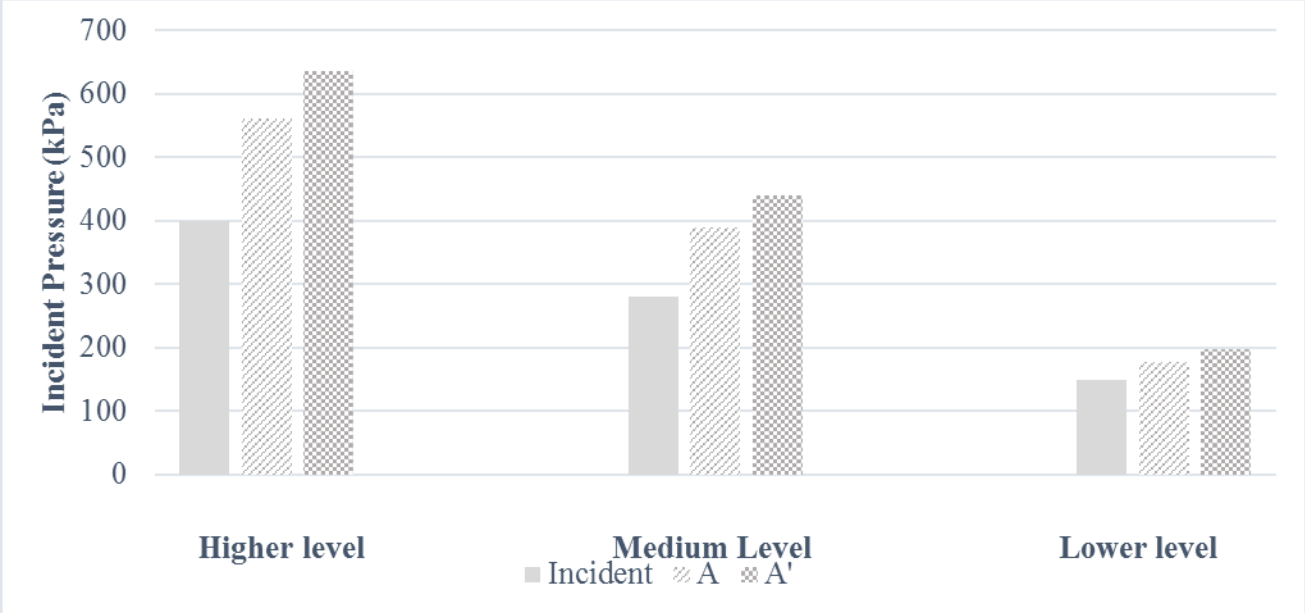

Figure 20. Comparison of the peak incident over pressure and ICPs at the actual sensor location (A) and an assumed near front location (A') for frontal region at the three levels of blast.

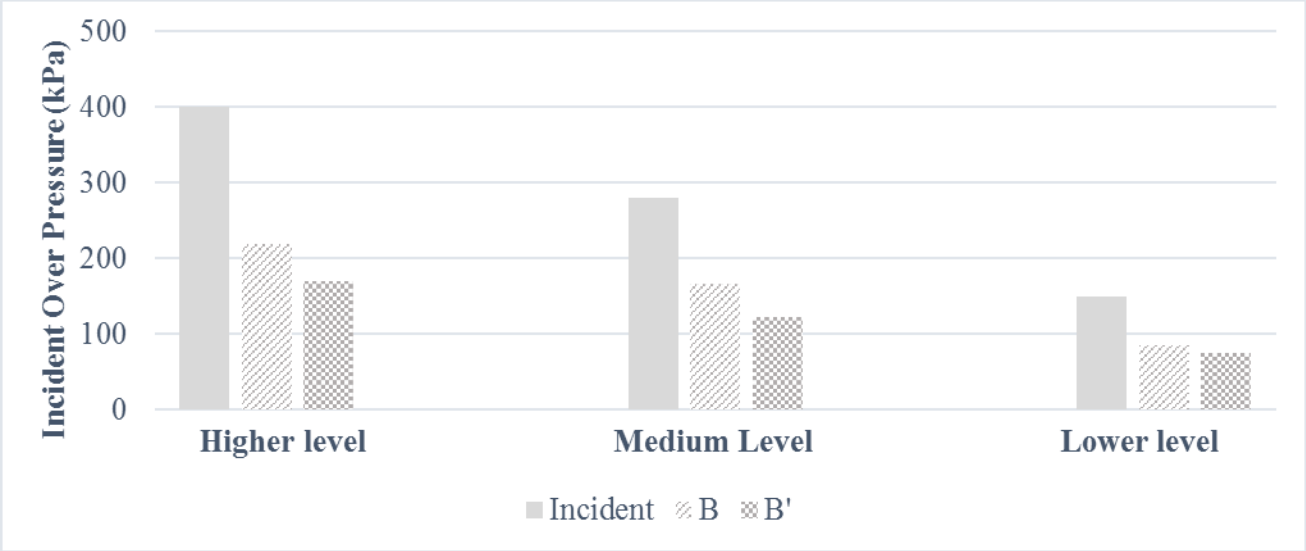

Figure 21. Comparison of the peak incident over pressure and ICPs at the actual sensor location (B) and an assumed far rear end location (B') for occipital region at the three levels of blast.

4. Conclusion:

To conclude, an FE model of a 55-kg Yucatan pig head was developed to simulate the biomechanical responses of the pig brain in an open field blast environment. Simulation results showed that an open field explosion can be replicated with the help of a 2D to 3D mapping technique using an MMALE formulation. Further, the interaction between the shock wave and the pig head can be simulated with the help of a coupling algorithm available in a non-linear explicit FE code in LS-DYNA. The measured peak ICPs at three levels of incident over pressure levels (low, medium and high) were compared with the FE model predicted ICPs at the similar sensor locations. Reasonable agreement was found between the experimental and numerical results, except at the frontal location. The FE model predicted a higher peak pressure at that location than the measured values. One possible reason might be related to air bubbles entrapped within the frontal fluid filled sinus cavity adjacent to the frontal ICP sensor. This argument is further supported by the parametric study using numerical models with holes at that location by removing some elements. Further studies will be aimed at correlating different biomechanical responses from the validated model with histological results, when they become available.

References:

Schmidt V. (2015) "Comparative anatomy of the pig brain - An integrative magnetic resonance imaging (MRI) study of the porcine brain with special emphasis on the external morphology of the cerebral cortex" Dissertation at the University of Gießen, Germany.

Cernak I., A. C. Merkle, V. E. Koliatsos, J. M. Bilik, Q. T. Luong, T. M. Mahota, L. Xu, N. Slack, D. Windle and F. A. Ahmed. (2011). “The pathobiology of blast injuries and blast-induced neurotrauma as identified using a new experimental model of injury in mice.” Neurobiology of disease 41: 538-551.

TASK IV REPORT

Task IV - Develop and validate a computer model of the human brain simulating the effects of a blast over-pressure

In this task, we report work the validation of the human brain model. This is a preliminary attempt at validating of the human head model against cadaveric brain response subjected to open-field overpressure using two of the three tests that have been carried out. The first test was not used because the cadaver brain was not properly perfused

1. Methods

To simulate the open-field blast tests we conducted, an 8 lb spherical C4 charge was modeled with a 4.86 kg TNT equivalent. The FE meshes of the spherical charge and the surrounding air adequate for the maximum standoff distance were developed (Figure 22). The FE head model was then embedded in the air mesh where its location and orientation with respect to the center of the charge conformed to the standoff distance and blast wave direction used in the cadaver tests. The open-field blast simulation technique, method and algorithm used were based on our previous blast simulation studies (Zhang et al., 2013). The head model used for the current effort has been improved and has been reported previously. Briefly, the major improvement included the addition of the eye/orbital components, the segregation of the 4 lobes, the refinement of the major cerebral structures, and the differentiation of the cerebellar white matter from the gray matter. Figure 23 shows the element clusters defined to approximate the ICP sensors locations placed in the cadaver brain. The element clusters representing the frontal, parietal, occipital and center ICP sensor locations were located in a para-sagittal brain section, approximately 10-12 mm off the midline and 5-7 mm below the brain surface in the corresponding lobes or 10 cm below the surface in the center of the brain. The element cluster representing the temporal sensor location was located 5 mm below the cortex in the temporal lobe.

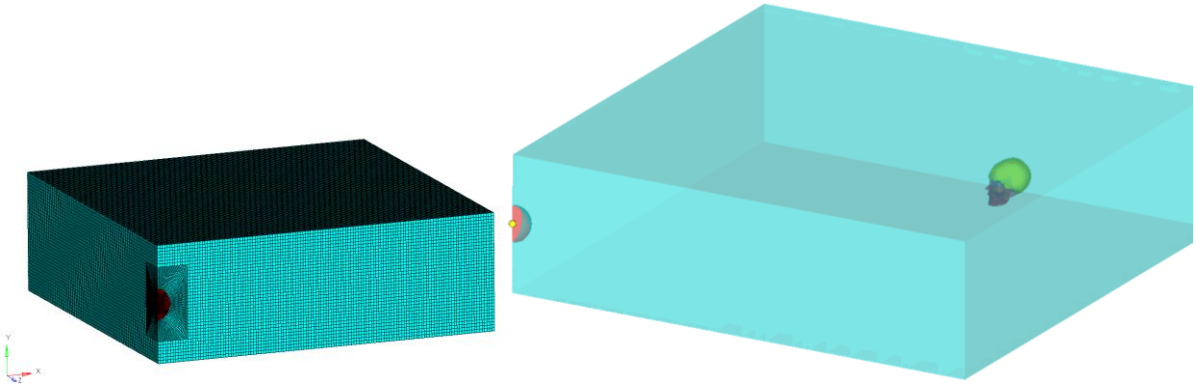

Figure 22. FE mesh of the TNT and air, and the head model embedded in the air mesh in a forward blast setup

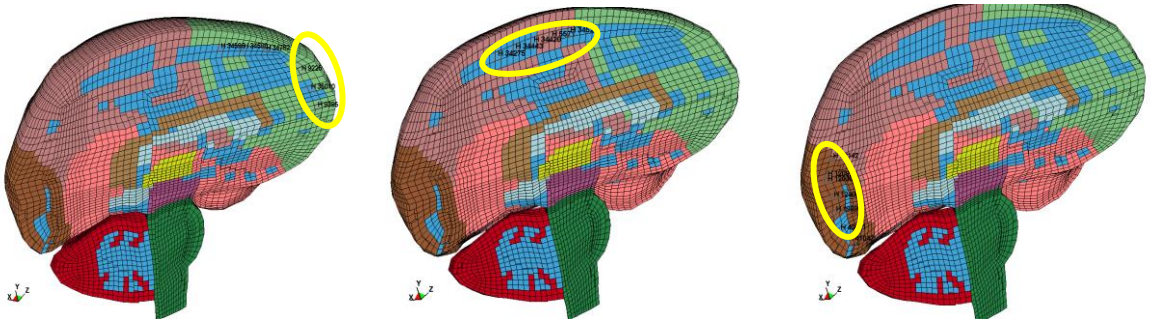

frontal location parietal location occpital location .

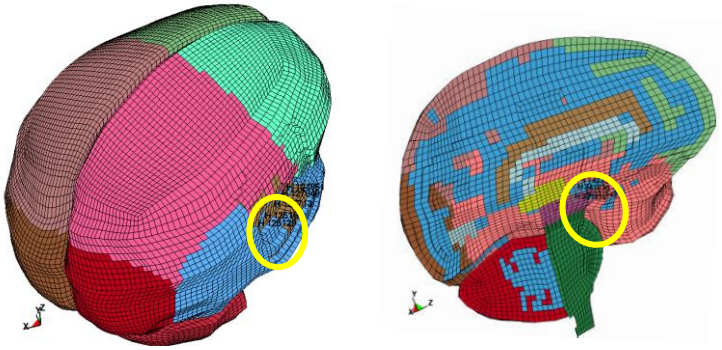

parietal location Center

Figure 23. The model element cluster defined for ICP calcualtions at the locations coresponding to the ICP sensors placed in the cadaver brain.

2. Results

Model results due to lateral blast

The model-predicted ICP at locations coincident with those of the pressure sensors resulting from lateral blast of 487 kPa overpressure (IOP) are compared with measured

data in Figure 24. The model-predicted peak ICPs at the frontal, parietal and temporal regions were comparable to the data measured by the sensors at the corresponding locations. However, the model under-predicted peak ICP at the occipital location and over-predicted ICP at the contrecoup temporal site. As for the temporal pressure at the coup site, although the peak ICP was consistent with the cadaver sensor data, the duration of the predicted pressure was much longer than the measured results. The cause of the discrepancy is under investigation and more test data will be needed to assess the discrepancy. It was also noted that the FE model predicted multiple waves after the first peak pressure wave, indicating the presence of a vibratory response in the model. This was presumably related to the use of head model only which may not have the same constraint and mass effect as offered by the full body in the cadaver test. Future efforts will focus on suppressing the oscillation.

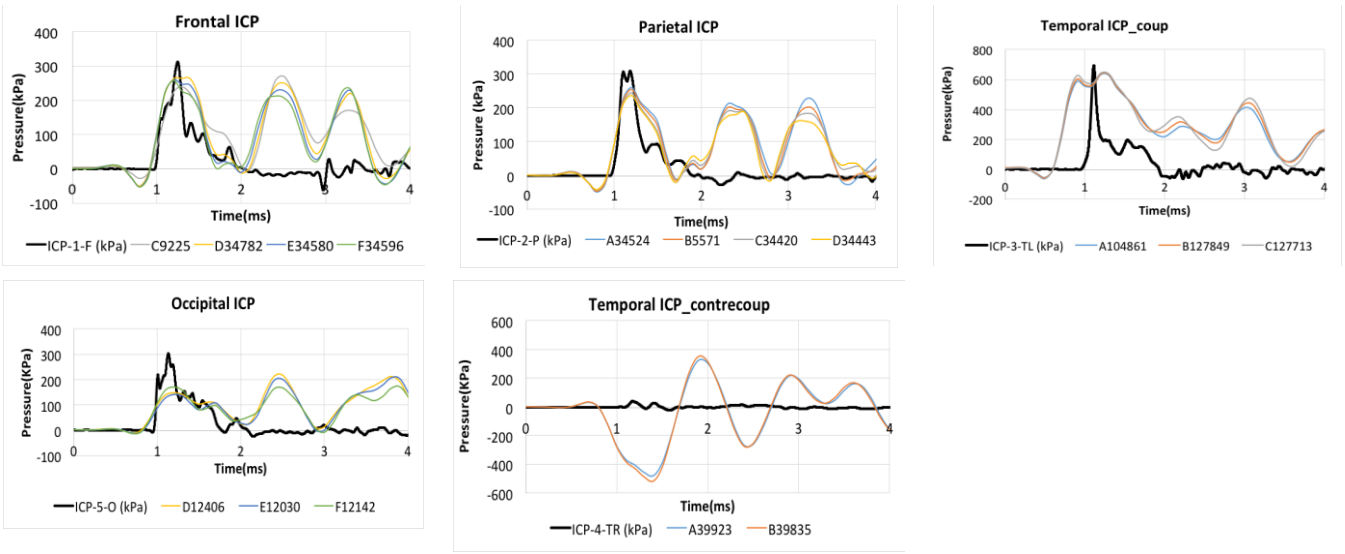

Figure 24. Lateral blast due to a peak IOP of 487 kPa: the model-predicted ICP and ICP sensor results (black line) are compared at different locations

Model results due to a frontal blast

The model-predicted ICP at the different locations resulting from a frontal blast of 440 kPa incident overpressure are compared with the ICP sensor data in Figure 25. The FE model predicted comparable peak ICP values in the parietal and central regions of the brain as the ICP sensor results although the durations of ICP responses were over predicted. The model-predicted ICP in the frontal (coup) and occipital (contrecoup) regions were higher than the results from the sensors in the same region. It was also observed that the pressure rise time appeared to be longer in model prediction as compared to the sensor measurements. This implies that the modeled brain tissue may have a greater damping effect than the cadaver brain tissue. It may also be due to the

inadequate sealing of the skull in the cadaver preparation. Similar to what was observed in the lateral blast simulation, the model-predicted ICP due to a frontal blast also exhibited vibrations in the various regions of the brain.

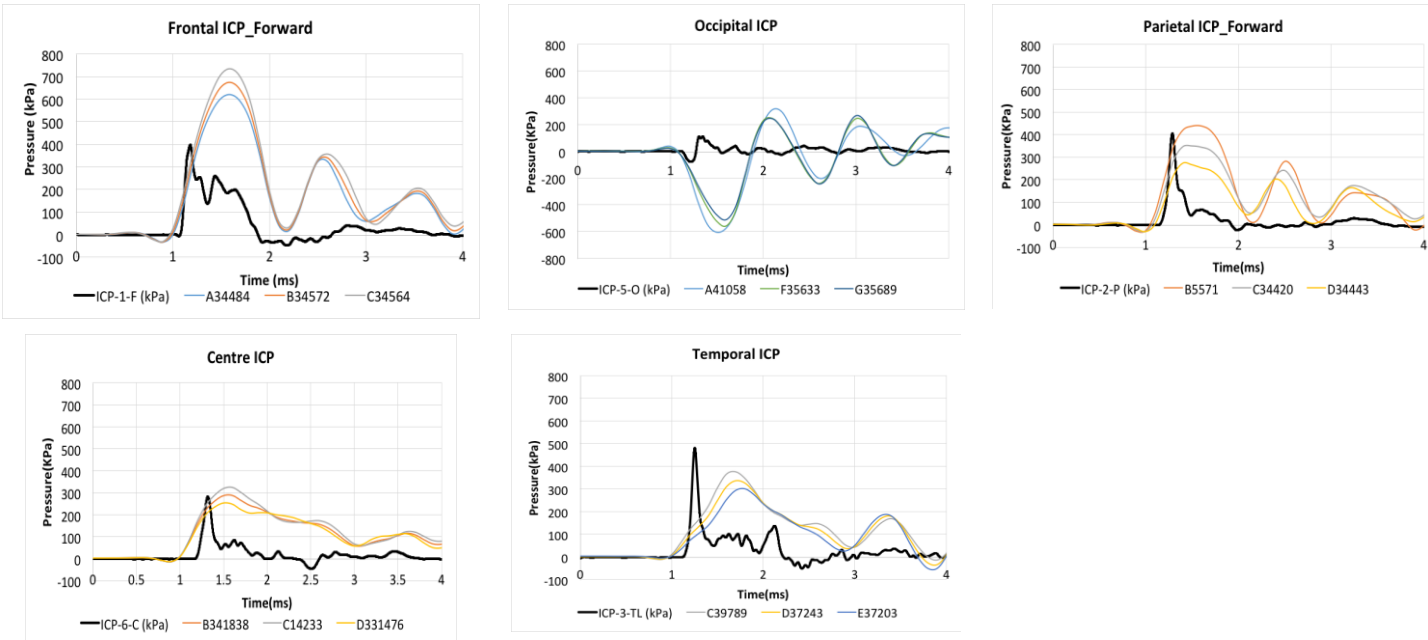

Figure 25. Frontal blast at 440 kPa IOP: the model-predicted ICP and ICP sensor results (black line) are compared at different locations.

Model-predicted brain strain response

The maximum principal strains (MPS) in the brainstem region and the coup site (temporal region for a lateral blast and frontal region for a frontal blast) were computed. The strains due to a forward blast with a peak IOP of 440 kPa and a lateral blast with a peak IOP of 487 kPa are shown in Figure 5. The brainstem strain was proximately 0.3 and 0.35 for the frontal and lateral blasts, respectively. Compared to the MPS in the brainstem, MPS at the coup site and midbrain region was less than 0.25 and 0.1, respectively in both the frontal and lateral blast. The brain MPS responses seemed to increase continuously even after the intracranial pressure response returned to zero, suggesting viscoelastic behavior of the brain tissue under the blast loading conditions. Although the predicted MPS time histories were comparable at the selected locations for the two blast directions, the peak IOP intensities used for the lateral and frontal blast were not identical. For a proper comparison of the effect of blast directions on the ICP and MPS responses it will be necessary to obtain more cadaveric test data and to conduct more simulations.

Frontal blast	Lateral blast

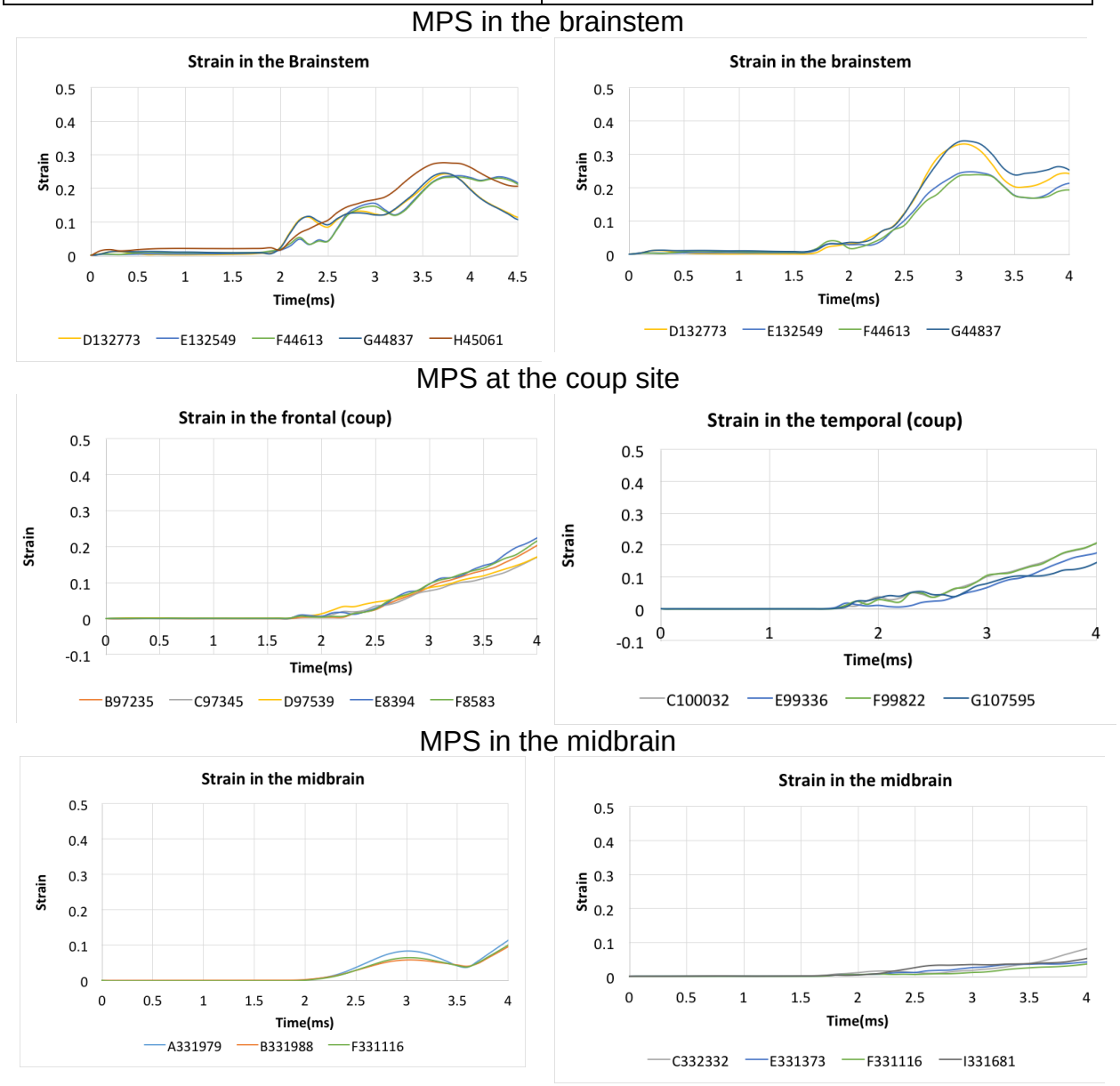

Figure 5: The model-predicted maximum principal strain in the brainstem, coup site and midbrain from a frontal blast (IOP: 440 kPa) and a lateral blast (IOP: 487 kPa)

3. Discussion

Overall, the model-predicted ICP decreased as the pressure wave propagated across the brain and eventually became negative (below atmospheric pressure) at the contrecoup site. The measured ICP data from available cadaver tests did confirm the existence of a pressure gradient which may not be consistent in all tests, partially due

the orientation of the cadaver head to the oncoming wave front direction. This orientation may not be consistent.

The current head model demonstrated a reasonable capability of predicting realistic pressure patterns. The model predicted the coup and contrecoup phenomenon and the predicted peak values were consistent with the ICP sensor recordings in both the lateral and frontal blast. To the best of our knowledge, this is the first time that coup and contrecoup pressures were measured and confirmed in the human cadaver head exposed to open-field blast loadings. The preliminary cadaver data and modeling results are revealing that both blast exposure and blunt impact are capable of inducing coup and contrecoup brain injury when the pressure or associated pressure impulse magnitude exceeds the tissue tolerance level. The preliminary finings will be confirmed when more cadaver test data become available.

The current effort is focused on the understanding of the brain model response pattern and physical process involved in open-field blast simulation. Further work will be done to improve the correlation results with the experimental data when more cadaver test data become available. The improvement to be envisioned include: 1) applying the additional effective mass and/or damping to reduce the oscillation, 2) applying the scaling method to scale the FE head model to match individual cadaver head size to accurately replicate head kinematics and pressure wave propagation, 3) conducting parametric studies of brain material properties on ICP responses and brain strain, 4) verifying that the simulated incident overpressure is comparable to the measured IOP, 5) investigating brain strain rate, pressure rate and other relevant biomechanical response parameters pertinent to blast induced TBI mechanism.

ADDITIONAL STUDIES

Under Task I, we received approval from IACUC of Wayne State University and ACURO of MRMC to add two procedures to our swine testing protocol. One was to monitor the electroencephalographic (EEG) signals from the swine brain pre- and post-blast. The second was to perform MRI scans of the swine brain pre- and post-blast. Both procedures were designed to collect additional information on the effects of primary blast on the brain.

The EEG study resulted in a journal paper which was accepted for publication recently by Brain Injury.

Magnetic Resonance Imaging (MRI) of Swine Brain

The second project involved the magnetic resonance imaging (MRI) of swine brain in an attempt to detect MRI changes after sustaining a blast overpressure exposure. Again, these were the noninstrumented animals used for histological studies and were exposed only once to pressures ranging from 420-450 kPa. The pigs were scanned a

day or so pre-blast and again on the 3rd day post-blast. Two sham pigs were also scanned, but only once.

We have conducted 12 *in vivo* scans using a 3T MRI scanner. This includes 5 pigs which were scanned pre- and post-blast and 2 sham pigs which were each scanned once. The *in vivo* study did not show any significant difference between pre- and post-blast MRI. Specifically, we examined the T2-FLAIR images for potential edema and susceptibility weighted imaging (SWI) images for possible bleeds. No abnormalities were identified.

To further investigate the microstructural white matter injury, which is related to diffuse axonal injury (DAI) or traumatic axonal injury (TAI), high quality (very high-resolution and high signal to noise ratio) diffusion tensor imaging (DTI) needs to be performed. However, due to several factors such as cranial thickness, the large volume of surrounding tissue (skin, fat, and muscles), scan time, and 3T human MRI limitations, we could not collect meaningful DTI images *in vivo* with a decent signal to noise ratio (SNR). Ex-vivo MRI scanning is an option. However, additional funding is necessary to continue this work

DISCUSSION

To the extent possible, we have completed all of our swine blast testing and are making progress on our histological studies of porcine brains. A computer model of the swine brain has been completed and validation is almost complete. For the human brain model, we do not have enough cadaver data for validation, having only done 3 of the 6 scheduled cadaver tests.

There is good histological evidence that the porcine brain sustained injury as a result of the primary open field blasts, particularly at high pressures. The various manifestations of axonal and neuronal injuries need to be studied further in order to determine the reasons for the observed changes. Perhaps, direct observation of cellular response to blast needs to be made to ascertain the mechanisms of injury. We have in mind the construction of a shock tube that can apply a blast wave to a living slice of mouse brain and that will allow observation of the transport of fluorescent molecules across cellular membranes as well as response of subcellular elements to a blast overpressure.

Based on what we know so far, there is injury to the axon as well as to the cell body of the neuron due to blast. The injury mechanism may not be the same as that for blunt impact. That is, in blunt impact, the axons are presumably injured by stretching but since the computed strains in the brain are low due to blast, the observed axonal injury may be due to a dynamic pressure wave. It has long been known that pressure waves can cause concussion but a mechanical explanation of how pressure waves injure brain cells is still unknown. This is another reason for the proposed study to make direct observations of cellular response to a blast wave, as described above.

CONCLUSIONS

1. The porcine brain is susceptible to blast overpressure and sustains both axonal and neuronal cell body injury when the pressure is high enough (above 400 kPa).
2. The measured intracranial pressure (ICP) in the swine brain is generally lower than the incident overpressure (IOP) with the parietal pressures being the highest and almost equal to the IOP.
3. Preliminary data from cadaver testing revealed that the ICP is also lower than the IOP, even with pressurization of the brain with artificial cerebral spinal fluid (CSF).
4. Computer models of the swine and human brain in response to blast have been developed. The predicted ICP was found to be comparable to experimental data in all regions of the brain except in the frontal region where the predicted pressure is larger than that observed experimentally. We exercised the model and found that air in the diploe layer of the skull or between the brain and skull can be the cause for this mismatch.
5. The observed injuries to brain cells require a logical explanation. That is, how does a pressure wave damage cells?
6. Further research involving the observation of cellular response to blast is recommended.

PUBLICATIONS AND PRESENTATIONS

Journal papers

Chen C, Zhou C, Cavanaugh JM, Kallakuri S, Desai A; Zhang L, King AI (2015) Quantitative Electroencephalography in a Swine Model of Blast Induced Brain Injury. Brain Injury. Manuscript accepted for publication by Brain Injury

Zhu F, Chou CC, Yang KH and King AI. On the development of a new biomechanical indicator for primary blast-induced brain injury. Chinese Journal of Traumatology (English Edition), 2015, 10.1016/j.cjtee.2014.10.001.

Zhu F, Chou CC, Yang KH and King AI. A theoretical analysis of stress wave propagation in the head under primary blast loading. Proceedings of the Institution of Mechanical Engineers, Part H, Journal of Engineering in Medicine, 2014, Vol. 228(5) 439–445.

Kallakuri S, Desai A, Mathei J, Dawe E, Feng K, Saif T, Jin X, Chen CY, Zhang L, Cavanaugh JM and King AI. Neuronal injury and glial changes are the hallmark of injury changes following open field blast exposure in the brain- an investigation of swine frontal lobe (*Manuscript in under review by PLOS-ONE)*

Conference papers

Zhu F, Gatti DL and Yang KH. Building a finite element model of axonal microscopic structures. In: Proceedings of WSU 75th Anniversary Symposium Injury Biomechanics, Prevention, Diagnosis & Treatment, August 14-16, 2014, Detroit, MI, USA.

Zhu F, Chou CC, Yang KH and King AI. Analytical modelling of stress wave response in the head under primary blast loading. In: Proceedings of WSU 75th Anniversary Symposium Injury Biomechanics, Prevention, Diagnosis & Treatment, August 14-16, 2014, Detroit, MI, USA.

Kalra A, Zhu F and Yang KH. Key parameters in the blast modeling using 2D to 3D ALE mapping technique. In: Proceedings of 13th International LS-DYNA Users Conference, June 2014, Detroit, MI, USA.

Kalra A, Zhu F, Chen C and Yang KH. A computational modeling of the biomechanical response of pig head under blast loading. In: Proceedings of 17th U.S. National Congress on Theoretical & Applied Mechanics, June, 2014, East Lansing, MI, USA.

Zhang L. Makwana. Biomechanical Responses of Human Head and Headform in Blast Exposure, at the 17th U.S. National Congress on Theoretical and Applied Mechanics, East Lansing, MI, June 16, 2014.

Zhang L, Sharma S, Makwana R, Wang L. Modeling of Brain Responses in Traumatic Blast Exposure. Proceedings of the Wayne State University 75th Anniversary Symposium, August 14th-16th, 2014.

Zhang L, Sharma S. Development and Validation of A Detailed Finite Element Model of Human Eye for Predicting Ocular Trauma. Proceedings of the Wayne State University 75th Anniversary Symposium, August 14th-16th, 2014.

S Kallakuri, A Desai, K Feng CY Chen, T Saif, X Jin, L Zhang, C Zhou, J Mathei, E Dawe, JM Cavanaugh, AI King. Open Field Primary Blast Exposure Induces Changes in Brain-Preliminary Results from Swine Prefrontal Cortex. Wayne State University Department of Biomedical Engineering 75th Anniversary Symposium, Detroit Marriott, August 14th-16th, 2014.

JM Cavanaugh, K. Feng, L. Zhang, S. Kallakuri, C. Chen, A. I. King. Mechanical Response and Brain Injury in Swine Subjected to Free-Field Blast. World Congress of Biomechanics, Boston, Massachusetts, 2014. Podium.

Kallakuri S, Desai A, Mathei J, Dawe E, Feng K, Chen Cy, Cavanaugh JM, Zhang L, King AI: Open field primary blast exposure induces neuronal and glial alterations in frontal cortex. B3-13; 33rd Annual Symposium of the National Neuortrauma Society, Santa Fe, New Mexico, June 28-July1, 2015

Ke Feng, Liying Zhang, Chaoyang Chen, Srinivasu Kallakuri, John M Cavanaugh, Albert I King, "Free Field Blast Induced Mechanical Response, Axonal Injury and Glial Changes in Swine Brain." BMES annual conference, Tampa, Florida October 2015.

Poster Presentations

Ke Feng, Liying Zhang, Chaoyang Chen, Srinivasu Kallakuri, John M Cavanaugh, MD, Albert I King, PhD. Biomechanical Response of swine exposed to open-field blasts. The 2015 Military Health System Research Symposium (MHSRS). August 2015.

Srinivasu Kallakuri, Alok Desai, Janine Mathei, Elizabeth Dawe, Ke Feng, Chaoyang Chen, Liying Zhang, John M Cavanaugh, Albert I King, Open field primary blast exposure induces neuronal and glial alterations in the brain - a preliminary investigation of swine frontal cortex. The 2015 Military Health System Research Symposium (MHSRS). August, 2015.

Feng K, Kallakuri S, Zhang LY, Chen CY, Cavanaugh JM, King AI. Mechanical Response and Brain Injury of Swine Subject to Free-Field Blast. Ohio State University, 2014 http://ibrc.osu.edu/symposium/past-symposiums/2014-symposium/2014-posters-manuscripts/

APPENDICES

Appendix 1 Ke Feng*, Liying Zhang, Xin Jin, Chaoyang Chen, Srinivasu Kallakuri, Tal Saif, John Cavanaugh and Albert King (Under review) Biomechanical responses of swine subjected to free-field blasts. Frontiers in Neurotrauma.

Appendix 2 Srinivas Kallakuri, Alok Desai, Ke Feng, Sharvani Tummala, Tal Saif, Chaoyang Chen, Liying Zhang, John M. Cavanaugh, Albert I. King (Under review) Neuronal injury and glial changes are hallmarks of open field blast exposure in swine frontal lobe

Appendix 3 Test Data from the 3rd Cadaver Test

Appendix I

Biomechanical responses of swine subjected to free-field blasts

Ke Feng*, Liying Zhang, Xin Jin, Chaoyang Chen, Srinivasu Kallakuri, Tal Saif, John Cavanaugh and Albert King

Abstract

Blast-induced traumatic brain injury (bTBI) is a signature wound of modern warfare. The current incomplete understanding of its injury mechanism impedes the development of strategies for effective protection of bTBI. Despite a considerable amount of experimental animal studies focused on the evaluation of brain neurotrauma caused by blast exposure, there is very limited knowledge on the biomechanical responses of the gyrenecephalic brain subjected to primary free-field blast waves imposed *in vivo*. This study aims to evaluate the external and internal mechanical responses of the brain against different levels of blast loading with Yucatan swine in free field. The incident overpressure (IOP) was generated using 3.6 kg of C4 charge placed at three standoff distances from the swine. Five swine were exposed to a total of 19 blasts. The three average peak IOP pressure levels in this study were 148.8, 278.9, and 409.2 kPa as measured by a pencil probe. The duration of the first positive wave was in the range of 2.1 - 3 ms. Pressure changes in the brain and head kinematics were recorded with intracranial pressure (ICP) sensors, linear accelerometers and angular rate sensors. The corresponding average peak ICPs were in the range of 79-143, 210-281, and 311-414 kPa designated as low, medium, and high blast level, respectively. Peak head linear accelerations were in the range of 120-412 g. A positive correlation between IOP and its corresponding biomechanical responses of the brain was also observed. This experimental data can be used to validate computer models of bTBI.

Keywords: free-field blast, head kinematics, traumatic brain injury, swine, intracranial pressure

Introduction

With the increasing use of explosives in modern warfare, exposure to blasts from improvised explosive devices has become the most common cause of injury to our soldiers.[1] The causes of blast-induced injury are usually complicated and can be due to one or more mechanisms.[2] Unlike the other well-studied categories of injury, the mechanisms and injury criteria of primary blast injury that directly result from the transmission of shock waves to the body, are the least well known although the physics of blast waves are well characterized.[3, 4] In the last 70 years, researchers have performed substantial work in this field and have been able to define the biological tolerance levels of the most vulnerable air-filled organs to primary blast such as the ears and lungs.[5-7] These criteria were developed based on the peak overpressure and duration. With the improved design and extensive use of personal protective equipment, mortality rate and severity of injuries level from blast explosives have significantly decreased in recent years. [8] However, there is an increase in mild to moderate close-head traumatic brain injury due to direct transmission of pressure waves into the head.[9] Patients with this type of injury are often found without any physically visible defects or brain damage identifiable by imaging, but show persistent symptoms such as fatigue, headaches, and delayed recall of memory.[10-12] It is still not clear how a blast wave interacts with the head and transfers complex energy through various parts of the cranium to cause brain injury.[13, 14] In order to develop better head protection from blast, the injury mechanisms and injury thresholds related to primary bTBI need to be defined based on the characteristic parameters of the blast wave, mechanical response of the brain and the skull as well as injury to the brain tissue.

Most studies have utilized shock tubes to produce overpressure.[15] The distinct advantages of shock tube are its economical function for repeated tests in laboratories and repeatability of the desired

overpressure by using membranes of the same thickness. However, the overpressure generated in shock tubes is different from a free-field blast wave. The positive duration of the overpressure is longer, and the peak pressure is more prolonged than in free-field blasts.[16, 17] Moreover, the shock tube confines the gas to travel in only one direction, causing non-negligible complex reflections. These characteristics would make the corresponding mechanical responses different from those in free-field blasts, in which test subjects can be exposed to a simple Friedlander wave without interference from reflections. Additionally, blast testing in the open field with proper settings can provide relevant physical parameters of blast conditions similar to those in the battlefield. In the real world, reflections of the shock wave from the ground are inevitable. To minimize the effect of reflected waves, we need to find the "triple point" utilizing appropriate standoff distances and the heights of burst. Due to compression of air and the heat generated, the reflected wave travels faster than the incident wave and eventually overtakes the incident overpressure (IOP) and two shock fronts merge into one. The merged overpressure called the "Mach stem" which travels horizontally on the ground surface. The point where the incident wave, reflected wave and the "Mach stem" meet is called the "triple point." This merged overpressure behaves in the same way as a free shock wave, which has a sudden pressure rise to a positive phase followed by a negative phase.[18]

In the meanwhile, the measurement of shockwave propagation patterns in an *in vivo* brain remains a significant challenge. Much research has been conducted with rats and swine to measure the ICP responses in the brain using shock tubes.[19-23] However, in most of the studies only a few sensors were installed and, in some cases, there was no detailed description of sensor locations.[19, 20, 22] This lack of accurate information constitutes an impediment to a full understanding of how a pressure wave interacts with various parts of the brain. In addition, the brain structures and skull thickness

vary widely between small and large animals. Biomechanical responses of large animals to blast overpressure are expected to be closer to those of the human and thus it would be more appropriate to study them instead of the smaller ones.

On the other hand, computational modeling can help elucidate the comprehensive responses of the head and brain to blast.[24-27] One of the hypotheses is that the scalp may exacerbate the pressure effects in the brain.[24] Others have shown that the skull flexure due to blast is a potential mechanism.[25] The distribution of intracranial pressure (ICP) and the kinetics of the head have been simulated in several models.[26-28] However, experimental data are still needed to validate these models.

With recognition of the limitations in bTBI research, there is a need to develop reliable and more operationally relevant animal models in this field. As a first step to characterize the effects of free-field blast on the head, this study exposed swine to free-field blasts generated by explosives at different IOP levels. Thus, the aim of this study was to provide data on mechanical responses of the swine in primary bTBI. To our knowledge, this would be the first set of published experimental biomechanical data from a large animal subjected to free-field blast overpressure.

Materials and methods

Animal preparation

This research protocol was reviewed and approved by the Institutional Animal Care and Use Committee and the USAMRMC ACURO. Five instrumented Yucatan swine (age 6-8 months, weight 50-60 kg) were exposed to repeated frontal free-field blasts to collect biomechanical data. Before instrumentation, all swine were acclimated for 6-8 days before tests to their new housing conditions. On the test date, the animal was transported in an ambulance to the blast site (ARES, Port Clinton, Ohio) under anesthesia (ketamine 20mg/kg intra muscular and xylazine 2mg/kg intra muscular). The ambulance was equipped with an examination table and equipment for physiological monitoring to ensure maintenance of the proper anesthetic level. Once at the test site, a surgical procedure to install ICP sensors was performed. Blood pressure, oxygen saturation, heart rate and respiratory rate were monitored before and in between blast exposures. During the tests the animal was maintained under anesthesia (propofol 12-20 mg/kg/hr Constant-Rate Infusion). To expose the swine to open field blast, the animal was placed prone in a specially designed canvas sling with holes for the extremities. The sling was supported by a steel body frame which was suspended from a metal I-beam that was 3.7 m off the ground. The I-beam was supported by two, steel A-frames, as shown in Figure 1. The body frame was tied down to the A-frames with straps to prevent excessive motion due to the blast wind. To prevent thoracic injuries from primary blast, the torso was wrapped in a lead sheet that had a density of 39 kg/m^2. A piece of 1.6 cm thick foam padding was placed between of the lead sheet and the animal. The snout of the animals was secured by webbing material to support the head during blast tests.

Free-field blast procedure

3.6 kg of C-4 was packed into a spherical shape to generate blast waves. The height of burst (HOB) was controlled by suspending the C4 from a metal chain and a 2-inch thick metal plate placed under the charge to eliminate debris and assure consistence of the reflected wave. To generate different levels of IOP, the explosive was placed at varying distances from the pig's head. Three levels of IOP were used in this study. Since the goal was to evaluate mechanical responses in non-fatal primary bTBI, the pressure levels were selected based on previous swine studies that were tested using shock tubes.[19, 23] These three pre-determined peak IOP levels were nominally designated as low (150 kPa), medium (300 kPa), and high (400 kPa). To attain a pure Friedlander waveform, the height of the triple point as a function of the horizontal distance from a given charge weight was calculated for a range of HOB.[29, 30] The HOB of the charge was computed to be 0.8 - 0.91 m with the height of the head of the test subject at or less than 0.91 m. The estimated horizontal distances from the charge and the HOB to produce the three different blast pressure levels were further verified by a finite element simulation (ConWep card in LS-Dyna, LSTC, Livermore, CA).

To record the IOP profile during each test, a pencil pressure sensor (137B24B, PCB Piezotronics, Depew, NY,) was placed near the animal at the level of its eyes while two backup pencil sensors were placed at the same height along a circular arc with a radius equal to the desired standoff distance. The sensors were mounted on a metal frame that was bolted to the concrete ground. A total of nine blast tests run at three standoff distances were conducted first to validate and finalize the calculated standoff distances based on the IOP measured from pencil probes. The current communication reports the results from frontal blast tests. Side and rear blasts were also performed but the results will be presented separately.

Instrumentation and data acquisition

Intracranial pressure (ICP) transducers (XCL-072-100A, Kulite, CA) were installed in the in the frontal, occipital, left and right temporal and parietal lobe and at the center of the brain. Holes in the skull were drilled using a drill bit with a stop collar and the transducers were installed and secured with a 1/4-inch diameter threaded copper hollow fitting, equipped with a threaded cap (Dorman, Colmar, PA). A 1/8-inch diameter cannula was inserted into the brain to guide the pressure sensor into place. The vertical distance between the brain surface and the tip of frontal, parietal, temporal, and occipital ICP transducers was 5-7 mm. The depth of the center ICP transducer was 10-12 mm. The diameter of the pressure transducers was 1.9 mm. The three linear accelerometers (7264D-2KTZ-2-360, Meggitt's Endevco, CA) and the three angular rate sensors (ARS-50K-HG, DTS, CA) were fastened to a single aluminum block (ARS HG Triax block, DTS, CA) and installed on top of the skull to monitor the motion of the head. To ensure rigid attachment of the accelerometer block, a 4 × 4-cm of scalp was removed from the posterior of the head to the lambda. Its location is shown in Figure 2 which also shows the approximate locations of the six ICP transducers. The X-axis was defined as the axial direction of the blast, the Y-axis was defined as being perpendicular to the sagittal plane of swine's head, and the Z-axis was normal to the transverse surface of the swine's head at the location of the sensor block. The detailed sensor locations are presented in Table 1. After all the tests were done, the instrumented animal was euthanized at the blast site with an overdose of sodium pentobarbital (120 mg/kg, intraperitoneally). A parallel group of non-instrumented animals also underwent similar blast tests for histological and biomarker studies. Results of these studies are reported separately.

The IOP and the biomechanical responses of the head, including the ICP, head linear acceleration, and head angular velocity were acquired at a sampling rate of 1,000,000 Hz using the DeweSoft

data acquisition system (SIRUS, Dewe Soft LLC.,OH) and DEWETRON data acquisition system (Dewe-3020, DEWETRON Inc. RI). Two high-speed digital camera systems (GX-8, HX-1, NAC Image, MN) were set up to record high-resolution videos of the blast event. One of the cameras was focused on the head of the instrumented swine and ran at 20,000 frames/second (fps). The other camera provided an overall view of the blast wave propagation from the charge to the swine test subject and ran at 10,000 fps. Data acquisition of all the sensors and both cameras were synchronized for each test.

Data processing and analysis

IOP and ICP data were filtered with a 100 kHz and 10 kHz Butterworth low pass filter, respectively. Linear acceleration and angular velocity data were filtered with a 2 kHz Butterworth low pass filter. All post data processing and statistical analysis were performed using DIAdem 2012 software (National Instruments Corporation, Austin, TX) and IBM SPSS Statistics (Version 22.0. Armonk, NY). All data were grouped into three IOP levels according to the recorded IOP by the pencil probe located next to the head of the swine. The duration of the blast wave was defined as the time the IOP stayed above ambient pressure and, was determined using Diadem. IOP impulse was defined as the area of the positive phase of the IOP wave and was obtained through integration. Peak ICP values were determined for each blast for statistical analysis. Linear regression models were constructed to predict the relative relationship between ICP readings within groups. ICP Box plots were drawn to show the distribution of pressure within each group. Paired t-tests were performed between IOP and ICP at each location in the same blast level. One-way analysis of variance (ANOVA) tests were performed to compare the mean peak ICP readings between various locations at the same blast level and the peak ICP readings at the same location

in different blast levels. Average Peak ICP readings for each test were correlated with their peak IOP values.

The peak resultant acceleration was calculated based on the data measured by the three accelerometers. Similarly, the resultant angular velocity was calculated from results acquired by the three angular rate sensors. Linear regression models were used to describe the relationship between the peak resultant acceleration, peak resultant angular velocity and the peak IOP. One-way ANOVA test of peak resultant acceleration was performed between low, medium, and high blast levels. No data at high blast level was collected due to sensor cable failure and signal anomalies. Independent t-tests were performed to compare the resultant angular velocities between the low and medium pressure levels.

Results

Intracranial Pressure response

The results of a total of 19 frontal blasts are reported in this study, using five swine. Plots of a typical set of IOP and ICP curves are shown in Figure 3. The peak IOP, duration, and IOP impulse of each test are summarized in Table 2. In our study, peak IOPs ranged from 143 to 461 kPa. The impulses ranged from 156 to 239 Pa-s. The test results were then divided into three pressure level groups based on the IOP results (Table 3). The average peak IOP values were 149, 279, and 409 kPa for the low, medium, and high blast levels tested. The average peak ICP at various locations of the brain were in the range of 79-144 kPa at the low blast level, 209-282 kPa at the medium blast level, and 312-415 kPa at the high blast level.

Scatter plots show that peak ICPs increased with peak IOP at every instrumented location (Figure 4). More specifically, ICP peak values correlated well with peak IOP in all the three blast pressure

levels using linear regression models. The overall ICP responses were close or lower than its IOP at each blast level. At the low blast level, peak ICP responses of occipital and center regions were significantly lower than the peak IOPs (paired *t-test, $p < 0.05$*), with no significant differences in other regions of the brain (paired *t-test*, $p > 0.05$). At the medium blast level, no significant difference was found between peak ICP responses and peak IOP (paired *t-test, $p > 0.05$*). At the high blast level, peak ICPs were not significantly different from the peak IOPs (paired *t-test, $p > 0.05$*), except that in the center regions where the peak ICPs were significantly lower compared with the peak IOPs (paired *t-test, $p < 0.05$*) (Figure 5). There was no statistically significance difference in peak ICPs between various locations at the low, medium and high levels (ANOVA, *$p > 0.05$*). The frontal ICP at the low blast level was significantly lower than that at the medium and the high blast level (ANOVA, PostHoc LSD, *$p < 0.05$*). However, there was no significant difference of the peak frontal ICPs between the medium and the high blast level (ANOVA, PostHoc LSD, *$p > 0.05$*). Similarly, the occipital ICP at low blast level was lower than that at the medium and the high blast level (ANOVA, PostHoc LSD, *$p < 0.05$*). No significant difference was found with the occipital ICPs between the medium and high blast level (ANOVA, PostHoc LSD, *$p > 0.05$*). The peak center ICP values at the medium and the high blast level were both significantly higher than that at the low blast level (ANOVA, PostHoc LSD, *$p < 0.05$*). Statistical analysis also showed significant differences of the peak ICP between the medium and the high blast levels (ANOVA, PostHoc LSD, *$p < 0.05$*) (Figure 6). Average peak ICP peak values in each test correlated well with peak IOPs (Figure 7).

Head kinematics

In this study, we characterized the head motion with its linear acceleration and angular velocity. Typical time histories of the three linear accelerometers and the three angular rate sensors are

shown in Figure 8A and 8B respectively. The resultant linear accelerations and the resultant angular velocities increased linearly with IOP (Figure 9A and 9B). The resultant accelerations at high blast levels were significantly higher than that at low and medium blast levels (ANOVA, PostHoc LSD, $p < 0.05$), but there was no statistical significance between the low and the medium blast levels (ANOVA, PostHoc LSD, $p > 0.05$). The resultant angular velocity at the medium blast level was significantly higher than that at the low blast level (independent *t-test*, $p < 0.05$). The durations of the linear acceleration were typically less than 3 ms, indicating that there was little translational movement of the head during primary blast.

Discussion

Animals are commonly used to study traumatic brain injury (TBI).[2, 31] In this study, we chose Yucatan pigs as the body mass and skull thickness are closer to those of the human. Also, with a larger body size, biological tolerance level of air-filled organs to blast is believed to be higher.

This study exposed live swine subjects to free-field blast loading at various pressures and durations by changing the standoff distance between the charge and the swine. Of the five swine tested, two expired just before the blast testing, and one died during the tests. This resulted in 8 of the 19 blasts being performed on expired animals. However, the ICP responses showed little difference between expired animals and live animals. The potential causes of death could be related to complications from anesthesia and surgical procedure to insert ICP sensors. Additionally, the parallel group of non-instrumented animals was subjected to medium and high blast overpressure at the same blast test condition. Observation of the brain harvested after perfusion performed after 3 days of survival showed no gross injury. Preliminary histological results from the frontal sections of the blast

showed evidence of neuronal injury in the form of beta amyloid precursor protein immunoreactive zones in the gray and white matter from both blast exposure groups as compared to sham. Neuronal injury was also supported by neurofilament light chain immunohistochemistry. Furthermore, an obvious increase in the number of astrocytes and microglia was also observed in the blast exposed sections compared to sham sections. Based on our knowledge of blast physics, the blast wave produces highly variable pressures both spatially and temporally [32] To fulfill this goal of defining mechanical response of the brain to blast, we analyzed the ICP in different regions of the brain at various blast IOP levels. All previous studies have addressed the mechanical responses of the brain to blast with post-mortem human subjects (PMHS),[33] rats,[20, 22, 34-36] and swine [19, 23, 37, 38] models using compressed-gas shock tubes in a laboratory environment or enclosed space. Although some of these models provided crucial information on the correlation between IOP levels and injury responses, challenges with shock tube tests still exist, including animal positioning, orientation, and interpretation of the effect of the relatively longer duration of the blast.[39] One previous animal model placed the animal head right outside of shock tube.[23]It brought dramatic changes to the IOP characteristics including the formation of a strong vortex flow and elevated dynamic blast pressure and impulse, which deviated significantly from the free-field blast scenario. Data from rat blast models tested in shock tubes recorded positive phase durations in the range of 4-18 ms,[20, 22, 34, 36] which would render the equivalent human duration much longer than that of a free field blast. Hence, shock tube test results need to be carefully investigated and compared with free-field explosive detonations. In this study, all experiments were performed in an open field blast environment. To minimize multiple waveforms from ground reflections, we placed the animal below the triple point and exposed it to the Mach stem.[4] The IOPs were typical free-field Friedlander blast waves in the Mach stem region based on our analysis of the IOP data.

This study provided detailed ICP response in the swine brain subjected to free-field blasts. Historically, some animal tests have been designed and carried out in an attempt to investigate the mechanism of shock wave transmission to the brain, but only a few animal studies recorded direct pressure within the brain tissue during exposure to blast.[20, 22, 23, 38] In our study, the results have demonstrated that ICP followed a trend of increasing magnitude with increased blast severity.

The relationship between ICP and IOP has been determined in several animal blast studies. We showed that, at different locations in the brain, peak ICP values were close to or lower than the IOP. One similar observation was made by another group investigating the mechanical response of the swine brain subjected to left-sided blasts in a shock tube.[23]The peak IOPs ranged from 110 to 740 kPa with scaled durations from 1.3 to 6.9 ms. ICPs ranged from 80 to 390 kPa and were lower than the IOPs and notably lower than the reflected pressures of 300-2830 kPa. Another swine study by Bauman [19] was performed in both a shock tube and in a simulated building with frontal blasts.[19] The recorded IOP data showed that the test animal was exposed to multiple shock waveforms. Fiber-optic pressure transducers were used to record pressure from within the forebrain, thalamus, and hindbrain of the swine without specifying details related to the locations of transducers. The ICP results showed that for IOP levels of 100-250 kPa, the peak ICP values at the three locations were lower than the IOPs.[38]

In addition to the use of swine, smaller animals like rats have also been used. In a rat study, an optic fiber pressure sensor was used to record shock tube generated ICPs. The animals were exposed to a low level blasts of about 40 kPa and the recorded peak ICPs were close to but lower than the IOP in both the frontal and lateral regions of the brain.[20] However, this study only used one ICP sensor in each test, and the results of the study were not statistically analyzed. There were also some discrepancies between findings in the peak ICP values compared to the peak IOP values

in rat models. Leonardi et al. reported that peak ICPs in rats were larger than the peak IOPs and suggested that skull flexure due to an immature skull suture could be the source of the pressure increase.[22]One recent study with cadaver rats also showed a higher peak ICP compared to the peak IOP values at different IOP levels.[40]However, the location of the ICP sensor in the brain was not described, and the torso was not properly shielded from the shockwave. Also, the impulse produced in this study was in the range of 165- 497 Pa-s, larger than what we used in this study (160-240 Pa-s).

Blast studies have also been performed on PMHS. In one PMHS study, using a shock tube, four fiber optic sensors were implanted in the right frontal cortex, right lateral ventricle, right parietal lobe and right occipital lobe with the respective depths of the tip of the sensors from the outer surface of the skull being 30, 30, 65, and 30 mm.[33] At each IOP level, the peak ICP values in the frontal lobe were higher than its peak IOP value. This observation was not seen at other locations of the brain. Also, most of the computer models indicated higher peak ICP compared with IOP readings.[13, 27, 38, 41-43]

The discrepancy between measured and model predicted ICP and IOP readings could be due to several causes. One would be the highly nonlinear relationship between ICP at various locations and the IOP wave.[38] Due to the impedance mismatch between the skull and the brain, ICP peak values tend to be higher at the boundaries and lower in the central region.[44] With respect to the location of transducers, computer models can precisely pinpoint the coup and countercoup regions of the brain. The location of the ICP sensors in animal experiments was limited by surgical techniques. The depths of sensors below the skull in all experimental tests were different or not described in detail. Therefore, the ICP readings vary in the published literature as described above. Another reason for ICP differences seen in rats and pig is possibly due to the morphological

differences between species. Compared to rats, pigs have a much thicker skull with a complex diploe layer that is full of voids. Computer models, on the other hand, may have oversimplified the skull and yielded predictions that did not match experimental data.

Both linear and angular motions of the head were acquired in our tests. The arrival of the ICP wave is almost simultaneous with head motion. Thus the motion is due to the primary blast wave (Figure 10). However, the duration of the motion is relatively short (1-2 ms), which resulted in the maximum head displacement around 2 ms. Similar observations were made by Shridharani et al. also using swine subjects.[23] They found strong correlations (R^2 = 0.9) between peak resultant acceleration and peak IOP in the range of 110 to 740 kPa in a linear model. Their positive phase duration was around 3 ms, and the maximum head displacement was 7.5 mm. Thus, the observed acceleration in these two studies was likely due to the primary shock wave. Well after the passage of the shock wave, we observed inertial global head movement but the head acceleration due to the blast wind or tertiary blast was not significant compared to the initial acceleration due to the primary shock wave.

Conclusions

The data reported here were acquired from live, anesthetized swine exposed to primary blast waves. This is the first large animal model exposed to free-field blasts in which detailed internal pressure measurements were made at various locations. Head motion due to primary blast waves was also measured. The mechanical responses of swine need to be scaled to the human head to determine human response. However, due to the morphological differences between the two species, scaling laws can be difficult to develop. Also, the limited sample size should also be taken into consideration. Due to time limitations to complete nine blast tests on a single animal in 8 hours and failure of the data acquisition system on one occasion, data were available from 19 tests on 5

animals. Additional testing of more animals should improve the statistical significance of the results.

In summary, the results of this study provided a set of detailed biomechanical response data of swine skull and brain during exposure to primary blast waves, with the peak IOPs ranging from 143 to 461 kPa, and the impulses ranging from 156 to 239 Pa-s. The overall ICP responses were close or lower than its IOP at each blast level. More specifically, peak ICP values at the frontal, parietal, and temporal were statistically the same as its IOP values. Peak ICP values at the frontal, central, and occipital regions were significantly elevated at the medium and high blast levels compared with the low blast levels. Furthermore, only at central location, was the ICP significantly different between the medium and high pressures tests. Both the linear acceleration and the angular velocity increased with blast levels. Although the head acceleration was high, its duration was less than 2 ms. It is unlikely that the brain would be able to respond to this type of acceleration input. The experimental data can be used to validate computer models.

Acknowledgment

This research was supported by MRMC Contract No. W81XWH-12-2-0038, US Army. The views, opinions and/or findings contained in this paper are those of the author(s) and should not be construed as an official Department of the Army position, policy or decision unless so designated by other documentation. This study was conducted with assistance from WSU Veterinary Surgical Services, Team Wendy LLC and ARES, Inc. We thank Alok Desai, Haonan Fan, and Chengpeng Zhou for their technical support.

References

1. Warden, D.L. and French, L. (2005). Traumatic brain injury in the war zone. The New England journal of medicine 353, 633-634.
2. Risling, M. and Davidsson, J. (2012). Experimental animal models for studies on the mechanisms of blast-induced neurotrauma. Frontiers in neurology 3, 30.
3. Nakagawa, A., Manley, G.T., Gean, A.D., Ohtani, K., Armonda, R., Tsukamoto, A., Yamamoto, H., Takayama, K. and Tominaga, T. (2011). Mechanisms of primary blast-induced traumatic brain injury: insights from shock-wave research. Journal of neurotrauma 28, 1101-1119.
4. Bass, C.R., Panzer, M.B., Rafaels, K.A., Wood, G., Shridharani, J. and Capehart, B. (2012). Brain injuries from blast. Annals of biomedical engineering 40, 185-202.
5. Richmond, D.R., Damon, E.G., Bowen, I.G., Fletcher, E.R. and White, C.S. (1967). Air-blast studies with eight species of mammals. Techn Progr Rep DASA 1854. Fission product inhalation project [technical progress report]. Lovelace Foundation for Medical Education and Research, 1-44.
6. Richmond, D.R., Damon, E.G., Fletcher, E.R., Bowen, I.G. and White, C.S. (1967). The relationship between selected blast-wave parameters and the response of mammals exposed to air blast. Techn Progr Rep DASA 1860. Fission product inhalation project [technical progress report]. Lovelace Foundation for Medical Education and Research, 1-36.
7. White, C.S., Bowen, I.G. and Richmond, D.R. (1965). Biological tolerance to air blast and related biomedical criteria. CEX-65.4. CEX [reports]; civil effects exercise. U.S. Atomic Energy Commission, 1-239.
8. Wood, G.W., Panzer, M.B., Shridharani, J.K., Matthews, K.A., Capehart, B.P., Myers, B.S. and Bass, C.R. (2013). Attenuation of blast pressure behind ballistic protective vests. Injury prevention : journal of the International Society for Child and Adolescent Injury Prevention 19, 19-25.

9. Kennedy, J.E., Jaffee, M.S., Leskin, G.A., Stokes, J.W., Leal, F.O. and Fitzpatrick, P.J. (2007). Posttraumatic stress disorder and posttraumatic stress disorder-like symptoms and mild traumatic brain injury. Journal of rehabilitation research and development 44, 895-920.
10. Heltemes, K.J., Holbrook, T.L., Macgregor, A.J. and Galarneau, M.R. (2012). Blast-related mild traumatic brain injury is associated with a decline in self-rated health amongst US military personnel. Injury 43, 1990-1995.
11. Elder, G.A. and Cristian, A. (2009). Blast-related mild traumatic brain injury: mechanisms of injury and impact on clinical care. The Mount Sinai journal of medicine, New York 76, 111-118.
12. Gupta, R.K. and Przekwas, A. (2013). Mathematical Models of Blast-Induced TBI: Current Status, Challenges, and Prospects. Frontiers in neurology 4, 59.
13. Zhang, L., Makwana, R. and Sharma, S. (2013). Brain response to primary blast wave using validated finite element models of human head and advanced combat helmet. Frontiers in neurology 4, 88.
14. Przekwas, A., Tan, X., Harrand, V., Reeves, D., Chen, Z., Sedberry, K. and Chancey, V. (2011). Integrated experimental and computational framework for the development and validation of blast wave brain biomechanics and helmet protection. In: *Proc. HFM-207 NATO Symposium on a Survey of Blast Injury Across the Full Landscape of Military Science*.
15. Rafaels, K.A., Bass, C.R., Panzer, M.B., Salzar, R.S., Woods, W.A., Feldman, S.H., Walilko, T., Kent, R.W., Capehart, B.P., Foster, J.B., Derkunt, B. and Toman, A. (2012). Brain injury risk from primary blast. The journal of trauma and acute care surgery 73, 895-901.
16. Reneer, D.V., Hisel, R.D., Hoffman, J.M., Kryscio, R.J., Lusk, B.T. and Geddes, J.W. (2011). A multi-mode shock tube for investigation of blast-induced traumatic brain injury. Journal of neurotrauma 28, 95-104.
17. Sundaramurthy, A. and Chandra, N. (2014). A parametric approach to shape field-relevant blast wave profiles in compressed-gas-driven shock tube. Frontiers in neurology 5, 253.
18. Ben-Dor, G. (2007). Shock wave reflection phenomena. Vol 2. Springer.
19. Bauman, R.A., Ling, G., Tong, L., Januszkiewicz, A., Agoston, D., Delanerolle, N., Kim, Y., Ritzel, D., Bell, R., Ecklund, J., Armonda, R., Bandak, F. and Parks, S. (2009). An introductory characterization of a combat-casualty-care relevant swine model of closed head injury resulting from exposure to explosive blast. Journal of neurotrauma 26, 841-860.
20. Chavko, M., Koller, W.A., Prusaczyk, W.K. and McCarron, R.M. (2007). Measurement of blast wave by a miniature fiber optic pressure transducer in the rat brain. J Neurosci Methods 159, 277-281.
21. Long, J.B., Bentley, T.L., Wessner, K.A., Cerone, C., Sweeney, S. and Bauman, R.A. (2009). Blast overpressure in rats: recreating a battlefield injury in the laboratory. Journal of neurotrauma 26, 827-840.
22. Leonardi, A.D., Bir, C.A., Ritzel, D.V. and VandeVord, P.J. (2011). Intracranial pressure increases during exposure to a shock wave. Journal of neurotrauma 28, 85-94.
23. Shridharani, J.K., Wood, G.W., Panzer, M.B., Capehart, B.P., Nyein, M.K., Radovitzky, R.A. and Bass, C.R. (2012). Porcine head response to blast. Frontiers in neurology 3, 70.
24. Nyein, M.K., Jason, A.M., Yu, L., Pita, C.M., Joannopoulos, J.D., Moore, D.F. and Radovitzky, R.A. (2010). In silico investigation of intracranial blast mitigation with relevance to military traumatic brain injury. Proceedings of the National Academy of Sciences of the United States of America 107, 20703-20708.
25. Moss, W.C., King, M.J. and Blackman, E.G. (2009). Skull flexure from blast waves: a mechanism for brain injury with implications for helmet design. Physical review letters 103, 108702.
26. Lockhart, P., Cronin, D., Williams, K. and Ouellet, S. (2011). Investigation of head response to blast loading. The Journal of trauma 70, E29-36.
27. Chafi, M.S., Karami, G. and Ziejewski, M. (2010). Biomechanical assessment of brain dynamic responses due to blast pressure waves. Annals of biomedical engineering 38, 490-504.
28. Wang, C., Pahk, J.B., Balaban, C.D., Miller, M.C., Wood, A.R. and Vipperman, J.S. (2014). Computational study of human head response to primary blast waves of five levels from three directions. PloS one 9, e113264.

29. De Rosa, M., Fam, F., Palleschi, V.V., Singh, D.P. and Vaselli, M. (1992). Derivation of the critical angle for Mach reflection for strong shock waves. Physical review. A 45, 6130-6132.
30. Ivanov, M.S., Vandromme, D., Fomin, V.M., Kudryavtsev, A.N., Hadjadj, A. and Khotyanovsky, D.V. (2001). Transition between regular and Mach reflection of shock waves: new numerical and experimental results. Shock Waves 11, 199-207.
31. Cernak, I. (2014). Blast-induced neurotrauma models and their requirements. Frontiers in neurology 5, 128.
32. Ngo, T., Mendis, P., Gupta, A. and Ramsay, J. (2007). Blast loading and blast effects on structures–an overview. Electronic Journal of Structural Engineering 7, 76-91.
33. Bir, C. (2011). Measuring blast-related intracranial pressure within the human head. DTIC Document.
34. Huber, B.R., Meabon, J.S., Martin, T.J., Mourad, P.D., Bennett, R., Kraemer, B.C., Cernak, I., Petrie, E.C., Emery, M.J., Swenson, E.R., Mayer, C., Mehic, E., Peskind, E.R. and Cook, D.G. (2013). Blast exposure causes early and persistent aberrant phospho- and cleaved-tau expression in a murine model of mild blast-induced traumatic brain injury. Journal of Alzheimer's disease : JAD 37, 309-323.
35. Gullotti, D.M., Beamer, M., Panzer, M.B., Chen, Y.C., Patel, T.P., Yu, A., Jaumard, N., Winkelstein, B., Bass, C.R., Morrison, B. and Meaney, D.F. (2014). Significant head accelerations can influence immediate neurological impairments in a murine model of blast-induced traumatic brain injury. Journal of biomechanical engineering 136, 091004.
36. Goldstein, L.E., Fisher, A.M., Tagge, C.A., Zhang, X.L., Velisek, L., Sullivan, J.A., Upreti, C., Kracht, J.M., Ericsson, M., Wojnarowicz, M.W., Goletiani, C.J., Maglakelidze, G.M., Casey, N., Moncaster, J.A., Minaeva, O., Moir, R.D., Nowinski, C.J., Stern, R.A., Cantu, R.C., Geiling, J., Blusztajn, J.K., Wolozin, B.L., Ikezu, T., Stein, T.D., Budson, A.E., Kowall, N.W., Chargin, D., Sharon, A., Saman, S., Hall, G.F., Moss, W.C., Cleveland, R.O., Tanzi, R.E., Stanton, P.K. and McKee, A.C. (2012). Chronic traumatic encephalopathy in blast-exposed military veterans and a blast neurotrauma mouse model. Science translational medicine 4, 134ra160.
37. Saljo, A., Arrhen, F., Bolouri, H., Mayorga, M. and Hamberger, A. (2008). Neuropathology and pressure in the pig brain resulting from low-impulse noise exposure. Journal of neurotrauma 25, 1397-1406.
38. Zhu, F., Skelton, P., Chou, C.C., Mao, H., Yang, K.H. and King, A.I. (2013). Biomechanical responses of a pig head under blast loading: a computational simulation. International journal for numerical methods in biomedical engineering 29, 392-407.
39. Needham, C.E., Ritzel, D., Rule, G.T., Wiri, S. and Young, L. (2015). Blast Testing Issues and TBI: Experimental Models That Lead to Wrong Conclusions. Frontiers in neurology 6, 72.
40. Skotak, M., Wang, F., Alai, A., Holmberg, A., Harris, S., Switzer, R.C. and Chandra, N. (2013). Rat injury model under controlled field-relevant primary blast conditions: acute response to a wide range of peak overpressures. Journal of neurotrauma 30, 1147-1160.
41. Moore, D.F., Jerusalem, A., Nyein, M., Noels, L., Jaffee, M.S. and Radovitzky, R.A. (2009). Computational biology - modeling of primary blast effects on the central nervous system. NeuroImage 47 Suppl 2, T10-20.
42. Zhu, F., Mao, H., Dal Cengio Leonardi, A., Wagner, C., Chou, C., Jin, X., Bir, C., Vandevord, P., Yang, K.H. and King, A.I. (2010). Development of an FE model of the rat head subjected to air shock loading. Stapp car crash journal 54, 211-225.
43. Taylor, P.A. and Ford, C.C. (2009). Simulation of blast-induced early-time intracranial wave physics leading to traumatic brain injury. Journal of biomechanical engineering 131, 061007.
44. Meyers, M.A. (1994). Dynamic behavior of materials. Wiley: New York.

Tables

Table 1. Summary of the location of all sensors.

Sensor	Location
Frontal ICP	2.5 cm anterior to Bregma, 0.5 cm left of midline.
Parietal ICP	At the level of Bregma, 0.5 cm left of midline.
Center ICP	At the level of Bregma, 0.5 cm right of midline.
Left temporal ICP	0.5 cm anterior to Bregma, 1.0 cm left of midline.
Right temporal ICP	0.5 cm anterior to Bregma, 1.0 cm right of midline.
Occipital ICP	1.5 cm posterior to Bregma, 0.5 cm left of midline.
Accelerometer block	2.5 cm posterior to Bregma, on the midline.

Table 2: The summary of IOPs in this study: peak values, duration of the first positive wave and the impulse of the first positive waveform. **** indicates test in which swine had already expired during testing.***

Test ID	Peak Incident Pressure (kPa)	Duration (ms)	Impulse (Pa-s)
*1	150.3	2.8	170.3
*2	142.7	2.9	155.7
3	150.3	2.9	158.3
4	148.2	2.9	160.3
5	152.4	3.1	161.0
6	218.0	2.1	193.9
7	253.4	2.2	195.7
8	255.2	2.0	194.9
9	324.2	2.3	194.1
*10	285.5	2.3	207.7
*11	284.1	2.1	198.1

12	285.4	2.0	196.4
13	325.4	2.0	204.0
14	366.0	1.6	205.4
*15	441.3	1.7	225.2
*16	413.7	1.6	229.6
*17	460.6	1.7	239.2
*18	341.3	2.4	228.8
19	432.3	2.4	222.9

Table 3: IOP peak values vs ICP peak values at low, medium, and high IOP levels

Test	Biomechanical responses , ICP peak values, mean±SE						
	IOP	Frontal	Parietal	Left Temp	Right Temp	Occipital	Center
Low	148.8±1.7	97.6±19.7	144.2±18.0	142.8±0.0	147.9±0.0	78.9±13.4	93.7±17.0
Medium	278.9±13.9	236.5±30.7	276.0±62.4	281.6±35.0	253.1±46.8	209.1±34.5	228.1±29.5
High	409.2±18.9	311.7±29.1	414.6±0.0	386.4±7.1	325.5±8.6	328.2±26.7	327.2±17.0

Figures

Figure 1: Blast experiment test set-up. The photograph on the left shows the anesthetized swine placed in a lead-covered sling hanging from a metal beam which is attached to two A-Frames. The arrow at “A” points to the C4 charge. Arrow B shows the pencil pressure sensor used to record the IOP. Arrow C shows the head of the test animal facing in the direction of the oncoming blast wave front. Arrow D shows the location of high-speed cameras and their shielding. The right photograph shows the swine in a sling anchored to the A-frames and covered with a foam-lined lead shield protecting the torso.

Figure 2: Top view of the location of ICP sensors relative to the skull of the swine

Figure 3: Pencil reading from a medium level blast (A) and the ICP results in the swine brain from the same blast (B). The positive phase duration of the IOP was 2.30 ms, and the impulse of the IOP was 207.7 Pa*s.

Figure 4: Scatter plots of ICP vs IOP at different locations of the brain. The x axis is the IOP and the y axis is the ICP, both in units of kPa. A linear regression model and R^2 values are shown in each plot.

Figure 5: Peak ICP readings for different levels of blast. Peak ICPs in different regions of the brain within each blast level group were not statistically different from each other.

Figure 6: ICP peak values in the frontal, central and occipital regions of the brain showed a significant increase with increasing blast levels. Student's t-tests indicated a significant difference between blast levels. (* $p<0.05$)

Figure 7: Scatter plots of average ICP peak values of different locations at each test IOP.

Figure 8: Sample time-history plots of the acceleration and angular rate measured on the swine head with instrumentation mounted to the skull. The left plot shows linear acceleration (g) in the x, y and z directions. The right plot shows angular velocity (rad/s) in the x, y and z directions.

Figure 9: Scatter plots of the motion of the head, showing the relationship between the peak IOP (abscissa) and the resultant linear acceleration (ordinate, left graph), or the resultant angular velocity (ordinate, right graph). These variables correlated well with the peak IOP in linear regression models.

Figure 10: The relationship between ICP and head motion (resultant linear head acceleration and angular velocity) demonstrated that primary blast imparted a severe acceleration to the head, albeit the duration was very short.

Neuronal Injury and Glial Changes are Hallmarks of Open Field Blast Exposure in Swine Frontal Lobe

Srinivasu Kallakuri*, Alok Desai, Ke Feng, Sharvani Tummala, Tal Saif, Chaoyang Chen, LiYing Zhang, John M Cavanaugh and Albert I King

Department of Biomedical Engineering, Wayne State University, Detroit, Michigan, United States of America

*Corresponding Author:

E-mail: skallakuri@wayne.edu (SK)

Abstract

With the rapid increase in the number of blast induced traumatic brain injuries and associated neuropsychological consequences in veterans returning from the operations in Iraq and Afghanistan, the need to better understand the neuropathological sequelae following exposure to an open field blast exposure is still critical. Although a large body of experimental studies have attempted to address these pathological changes using shock tube models of blast injury, studies directed at understanding changes in a gyrencephalic brain exposed to a true open field blast are limited and thus forms the focus of this study. Anesthetized, male Yucatan swine were subjected to forward facing medium blast overpressure (peak side on overpressure 224-332 kPa; n=7) or high blast overpressure (peak side on overpressure 350-403 kPa; n=5) by detonating 3.6 kg of composition-4 charge. Sham animals (n=5) were subjected to all the conditions without blast exposure. After a 3-day survival period, the brain was harvested and sections from the frontal lobes were processed for histological assessment of neuronal injury and glial reactivity changes. Significant neuronal injury in the form of beta amyloid precursor protein immunoreactive zones in the gray and white matter was observed in the frontal lobe sections from both the blast exposure groups. Neuronal injury was further supported by neurofilament light chain immunohistochemistry. A significant increase in the number of astrocytes and microglia was also observed in the blast exposed sections compared to sham sections. We postulate that the observed acute injury changes may progress to chronic periods after blast and may contribute to short and long-term neuronal degeneration and glial mediated inflammation.

Introduction

Operations Iraqi Freedom (OIF) and Enduring Freedom (OEF) have highlighted the emergence of Blast Induced Neurotrauma (BINT) and the associated mild traumatic brain injury (mTBI) as the signature wound in returning service members [1,2]. Shell shock and post concussive syndrome had a similar prominence during World Wars I and II [3]. With much of these injuries more recently sustained following exposure to an improvised explosive device, basic understanding of the mechanisms and pathological changes in the central nervous system following an open field blast exposure still remains an area of intense research focus. What is still not well studied is whether exposure to primary blast wave causes changes in the gyrencephalic brain. Understanding the pathological changes in the brain following an open field exposure is important considering the complex neurological problems reported in the exposed service members. For example, the history of blast related mTBI has been significantly associated with post traumatic stress disorder (PTSD) and other physical problems in veterans from OIF [4] as well as those from OEF and Operation New Dawn [5,6]. In addition, the number of exposures also appears to be contributing to the neuropsychological sequelae with increased symptom reporting, as revealed by significant Neurobehavioral Symptom Inventory (NSI) scores in veterans with increased blast exposures [7]. There were also reports of abnormal hormonal levels in one or more pituitary axes [8] in those affected by blast mTBI. Visual dysfunction [9,10] and co-occurrence of auditory, visual and vestibular impairment referred to as multisensory impairment (MSI) was also reported [11] in blast victims. In a sample assessment of veterans, a diagnosis of non-epileptic seizures was suspected in 44% of the samples

studied and PTSD was confirmed in 81% of these samples studied. Exposure to blast was considered as the mechanism of the TBI [12] in these samples. In fact, TBI independent of an injury mechanism (blast or non-blast) has been described as a primary driver of adverse outcomes in an analysis of US military personnel [13].

The pathological basis of these blast-induced changes is still not well understood. A diffusion tensor imaging analysis of service members revealed that blast mTBI was associated with a pattern of lower white matter integrity, with a larger number of low fractional anisotropy (FA) voxels in those with more than one blast mTBI than in individuals with a single blast injury [14]. Others, albeit using a limited number of blast exposed soldiers also reported abnormalities consistent with cerebellar white matter injury in 3 of 4 subjects studied using diffusion tensor imaging [15]. Compared to control subjects, veterans with blast mTBI also showed neurometabolic changes with significant reductions in the ratio of N-acetylaspartate to choline (NAA/Ch) and N-acetyl aspartate to creatine (NAA/Cr) in the anterior portions of the hippocampus [16].

With limitations in studying brain pathological changes in the blast victims, several animal models using a shock tube system to simulate blast overpressure exposure have gained prominence. Behaviorally, transient anxiety-like behavior in an open field arena was reported in mice subjected to 172-276 kPa blast overpressure with symptoms becoming prominent in those exposed to 345-414 kPa [17]. In rats exposed to blast waves with peak reflected overpressures of either 100 or 450 kPa (39 or 110 kPa incident pressure respectively), FA revealed significant brain abnormalities as evidenced by greater numbers of significant voxels in animals exposed to high-blast compared to low-blast. The decreased FA was observed prominently in the cortex,

thalamus and ipsilateral ventral hippocampus [18]. In mice exposed to blast overpressure via a shock tube, Huber et al reported elevated phospho and cleaved-tau species in neurons, as well as elevated manganese superoxide-dismutase levels by 24 hours with the aberrant tau species persisting for at least 30 days post-exposure in the hippocampus [19]. Electrophysiolgically, recordings from the corpus callosum of rat brain slices exposed to blast in the range of 28 kPa indicated greater deficits in unmyelinated fibers relative to myelinated fibers. There was a reduced compound action potential amplitude at 14 days post-injury [20]. Mice subjected to open field explosion (35 and 17 kPa), demonstrated behavioral changes with increased blood brain barrier permeability, increased FA and decreased radial diffusivity that correlated with sites of up-regulation of manganese superoxide dismutase 2 in neurons and CXC-motif chemokine receptor 3 around blood vessels in the fiber tracts [21].

Histologically, in rats subjected to sub-lethal open field blast overpressure (49 kPa or 77 kPa), darkened and shrunken cortical neurons were observed one day after blast with signs of recovery by 4 and 7 days after blast [22]. They also reported increased number of cells with amyloid precursor protein staining in the white matter [22] with some reporting multi focal axonal injury in the cerebellum, corticospinal tract and optic tract in mice subjected to a static blast pressure of 68 kPa using a shock tube [23]. Blast induced swollen neurons and myelin debris in the hippocampus [24] and accumulation of phosphorylated neurofilament-heavy chain (pNF-H) in neuronal perikarya of the cortex attributed to a disturbed axonal transport machinery was also reported [25]. Using silver impregnation technique, investigators have also shown axonal pathology in the cortex and cerebellum of swine exposed to blast pressures of

379 or 538 kPa [26] and in deep cerebellar white matter tracts and various brainstem regions of rats with body shielding exposed to a single 241 kPa blast wave [27]. Others showed cytoskeletal damage in the cortex and hippocampus 7 days after blast exposure using neurofilament immunohistochemistry [28]. With the evidence of axonal injury potentially in the form of impaired axoplasmic transport (IAT) in various blast models, it was reasoned that immunostaining for beta amyloid precursor protein (β-APP) and neurofilament light chain, the markers of traumatic axonal injury [29,30] may offer valuable clues on the extent of neuronal injury in the swine brain following blast exposure.

Glial alterations are another key component of blast induced injury changes in the brain [31]. Alterations related to astrocytes in the brain were prominently shown by several investigators using glial fibrillary acidic protein immunohistochemistry [32-37]. Current research also supports profound microglial activation following blast [38-45] in various animal models. However, studies aimed at understanding changes related to axonal injury and glial proliferation and their quantification in a gyrencephalic brain after a primary blast exposure are limited. Thus, the purpose of this study was to assess neuronal and glial reactivity changes in brains from male Yucatan swine subjected to a single open field blast exposure. Our results from analyses of sections encompassing the frontal lobe of the brain show neuronal and glial injury changes in the gray and white matter regions following open field blast exposure.

Materials and Methods

Animal preparation

All procedures were approved by the Institutional Animal Care and Use Committee (IACUC,Wayne State University, Detroit, MI) and the United State Army Medical Research and Materials Command Animal Care and Use Review Office (USAMRMC ACURO). All animals (male Yucatan swine 50-60 kg, Sinclair Bio Resources LLC, Columbia, MO 65205) were allowed to acclimate to their new housing conditions in the animal quarters prior to any test procedure. On the day of the test, each animal was sedated by an initial intramuscular injection of Ketamine (10 mg/kg once) and xylazine (2 mg/kg once) or ketamine (10 mg/kg once), dexmedetomidine 0.04 mg/kg IM and acepromazine 0.1 mg/kg IM in the case of animals subjected to high blast overpressure in the open field blast. Animals subjected to high blast overpressure were also administered buprenorphine sustained release 0.12-0.24 mg/kg (subcutaneous) prior to blast exposure.

Following the initial anesthesia, the animal was intubated and was allowed to breathe spontaneously. Additional ventilatory support was given by an Ambu bag as needed. In animals exposed to medium blast overpressure open blast and sham procedures, anesthesia was maintained by an intravenous infusion of Propofol 12-20 mg/kg. In animals subjected to high blast overpressure, anesthesia was further maintained by intravenous injection of ketamine 5-10 mg/kg/hr and dexmedetomidine 0.005-0.018 mg/kg. Supplemental intra venous (IV) fluids were administered (LRS 5-10 cc/kg/hr IV) via an intravenous catheter placed in an ear vein. All the animals were

transported in an emergency medical services (EMS) vehicle to a test site (Ares Inc. Port Clinton, OH) for open field blast exposure.

Animal preparation

All the blast tests were performed on days with no rain or snow. Open field blast overpressure was generated by detonating 3.6 kg of a spherical composition-4 (C4) charge. To attain a single Friedlander waveform, the height of burst was determined to be 0.8 -0.9 m and was achieved by suspending the C4 from a metal chain. The animal with an abdominal and thoracic lead shielding (39 kg/sq m) was suspended prone in a canvas harness. The harness was further supported by a steel frame which was suspended from a metal beam (3.7 m off the ground) mounted on two A-frames (S1 Fig). The height of the triple point as a function of the horizontal distance from charge was calculated for the given height of the burst. To expose animal's head below the triple point, the animal was suspended 0.9 m above the ground. The snout of the animal also was supported by two webbing straps to minimize head motion. The eye level was at 0.9 m (3 ft) above the ground with the head facing the direction of the wave propagation (S1 Fig). After proper alignment of the head with respect to the center of the C4 charge, the steel frame was further tied to four hooks cemented to the concrete ground with straps to prevent excessive motion during the blast exposure.

The intensity of the two blast exposures (medium versus high) was achieved by changing the stand-off distance between the animal's head and the center of the C4 charge (Table 1). The actual side-on overpressure was measured by a pencil probe (PCB137A24, PCB Piezotronics, Depew, New York 14043) mounted on a metal

frame that was bolted to the ground and placed next to the animal's head at the same height (0.9 m). The overpressure data was acquired at a sampling rate of 1 MHz using the SIRIUS HS-ACC MODULE (DEWESoft, Slovenia). Blast animals were divided into two groups that were exposed either to a single medium blast overpressure (stand-off distance = 3.6 m, n=7) or high blast overpressure (stand-off distance = 3.1 m, n=5; S1 Fig). Sham animals (n=5) were exposed to identical test conditions but were not subjected to blast exposure.

Stable heart rate with no jaw tone, palpebral reflex, and limb withdrawal reflex were used as indicators of adequate depth of anesthesia. Immediately before/during/after blast, SpO2 and heart rate were monitored by pulse oximetry. Body temperature was monitored continuously by a rectal thermometer. At lower ambient temperatures, supplemental heat (water circulating heating pad or Thermacare Heat Wraps) was provided to maintain body temperature.

Sham	**Medium Blast Overpressure**	**High Blast Overpressure**
Swine 1	Swine1: 223.5 kPa	Swine1: 359.9 kPa
Swine 2	Swine 2: 332.3 kPa	Swine 2: 359.9 kPa
Swine 3	Swine 3: 305.4 kPa	Swine 3: 403.3 kPa
Swine 4	Swine 4: 222 kPa	Swine 4: 403.3 kPa
Swine 5	Swine 5: 262.7 kPa	Swine 5: 350.3 kPa
	Swine 6: no data	
	Swine 7: 290.3 kPa	

Table 1 shows the number of animals studied for each group and the recorded open field blast overpressure.

Brain tissue processing

All animals were allowed to survive for 3 days after blast or sham procedures. At the end of their survival period, each animal was first injected with Heparin followed by an overdose of sodium pentobarbital and prepared for transcardial perfusion by 4% paraformaldehyde. After ensuring that there was no noxious and palpebral response, the animal was placed supine on a surgical table. The left and right common carotid arteries were exposed and traced inferiorly to the point of their origin in the aortic arch and the connector end of an intravenous tube was inserted into the right common carotid artery and was secured in place by a suture. Each animal was perfused first with 1 liter of saline followed by 8-10 liters of 4% paraformaldehyde. The venous return was collected from the right atrium by a suction pump. The perfusion of lower body was minimized by clamping the aorta just inferior to the heart. Following perfusion, the brain was removed and post-fixed in 4% paraformaldehyde with 20% sucrose until processing for immunohistochemical analyses.

Each harvested brain was cut into 5 mm blocks using a swine brain slicer (Zivic Instruments, Pittsburgh, PA 15237). Each block was then further cut into 35-40 μm thick serial sections (S2 Fig). A total of twenty-four pairs of sections from each of the six blocks were collected in phosphate buffered saline-filled 2 ml vials and stored at 4^{o}C. Then some of the designated sections were probed by various stains to assess cellular injury changes. For each stain, two sections from each block were used. Briefly, the sections were subjected to antigen retrieval by incubation in a citrate buffer (pH 6.0) at 90^{o}C for 1 hour. Then they were immersed for 1 hour in 0.6% hydrogen peroxide to quench endogenous peroxidase activity.

For assessing axonal injury changes, individual sections were subjected to incubation in antibodies against beta amyloid precursor protein (β-APP; 1:250, Cat # 51-2700, Life Technologies, Grand Island, NY), neurofilament light chain (NF-L; 1:5000, Cat#AB9568; Millipore, Temecula CA) or neurofilament-medium chain (NF-M; 1:750; cat # 34-1000, Invitrogen, Camarillo, CA, 1:750). For assessing astrocytic changes, a set of representative sections were incubated in a solution containing antibodies against glial fibrillary acidic protein (GFAP for identifying astrocytes, cat # NE1015, Calbiochem, La Jolla, CA; 1:5000). Microglial activation was detected by incubating a separate set of sections in a solution containing antibodies against ionized calcium-binding adapter molecule 1 (Iba1, cat # 019-19741, Wako Chemicals, Richmond, VA; 1:20000). All the antibody solutions were diluted in 2% normal goat serum (Vector Laboratories, Burlingame, CA) mixed in 1% bovine serum albumin (BSA). After respective primary antibody incubation, sections were incubated in a solution containing a 1:500 dilution of respective biotinylated secondary antibody (Vector Laboratories, Burlingame, CA) followed by exposure to Vectastain Elite ABC reagent. Finally, the peroxidase activity was developed by brief incubation in 3, 3'-diaminobenzidine and hydrogen peroxide. The sections were washed, dehydrated and cover slipped using DPX (Sigma Aldrich). In control incubations, normal goat serum was substituted for primary antibody.

Quantification of β-APP immunoreactivity

The presence of neuronal injury as evidenced by β-APP reactive zones was quantified from one section of each block from sham (n= 5 animals x 6 sections per animal = 30 total sections), medium blast overpressure (n=7 animals x 6 sections per animal = 42

total sections) and high blast overpressure (n= 5 animals x 6 sections = 30 total sections) groups. In the gray matter, an immunoreactive zone was defined as the region encompassing intense β-APP-reactive cell bodies that was observed in various cortical layers including the molecular layer. In the white matter, immunoreactive zones were defined as aggregates of intense β-APP-reactive axon-like processes, individual retraction balls, axonal swellings or intensely stained stellate-like cells. For quantification, each section (encompassing the entire left and right hemispheres) was viewed under a light microscope (Leica DMLB, Leica Microsystems Ltd, Heerburg, Switzerland) at 50x magnification defined as the high power field. The presence or absence of β-APP immunoreactive zones in these high power fields was investigated by a blinded investigator and the total number of immunoreactive zones for each section was recorded.

Quantification of astrocytic and microglial reactivity

Quantification of astrocytes and microglia was performed using separate sets of sections stained for GFAP and Iba1 respectively. For astrocytic quantification in a blinded fashion in blast and sham groups, a x5 composite panoramic image from two sections each per block (sham n= 60 sections; medium blast overpressure n= 84 sections; high blast overpressure n= 60 sections) was taken using OASIS software (Objective Imaging Inc, Kansasville, WI 53139). These panoramic images were then used as a guide to obtain a series of five x100 images per hemisphere, which in turn were used for counting the number of astrocytes. As the GFAP staining was predominantly found in the white matter tracts, representative images spaced

approximately 5 mm apart encompassing the white matter regions were obtained. Then, the number of astrocytes in each such image (10 images per section; 120 images for six blocks per animal resulting in a total of 2040 images for all the 17 animals).

For quantifying microglia in blast and sham groups another x5 composite panoramic image from two sections each per block per stain (sham n= 60 sections; medium blast overpressure n= 84 sections; high blast overpressure n= 60 sections) was taken using OASIS software (Objective Imaging Inc, Kansasville, WI 53139). However, as microglia were observed in both the white and gray matter regions, using the x5 panoramic images as a guide, another set of five representative images at x100 magnification encompassing areas of both the white and gray matter were taken per hemisphere. This resulted in a total of another (10 images per section; 120 images for six blocks per animal) 2040 images for all the 17 animals for counting microglia. The number of astrocytes and microglia were quantified independently from their respective images using ImageJ. Each image was inverted using the invert option which results in a reverse image similar to the negative of a photograph and enables better delineation of cells of interest from their background.

The average number of axonal injury counts, astrocytes and microglia per group was calculated and compared statistically for group-wise differences using Statistical Package for the Social Sciences (SPSS, IBM) software. One-way analysis of variance (ANOVA) was used for comparisons across study groups. Post hoc LSD tests were used for pair-wise comparisons as appropriate. A probability level of $p < 0.05$ was considered statistically significant.

Serum analyses for injury markers

Besides collecting the brain for histological analyses, serum samples were collected before and at 6 hours, 24 hours, 48 hours and 72 hours after the blast or sham procedures. These samples were assessed for temporal changes in the expression of phosphorylated neurofilament heavy chain (pNF-H Elisa Kit, Encor Biotechnology, Gainesville, FL), glial fibrillary acidic protein (GFAP; cat#NS830, EMD Millipore, Billerica, MA) and interleukin-6 (IL-6; cat# ESIL6, Life Technologies, Carlsbad, CA) by enzyme-linked immunosorbent assay (ELISA) as per the manufacturer's instructions. The ELISA data were analyzed by generalized estimating equations (GEE) with an exchangeable correlation structure and robust standard errors. Baseline biomarker data were entered as a covariate to address possible baseline imbalance.

Results

Axonal injury: β-APP immunohistochemistry

Our investigation revealed more prominent β-APP immunoreactive zones in the open field blast exposure group than in the sham group (Fig 1A). Sections from both the high and medium blast overpressure groups showed a significantly higher number of immunoreactive zones ($p<0.05$) compared to those from the sham group. In addition, the number of immunoreactive zones in the high blast overpressure group were significantly higher than those in the medium blast overpressure group ($p<0.05$). One striking observation was the presence of patches of β-APP reactive zones both in the white and gray matter. Immunoreactive zones in the gray matter were observed in various cortical layers characterized by 1-3 intensely stained cell bodies with plaque-like deposits with extended processes of the cell bodies. These immunoreactive zones were also observed in the sub-pial regions of the cortex (Fig 1B). The immunoreactive zones in the white matter were associated with stellate-like cells with their dark stained processes surrounded by retraction balls and axons showing signs of swellings (Fig 1C). Other components of β-APP immunoreactive zones in the white matter regions were the presence of axons undergoing pathological changes. These pathological changes were in the form of single or multiple axonal swellings, swollen axons with terminal retraction balls and retraction balls with or without tail-like profiles (Fig 1D and 1E). These axonal injury profiles were particularly predominant in the sub-cortical coronal radiations ending in various sulci, more so in the dorsal aspect of the cerebral hemispheres. Other areas that also showed injured axons were internal capsule, white matter bundles of the striatum, and white matter fibers near the vomiro nasal organ.

Occasionally, axonal injury was also observed in the periventricular white matter tracts and corpus callosum.

Axonal injury: NF-L and NF-M immunohistochemistry

Axonal injury was also assessed by neurofilament light chain immunoreactivity. In brain sections from swine exposed to medium and high blast overpressure, many NF-L reactive axons with uniform caliber and well-stained axonal core were observed. However, some large caliber axons with altered morphology were also observed (Fig 2A-C). These axons tended to have membrane boundaries that appeared to be disrupted in the form of semilunar empty space or occasionally with filamentous projections originating from their membranes. Besides, some of the large caliber axons appeared to be swollen and at times with the presence of vacuoles in their axonal core. In addition, some axons with terminal retraction bulbs appearing as clubs were also observed. The location of these observed changes was predominantly in the sub-cortical white matter tracts. In the corpus callosum, no such prominent observations could be made considering the predominant nature of small fiber axons in its population. Qualitatively, in sections from sham animals, NF-L reactive axons running for extended lengths in the white matter tracts were observed. These axons appeared to have uniform caliber with well stained NF-L reactive core (Fig 2D). Axonal injury changes assessed by NF-M immunohistochemistry revealed putative RMO14 immunoreactive axons that appeared to be linear with occasional swollen regions (arrow) and vacuolations (Fig 3).

Astrocytic reactivity changes

In all the sections from the six blocks of the frontal lobes, the astrocytes were almost exclusively localized to the white matter tracts highlighting them as distinct pathways (Fig 4) and thus images were exclusively obtained from the white matter tracts for the purpose of quantification. Although astrocytes in other areas of the cortex and sub-pial regions were observed they were less prominent than in white matter tracts. Quantification of images revealed a significantly high number ($p<0.05$) of GFAP reactive astrocytes (Fig 5A histogram) in sections from both the medium and high blast overpressure blast groups compared to those from sham (Fig 5B). Furthermore, astrocyte counts in sections from high blast overpressure group were also significantly high compared to those from medium blast overpressure (*$p<0.05$)*. Astrocytes in the blast group tended to be intensely stained by GFAP with numerous processes (Fig 5C and 5D). In addition, astrocytes in the blast groups appeared to undergo morphological changes with enlarged cell bodies (Fig 5D; S3 Fig).

Microglial reactivity changes

In the case of microglia, they were observed throughout the layers of the cortex, sub cortical white matter tracts and other structures with no specific distribution pattern. The number of microglia in both the blast groups was higher than in sections from sham group ($p<0.05$*;* Fig 6A). Unlike astrocytes, the microglial counts in the medium blast overpressure blast group were significantly higher than in the high blast overpressure group (*$p<0.05$)*. Compared to sham (Fig 6B), microglia in the blast group (Fig 6C and 6D) tended to be more oval in shape with limited number of processes.

Serum biomarker changes

ELISA data from the three markers was compared for statistical significance using generalized estimating equations. Baseline biomarker data were entered as a covariate to address possible baseline imbalance. Of the three biomarkers analyzed, there was some evidence of higher glial fibrillary acidic protein levels in the high blast overpressure group than the sham group ($p = 0.08$). No apparent difference in glial fibrillary acidic protein levels was found between sham and medium blast overpressure group. No significant changes were observed with regard to the serum levels of phosphorylated neurofilament heavy chain and interleukin 6.

Discussion

To our knowledge, this study is the first of its kind to attempt to address the fundamental question whether an open field blast exposure causes injurious changes in the gyrencephalic brain. Although there were other studies that attempted to address the same question in a gyrencephalic model using explosives, animals in those studies were exposed to a simulated open field blast by positioning the animal either in a shock tube, high mobility multipurpose wheeled vehicle surrogate or in a four-sided building with no roof using a moderate charge [26,37,46]. Another previous open field blast study (2.1 kg explosive) positioned the animal on a steel shelf mounted to the concrete wall of the bunker and studied only physiological parameters such as respiration, circulation and cortical activity but no histological analyses of brain for injury changes as in the current study [47]. Säljö et al on the other hand, offers some details on the effects of repetitive blast pressure (3 times during a 10-15 minute period) in swine exposed to low level noise produced by various weapons (a howitzer, a bazooka, an automatic rifle) or underwater explosives [48]. They reported that animals exposed to bazooka (Pmax 42 kPa) and automatic rifle (Pmax 23 kPa) showed significant increase in subarachnoidal and small parenchymal bleedings in cortical regions with occipital lobe and cerebellum being the most predominantly affected structures. Animals exposed to howitzer blasts at 30 kPa although displayed parenchymal and subarachnoid hemorrhages, they were not significantly different from that of controls due to the limitations in the number of animals. Säljö et al concluded that low levels of blast causes brain edema as indicated by increased bioelectric impedance, an increase in intracranial pressure, small brain hemorrhages and impaired cognitive function [49].

In our study the animals were exposed to higher open field blast pressure than these animals and the likelihood of such hemorrhages although possible was not investigated as the focus was to study neuronal injury and glial reactivity changes.

We studied injury changes in the brain following an open field blast in Yucatan swine suspended in a sling and positioned below the triple point and exposed to a single Friedlander wave form either at medium (range 222 kPa - 333 kPa; average 272±5 kPa) or high blast overpressure (range 350-403 kPa; average 375±3 kPa). Our lowest medium blast overpressure of 222 kPa was similar to the mean shock tube blast pressure (241±8 kPa) reported by de Lanerolle et al (2011) in Yorkshire swine. Besides, the shock tube pressures reported by de Lanerolle et al ranged from 131-365 kPa [37] with their lowest pressure range far lower than in our study. In our experience there were no mortalities in both the medium and high blast overpressure groups. These pressures were very close to those utilized by de Lanerolle et al (2011) who reported shock tube and vehicular blast pressures in the range of 255-365 kPa with potentially long durations that may be a contributing factor for the observed mortality [37]. Furthermore, the medium and high blast overpressures used in our study are higher than those used by Gyorgy et al (2011**)** who used three different blast overpressures of <152 kPa, 138-276 kPa and >276 kPa respectively on Yorkshire swine and reported time dependent changes in serum biomarkers [50].

This initial report offers data on neural, astrocytic and microglial changes from the most anterior aspect of the brain to about 30 mm posterior. Our findings suggest, that open field blast exposure causes neuronal injury and marked increase in the number of astrocytes and microglia as early as three days after blast in the cortical gray

and white matter regions of the frontal lobe. Although not investigated, it is plausible that these injury changes can progressively evolve and can extend to more chronic time periods as supported by the findings from de Lanerolle et al who also studied changes two weeks after blast in swine [37]**.** Neuronal injury in the form of beta amyloid immunoreactive cell bodies, stellate cells, axonal swellings and retraction balls in sections from blast group was observed. The axonal injury in the form of terminal retraction balls and beaded profiles was very similar to previous findings of diffuse axonal injury following traumatic brain injury induced by an impact acceleration device [51]. Furthermore, the microscopic nature of these changes may not allow them to be detected either by routine or advanced radiological assessments and may render diagnosis of blast related pathology even more difficult. The immunoreactive zones in gray matter may suggest accumulation of β-APP in the cell bodies that may be related to impaired axoplasmic transport and its ultimate release into the surrounding extracellular matrix, which in turn can trigger neurotoxicity presuming its breakdown into the smaller amyloid beta fragments which still needs further validation. An increased cytoplasmic β-APP staining in the perikarya following traumatic brain injury also was previously reported [52,53]. Additionally, up-regulation of β-APP in cells including Purkinje cells and hippocampal neurons has been reported in a rodent model of cranial blast [54]. Furthermore, some of the beta amyloid stained regions in the white matter resembled glial cells with projections, which may suggest a breakdown of amyloid precursor protein and its potential uptake by the microglial cells as a way of clearance. This is further supported by the increase in the number of microglia in both the gray and white matter regions of sections from the blast exposure groups compared to sham. In

fact, Ryu et al recently reported APP positive axonal abnormalities in several brain sites from veterans that suffered blast injury. The changes particularly appeared as clusters of axonal spheroids or varicosities in a honeycomb pattern with perivascular distribution in the medial dorsal frontal white matter [55]. Our observation of axonal retraction balls and spheroids is similar to their observation. The honeycomb appearance of immunoreactivity in their study may be related to the presence of staining around microglial cells that may be responsible for the characteristic honeycomb appearance in the white matter tracts and may need to be validated by dual labeling immunofluorescence for β-APP and microglial markers. β-APP reactive axonal profiles in the medium and high blast overpressure group were observed in sections encompassing the prefrontal and frontal lobes predominantly in the dorsal sub cortical white matter structures. These frontal lobe axonal changes were further supported by NF-L and NF-M immunoreactive axons. Axonal changes evidenced by NF-L immunoreactive swollen profiles, with vacuolations and club-like terminations were observed in various sub cortical white matter tracts. In fact NF-L immunohistochemistry was previously used to show the pathogenesis of diffuse axonal injury following traumatic brain injury [56] with others showing cell body changes evidenced by accumulation of phosphorylated neurofilament heavy chain in rats exposed to explosive blast in a shock tube [25]. Although this needs further validation, we also show some putative signs of neurofilament compaction using RMO-14 antibodies. Neurofilament compaction is one of the components of traumatic axonal injury revealed by RMO-14 antibodies [57] with the other being impaired axoplasmic transport revealed by β-APP immunohistochemistry [51,57]. In fact, the predominance of β-APP reactive profiles in

the blast groups supports the dominance of impaired axoplasmic transport which was reported to be localized to the thin caliber axons [58] as revealed by very thin β-APP reactive profiles especially in the sub cortical white matter. In addition, the utility of β-APP immunohistochemistry was also reported by other investigators studying blast related changes in rodents [27,59]. Another question that needs to be asked is whether the observed white matter injury has the same etiology as that seen in blunt impact where axonal strains are likely to be high, whereas in blast exposure, the axonal strains are predicted to be low by computer models.

The presence of a high number of GFAP reactive astrocytes delineating the white matter in the blast swine brain sections is another hallmark of this study with the number of astrocytes increasing with increasing pressure. The presence of astrocytes delineating the white matter tracts implicates and supports their strong association with ongoing neuronal injury changes in the white matter tracts and to our knowledge this type of white matter delineation was never reported in a gyrencephalic blast brain injury model. De Lanerolle et al also reported astrocytes in subpial cortex and white matter of Yorkshire swine, an observation similar to our findings. However, quantitatively, they reported significant astrocyte increase in regions of hippocampus in swine exposed to blast in a vehicle and building but not in the shock tube setting [37]. On the other hand, Bauman et al using two Yorkshire swine exposed to moderate peak pressure in a high mobility multipurpose wheeled vehicle (HMMVEE) showed astrocytosis in the ipsilateral superior corona radiata (exposed side) of the posterior frontal cortex as well as in multiple layers of the dentate gyrus. They also showed elevated GFAP levels in the ipsilateral frontal cortices of the two swine tested [26]. With the very limited swine

studies, much of the knowledge related to blast induced astroglial changes comes from several rodent blast studies [22,32,35,43,60-62]. For example, Svetlov et al showed peak GFAP accumulation in the hippocampus seven days after blast exposure to 358 kPa that persisted for 30 days post blast by western blot analysis with no significant accumulation in the cortex at any of the survival periods. They also showed significant serum and cerebrospinal GFAP levels at 24 hours and four days after blast respectively [32]. In a separate study that subjected rats either to composite or primary blast, prominent astrocytosis in the hippocampus was reported at 1 and 7 days after blast with elevated serum GFAP levels at 6 hours, 1 day and 7 days respectively following composite or primary blast [35]. Sajja et al using an established shock tube blast overpressure model, reported elevated GFAP levels 24 hours after exposure (117 kPa) but not after 48 hours [60]. Garman et al on the other hand, reported no prominent GFAP and Iba1 staining (although small number of reactive microglia was found in areas of neuronal death) in any of the survival periods studied (24 hours, 72 hours, 2 weeks) in rats subjected to head only exposed blast overpressure of 241 kPa [43]. Turner et al, using a tabletop shock tube, reported graded astrocytic reactivity in the corpus callosum based on the exposed peak overpressure [61] similar to our findings that showed an increased astrocyte count with increasing blast pressure. The histological observation of prominent GFAP in our study is further supported by high GFAP serum levels albeit insignificant in the high pressure group. Taken together, these findings may support GFAP to be a candidate biomarker of blast induced neurotrauma. In a study of Yorkshire pigs, Gyorgy et al did not report injury changes by histology, but showed a time dependent increase in S100B and also reported high

variability among animals [50]. Sevtlov et al showed a significant increase in blood GFAP levels by 24 hours with levels in CSF showing a decline and accumulation in a time dependent manner in rats [32].

Another striking observation from our study is the significant increase in the number of microglia in the medium blast overpressure swine sections compared to high blast overpressure and sham groups. This type of differential expression of microglia and astrocytes in swine blast has never been reported. In our study, microglia were observed in both the cortical and white matter regions with no preferential localization. However, de Lanerolle et al although reported no difference in the distribution of microglia in the superior frontal cortex and hippocampus between blast and controls, but observed prominently activated microglia in the central white matter and corpus callosum with no additional quantitative data in swine that survived for 2 weeks after blast [37]. The extent of microglial response at chronic time periods after open field blast is yet to be fully studied. Similar to astrocytes, much of the knowledge related to blast induced microglial changes comes from rodent studies using blast wave [38,41] and impulse noise [39]. Sajja et al in their recent report on pathological changes after low (69 kPa), moderate (97 kPa) and high (165 kPa) shock tube overpressures reported a differential expression of microglia and astrocytes seven days post blast survival period, a finding very similar to our observations. They reported significant increase in microglial reactivity in low pressure group alone with increase in astrocytes with increasing pressure [63]. This is different from Turner et al who reported an increase in the number of corpus callosum microglia with increasing pressure (217, 350, and 497 kPa) [36], Garman et al previously reported only slight evidence for microglial

activation in rats subjected to 241 kPa blast overpressure [27]. On the other hand, Kaur et al reported microglial cells in close association with some darkened dendrites in rats subjected to single non-penetrating blast [38]. A putative pathological implication for microglia comes from studies by Kane et al that showed an increased expression of microglial genes related to immune function and inflammatory responses in cultured microglia subjected to overpressure [44].

What are the potential implications of the observed astrocytic and microglial activation in the frontal lobes of the brain? One implication is their potential role in neurodegeneration. It was recently shown that transforming growth factor beta from immature astrocytes could initiate synaptic elimination in postnatal thalamus by regulating the expression of C1q, a subcomponent of C1 complex of complement activation in the retinal ganglion cells [64]. C1q can trigger classic complement pathway that can lead to tagging of the supernumerary synapses with C3b fragment derived from complement activation and their ultimate elimination by microglia [65,66]. Furthermore, the indiscriminate microglial invasion of cortical and sub cortical regions as observed in the current study may also have other neurodegenerative implications considering the enhanced β-APP immunoreactive zones. It was shown that microglial functions such as directed process motility and phagocytic activity were impaired in mice with Alzheimer's disease-like pathology (AD-like) with their impairment being temporally and spatially correlated with amyloid beta plaque deposition [67]. There may also be a bidirectional relationship between the activation of astrocytes and that of microglia. For example, the attenuation of reactive gliosis in a model of AD led to a high number of microglia in the vicinity of plaques and cortex [68]. Whereas the attenuation of astrocytic activation in a

mouse model of Batten disease was shown to be accompanied by increased number of microglia in the brain [69]. What could be the potential implication of differential astrocytic and microglial response as observed in this study? Does it mean that at lower pressures, cellular injury changes may be more discrete and modulated by microglia with high pressures leading to activation of both microglia and astrocytes with the latter playing a dominant role? It is very likely that astrocytes may serve as markers of injury severity. As their number increases with increasing pressure, there may be an array of neuronal and inflammatory injury changes as well as potential blood brain barrier permeability disruptions as indicated by their apparent high serum concentrations. Furthermore, the presence of astrocytes almost exclusively delineating white matter tracts may be an indication of the extensive white matter injury following blast exposure. In addition, it is also possible that mechanical perturbations in the tissue trigger astrocyte derived adenosine triphosphate release which may lead to rapid recruitment of microglia to the site of injury and can lead to both microglial and astrocytic reactivity responses [70]. The role of microglia and astrocytes contributing to the release of various inflammatory mediators has been well reported. For that matter, studies by Bauman et al and others have shown increased levels of tumor necrosis factor, interleukin 1 beta, and interferon-γ in cerebrospinal fluid and serum following blast [26,35] lending support also to the inflammatory nature of blast pathology.

In conclusion, our investigation of a gyrencephalic brain three days after open field blast exposure supports the presence of a robust neuronal injury accompanied by extensive astrocytic and microglial activation in the frontal lobes. The severity of the observed neuronal and astrocytic changes appeared to be proportional to the level of

blast exposure. The microglial response appears to be differential with high numbers at medium blast overpressure and low numbers at high blast pressure. Whether these injury changes extend to more posterior aspects and brainstem parts is a major aspect of our ongoing investigations. The functional implication of these observed changes may be related to neuronal, axonal and dendritic degeneration combined with a cascade of inflammatory mediator release. We postulate that the observed acute injury changes may progress to chronic periods after blast and may contribute to short and long-term neuronal degeneration and glial mediated inflammation.

Acknowledgements

This research was supported by the US Army through an MRMC Cooperative Agreement, Award No. W81XWH-12-2-0038. The authors would like to extend their sincere thanks Dr. Elizabeth Dawe, DVM and Ms. Janine Mattei, from Surgical Research Services, School of Medicine, Wayne State University for their invaluable technical help in preparing the swine for blast procedures. Our special thanks to Team Wendy LLC, Cleveland, OH and ARES, Inc., Port Clinton, OH. We also wish to thank Dr. Chengpeng Zhou, Ms. Heena Purkait, Mrs. Tong Shi, Ms. Natasha Gupta, Ms. Leena Penumalee and Ms. Ramya Maramraju for their valuable technical assistance during the course of this work. We also thank Dr. Scott Millis for his valuable assistance with statistical analysis.

References

1. Snell FI, Halter MJ (2010) A signature wound of war: mild traumatic brain injury. J Psychosoc Nurs Ment Health Serv 48: 22-28.
2. Eskridge SL, Macera CA, Galarneau MR, Holbrook TL, Woodruff SI, et al. (2012) Injuries from combat explosions in Iraq: injury type, location, and severity. Injury 43: 1678-1682.
3. Jones E, Fear NT, Wessely S (2007) Shell shock and mild traumatic brain injury: a historical review. Am J Psychiatry 164: 1641-1645.
4. Hoge CW, McGurk D, Thomas JL, Cox AL, Engel CC, et al. (2008) Mild traumatic brain injury in U.S. Soldiers returning from Iraq. N Engl J Med 358: 453-463.
5. Neipert L, Pastorek NJ, Troyanskaya M, Scheibel RS, Petersen NJ, et al. (2014) Effect of clinical characteristics on cognitive performance in service members and veterans with histories of blast-related mild traumatic brain injury. Brain Inj 28: 1667-1674.
6. Troyanskaya M, Pastorek NJ, Scheibel RS, Petersen NJ, McCulloch K, et al. (2015) Combat Exposure, PTSD Symptoms, and Cognition Following Blast-Related Traumatic Brain Injury in OEF/OIF/OND Service Members and Veterans. Mil Med 180: 285-289.
7. Reid MW, Miller KJ, Lange RT, Cooper DB, Tate DF, et al. (2014) A multisite study of the relationships between blast exposures and symptom reporting in a post-deployment active duty military population with mild traumatic brain injury. J Neurotrauma 31: 1899-1906.
8. Wilkinson CW, Pagulayan KF, Petrie EC, Mayer CL, Colasurdo EA, et al. (2012) High prevalence of chronic pituitary and target-organ hormone abnormalities after blast-related mild traumatic brain injury. Front Neurol 3: 11.
9. Magone MT, Kwon E, Shin SY (2014) Chronic visual dysfunction after blast-induced mild traumatic brain injury. J Rehabil Res Dev 51: 71-80.
10. Lemke S, Cockerham GC, Glynn-Milley C, Cockerham KP (2013) Visual quality of life in veterans with blast-induced traumatic brain injury. JAMA Ophthalmol 131: 1602-1609.
11. Pogoda TK, Hendricks AM, Iverson KM, Stolzmann KL, Krengel MH, et al. (2012) Multisensory impairment reported by veterans with and without mild traumatic brain injury history. J Rehabil Res Dev 49: 971-984.
12. Chen LL, Baca CB, Choe J, Chen JW, Ayad ME, et al. (2014) Posttraumatic epilepsy in operation enduring freedom/operation iraqi freedom veterans. Mil Med 179: 492-496.
13. Mac Donald CL, Johnson AM, Wierzechowski L, Kassner E, Stewart T, et al. (2014) Prospectively assessed clinical outcomes in concussive blast vs nonblast traumatic brain injury among evacuated US military personnel. JAMA Neurol 71: 994-1002.
14. Davenport ND, Lim KO, Armstrong MT, Sponheim SR (2012) Diffuse and spatially variable white matter disruptions are associated with blast-related mild traumatic brain injury. Neuroimage 59: 2017-2024.
15. Mac Donald C, Johnson A, Cooper D, Malone T, Sorrell J, et al. (2013) Cerebellar white matter abnormalities following primary blast injury in US military personnel. PLoS One 8: e55823.
16. de Lanerolle NC, Hamid H, Kulas J, Pan JW, Czlapinski R, et al. (2014) Concussive brain injury from explosive blast. Ann Clin Transl Neurol 1: 692-702.
17. Heldt SA, Elberger AJ, Deng Y, Guley NH, Del Mar N, et al. (2014) A novel closed-head model of mild traumatic brain injury caused by primary overpressure blast to the cranium produces sustained emotional deficits in mice. Front Neurol 5: 2.
18. Budde MD, Shah A, McCrea M, Cullinan WE, Pintar FA, et al. (2013) Primary blast traumatic brain injury in the rat: relating diffusion tensor imaging and behavior. Front Neurol 4: 154.

19. Huber BR, Meabon JS, Martin TJ, Mourad PD, Bennett R, et al. (2013) Blast exposure causes early and persistent aberrant phospho- and cleaved-tau expression in a murine model of mild blast-induced traumatic brain injury. J Alzheimers Dis 37: 309-323.
20. Park E, Eisen R, Kinio A, Baker AJ (2013) Electrophysiological white matter dysfunction and association with neurobehavioral deficits following low-level primary blast trauma. Neurobiol Dis 52: 150-159.
21. Rubovitch V, Ten-Bosch M, Zohar O, Harrison CR, Tempel-Brami C, et al. (2011) A mouse model of blast-induced mild traumatic brain injury. Exp Neurol 232: 280-289.
22. Pun PB, Kan EM, Salim A, Li Z, Ng KC, et al. (2011) Low level primary blast injury in rodent brain. Front Neurol 2: 19.
23. Koliatsos VE, Cernak I, Xu L, Song Y, Savonenko A, et al. (2011) A mouse model of blast injury to brain: initial pathological, neuropathological, and behavioral characterization. J Neuropathol Exp Neurol 70: 399-416.
24. Cernak I, Wang Z, Jiang J, Bian X, Savic J (2001) Ultrastructural and functional characteristics of blast injury-induced neurotrauma. J Trauma 50: 695-706.
25. Saljo A, Bao F, Haglid KG, Hansson HA (2000) Blast exposure causes redistribution of phosphorylated neurofilament subunits in neurons of the adult rat brain. J Neurotrauma 17: 719-726.
26. Bauman RA, Ling G, Tong L, Januszkiewicz A, Agoston D, et al. (2009) An introductory characterization of a combat-casualty-care relevant swine model of closed head injury resulting from exposure to explosive blast. J Neurotrauma 26: 841-860.
27. Garman RH, Jenkins LW, Switzer Iii RC, Bauman RA, Tong LC, et al. (2011) Blast exposure in rats with body shielding is characterized by diffuse axonal injury. Journal of neurotrauma.
28. Macgregor AJ, Dougherty AL, Galarneau MR (2010) Injury-Specific Correlates of Combat-Related Traumatic Brain Injury in Operation Iraqi Freedom. J Head Trauma Rehabil 26: 312-318.
29. Stone JR, Okonkwo DO, Dialo AO, Rubin DG, Mutlu LK, et al. (2004) Impaired axonal transport and altered axolemmal permeability occur in distinct populations of damaged axons following traumatic brain injury. Exp Neurol 190: 59-69.
30. Yaghmai A, Povlishock J (1992) Traumatically induced reactive change as visualized through the use of monoclonal antibodies targeted to neurofilament subunits. J Neuropathol Exp Neurol 51: 158-176.
31. Vandevord PJ, Leung LY, Hardy W, Mason M, Yang KH, et al. (2008) Up-regulation of reactivity and survival genes in astrocytes after exposure to short duration overpressure. Neurosci Lett 434: 247-252.
32. Svetlov SI, Prima V, Kirk DR, Gutierrez H, Curley KC, et al. (2010) Morphologic and biochemical characterization of brain injury in a model of controlled blast overpressure exposure. The Journal of trauma 69: 795-804.
33. Ahmed F, Gyorgy A, Kamnaksh A, Ling G, Tong L, et al. (2012) Time-dependent changes of protein biomarker levels in the cerebrospinal fluid after blast traumatic brain injury. Electrophoresis 33: 3705-3711.
34. Vandevord PJ, Bolander R, Sajja VS, Hay K, Bir CA (2011) Mild Neurotrauma Indicates a Range-Specific Pressure Response to Low Level Shock Wave Exposure. Annals of biomedical engineering.
35. Svetlov SI, Prima V, Glushakova O, Svetlov A, Kirk DR, et al. (2012) Neuro-glial and systemic mechanisms of pathological responses in rat models of primary blast overpressure compared to "composite" blast. Frontiers in neurology 3: 15.
36. Turner RC, Naser ZJ, Logsdon AF, DiPasquale KH, Jackson GJ, et al. (2013) Modeling clinically relevant blast parameters based on scaling principles produces functional & histological deficits in rats. Experimental neurology 248: 520-529.

37. de Lanerolle NC, Bandak F, Kang D, Li AY, Du F, et al. (2011) Characteristics of an explosive blast-induced brain injury in an experimental model. J Neuropathol Exp Neurol 70: 1046-1057.
38. Kaur C, Singh J, Lim MK, Ng BL, Yap EP, et al. (1995) The response of neurons and microglia to blast injury in the rat brain. Neuropathol Appl Neurobiol 21: 369-377.
39. Saljo A, Bao F, Hamberger A, Haglid KG, Hansson HA (2001) Exposure to short-lasting impulse noise causes microglial and astroglial cell activation in the adult rat brain. Pathophysiology 8: 105-111.
40. Hicks RR, Fertig SJ, Desrocher RE, Koroshetz WJ, Pancrazio JJ (2010) Neurological effects of blast injury. J Trauma 68: 1257-1263.
41. Readnower RD, Chavko M, Adeeb S, Conroy MD, Pauly JR, et al. (2010) Increase in blood-brain barrier permeability, oxidative stress, and activated microglia in a rat model of blast-induced traumatic brain injury. Journal of neuroscience research 88: 3530-3539.
42. Pun PB, Kan EM, Salim A, Li Z, Ng KC, et al. (2011) Low level primary blast injury in rodent brain. Frontiers in neurology 2: 19.
43. Garman RH, Jenkins LW, Switzer RC, 3rd, Bauman RA, Tong LC, et al. (2011) Blast exposure in rats with body shielding is characterized primarily by diffuse axonal injury. Journal of Neurotrauma 28: 947-959.
44. Kane MJ, Angoa-Perez M, Francescutti DM, Sykes CE, Briggs DI, et al. (2012) Altered gene expression in cultured microglia in response to simulated blast overpressure: possible role of pulse duration. Neuroscience letters 522: 47-51.
45. Sajja VS, Ereifej ES, Vandevord PJ (2014) Hippocampal vulnerability and subacute response following varied blast magnitudes. Neuroscience letters 570C: 33-37.
46. Gyorgy A, Ling G, Wingo D, Walker J, Tong L, et al. (2011) Time-dependent changes in serum biomarker levels after blast traumatic brain injury. J Neurotrauma 28: 1121-1126.
47. Axelsson H, Hjelmqvist H, Medin A, Persson JK, Suneson A (2000) Physiological changes in pigs exposed to a blast wave from a detonating high-explosive charge. Mil Med 165: 119-126.
48. Saljo A, Arrhen F, Bolouri H, Mayorga M, Hamberger A (2008) Neuropathology and pressure in the pig brain resulting from low-impulse noise exposure. J Neurotrauma 25: 1397-1406.
49. Saljo A, Mayorga M, Bolouri H, Svensson B, Hamberger A (2011) Mechanisms and pathophysiology of the low-level blast brain injury in animal models. Neuroimage 54 Suppl 1: S83-88.
50. Gyorgy A, Ling G, Wingo D, Walker J, Tong L, et al. (2011) Time-dependent changes in serum biomarker levels after blast traumatic brain injury. Journal of Neurotrauma 28: 1121-1126.
51. Kallakuri S, Li Y, Zhou R, Bandaru S, Zakaria N, et al. (2012) Impaired axoplasmic transport is the dominant injury induced by an impact acceleration injury device: An analysis of traumatic axonal injury in pyramidal tract and corpus callosum of rats. Brain research 1452: 29-38.
52. Itoh T, Satou T, Nishida S, Tsubaki M, Hashimoto S, et al. (2009) Expression of amyloid precursor protein after rat traumatic brain injury. Neurol Res 31: 103-109.
53. Kilbourne M, Kuehn R, Tosun C, Caridi J, Keledjian K, et al. (2009) Novel model of frontal impact closed head injury in the rat. J Neurotrauma 26: 2233-2243.
54. Kuehn R, Simard PF, Driscoll I, Keledjian K, Ivanova S, et al. (2011) Rodent model of direct cranial blast injury. J Neurotrauma 28: 2155-2169.
55. Ryu J, Horkayne-Szakaly I, Xu L, Pletnikova O, Leri F, et al. (2014) The problem of axonal injury in the brains of veterans with histories of blast exposure. Acta Neuropathol Commun 2: 153.
56. Povlishock JT (1993) Pathobiology of traumatically induced axonal injury in animals and man. Ann Emerg Med 22: 980-986.
57. Stone JR, Singleton RH, Povlishock JT (2001) Intra-axonal neurofilament compaction does not evoke local axonal swelling in all traumatically injured axons. Exp Neurol 172: 320-331.

58. Marmarou CR, Walker SA, Davis CL, Povlishock JT (2005) Quantitative analysis of the relationship between intra- axonal neurofilament compaction and impaired axonal transport following diffuse traumatic brain injury. J Neurotrauma 22: 1066-1080.
59. Koliatsos VE, Cernak I, Xu L, Song Y, Savonenko A, et al. (2011) A mouse model of blast injury to brain: initial pathological, neuropathological, and behavioral characterization. Journal of neuropathology and experimental neurology 70: 399-416.
60. Sajja VS, Galloway MP, Ghoddoussi F, Thiruthalinathan D, Kepsel A, et al. (2012) Blast-induced neurotrauma leads to neurochemical changes and neuronal degeneration in the rat hippocampus. NMR in biomedicine 25: 1331-1339.
61. Turner RC, Naser ZJ, Logsdon AF, DiPasquale KH, Jackson GJ, et al. (2013) Modeling clinically relevant blast parameters based on scaling principles produces functional & histological deficits in rats. Exp Neurol 248: 520-529.
62. Risling M, Plantman S, Angeria M, Rostami E, Bellander BM, et al. (2011) Mechanisms of blast induced brain injuries, experimental studies in rats. Neuroimage 54 Suppl 1: S89-97.
63. Sajja VS, Perrine SA, Ghoddoussi F, Hall CS, Galloway MP, et al. (2014) Blast neurotrauma impairs working memory and disrupts prefrontal myo-inositol levels in rats. Molecular and cellular neurosciences 59: 119-126.
64. Bialas AR, Stevens B (2013) TGF-beta signaling regulates neuronal C1q expression and developmental synaptic refinement. Nat Neurosci 16: 1773-1782.
65. Schafer DP, Lehrman EK, Kautzman AG, Koyama R, Mardinly AR, et al. (2012) Microglia sculpt postnatal neural circuits in an activity and complement-dependent manner. Neuron 74: 691-705.
66. Stevens B, Allen NJ, Vazquez LE, Howell GR, Christopherson KS, et al. (2007) The classical complement cascade mediates CNS synapse elimination. Cell 131: 1164-1178.
67. Krabbe G, Halle A, Matyash V, Rinnenthal JL, Eom GD, et al. (2013) Functional impairment of microglia coincides with Beta-amyloid deposition in mice with Alzheimer-like pathology. PLoS One 8: e60921.
68. Kraft AW, Hu X, Yoon H, Yan P, Xiao Q, et al. (2013) Attenuating astrocyte activation accelerates plaque pathogenesis in APP/PS1 mice. FASEB J 27: 187-198.
69. Macauley SL, Pekny M, Sands MS (2011) The role of attenuated astrocyte activation in infantile neuronal ceroid lipofuscinosis. J Neurosci 31: 15575-15585.
70. Burda JE, Bernstein AM, Sofroniew MV (2015) Astrocyte roles in traumatic brain injury. Exp Neurol.

Figure Legends

Figure 1: β-APP immunoreactivity in the blast and sham swine. 1A shows average number (± standard deviation, STD) of β-APP immunoreactive zones in the blast and sham swine sections. The number of β-APP immunoreactive zones in the medium blast overpressure sections were significantly higher than in sham (§) with those in sections from high blast overpressure being significantly higher compared to sections from sham (§) and medium blast overpressure (‡) groups ($p<0.05$; LSD; One-way ANOVA). 1B shows a gray matter immunoreactive zone from a representative high blast overpressure swine. 1C shows an immunoreactive zone with stellate-like profiles in the white matter tracts of a swine subjected to high blast overpressure. 1D and 1E show representative β-APP reactive retraction balls in the cortical white matter and internal capsule respectively.

Figure 2: NF-L immunoreactive large caliber nerve fibers in blast and sham sections. 2A shows an axon with swollen regions (arrows) in a brain section from the medium blast overpressure group. 2B and 2C show swollen axons with apparent vacuolations and retraction balls in a section from the high blast overpressure group. 2D shows a normal appearing axon in a section from the sham group.

Figure 3: RMO14 immunoreactivity showing NF-M immunoreactive large caliber axons in the cortical radiations. 3A shows normal looking axon in a sham brain section. 3B and 3C show apparently reactive axons. 3B shows an axon with an apparent vacuole like (arrow) presence in a section from medium blast overpressure group. 3C shows a

large caliber axon with a terminal putative enlargement preceded by vacuolated appearance (arrow) in a section from a high blast overpressure group.

Figure 4: Astrocytic reactivity in the white matter tracts. Representative panoramic images of sections of GFAP stained left hemispheres from a typical sham (A), medium (B) and high blast overpressure exposed swine. Arrows indicate white matter radiations into the cortex and other tracts that appeared to be clearly delineated from the gray matter. Note the intense staining of the neuropile. (CC= corpus callosum; LV= lateral ventricle; st = striatum; ac = anterior commissure)

Figure 5: Quantification of open field blast induced astrogliosis. 5A shows the astrocyte counts in the blast and sham groups. Astrocyte counts in sections from the high and medium blast overpressure group were significantly elevated compared to those from sham group. Astrocyte counts in the high blast overpressure group were significantly higher than in the medium blast overpressure group. 5B shows an image of lightly stained astrocytes in a representative sham section. 5C and 5D show increased astrocytic proliferation in medium and high blast overpressure exposed sections. Furthermore, astrocytes in blast sections appeared to be intensely stained with enlarged cell bodies and processes (5D).

Figure 6: Open field blast induced microglial proliferation. 6A shows extent of the microglial counts in the blast and sham groups. Microglial counts in sections from the high and medium blast overpressure blast groups were significantly high compared to those from sham group. 6B-D show representative images from sham, medium and

high blast overpressure exposed sections highlighting variations in microglial proliferation. Microglia in blast sections appeared to be enlarged in size.

Supporting Information

S1 Figure: Open field blast set-up. Figure shows swine suspended in slings in preparation for open field blast exposure. Red arrows point to two of the three pencil probes positioned to measure the incident pressure at the same standoff distance and height above the ground as the animal head. In this representative set-up, the swine with asterisk was the designated non-instrumented swine used for histological analyses. The other instrumented swine was used as part of a separate investigation to assess the brain biomechanical responses following open field blast exposure.

S2 Figure: Methodology of swine brain sectioning. 2A shows the brain slicer with a brain positioned and with blades inserted to harvest a 5 mm block shown in 2b. The arrow in 2B points to the hole made by inserting the tip of a glass pipette to identify the left hemisphere. 2C shows a series of representative blocks obtained from the anterior aspect of a swine brain. Each block was further sectioned into 35-40 µm thick sections. These blocks originate at the most anterior aspect of the frontal lobe and extend 30 mm posterior encompassing the corpus callosum, striatum, internal capsule, lateral ventricles and the septum.

S3 Figure: Astrocytes from sham (A), medium (B) and high blast overpressure (C) exposed groups.

Figure1

Click here to download Figure Fig_1A.tif

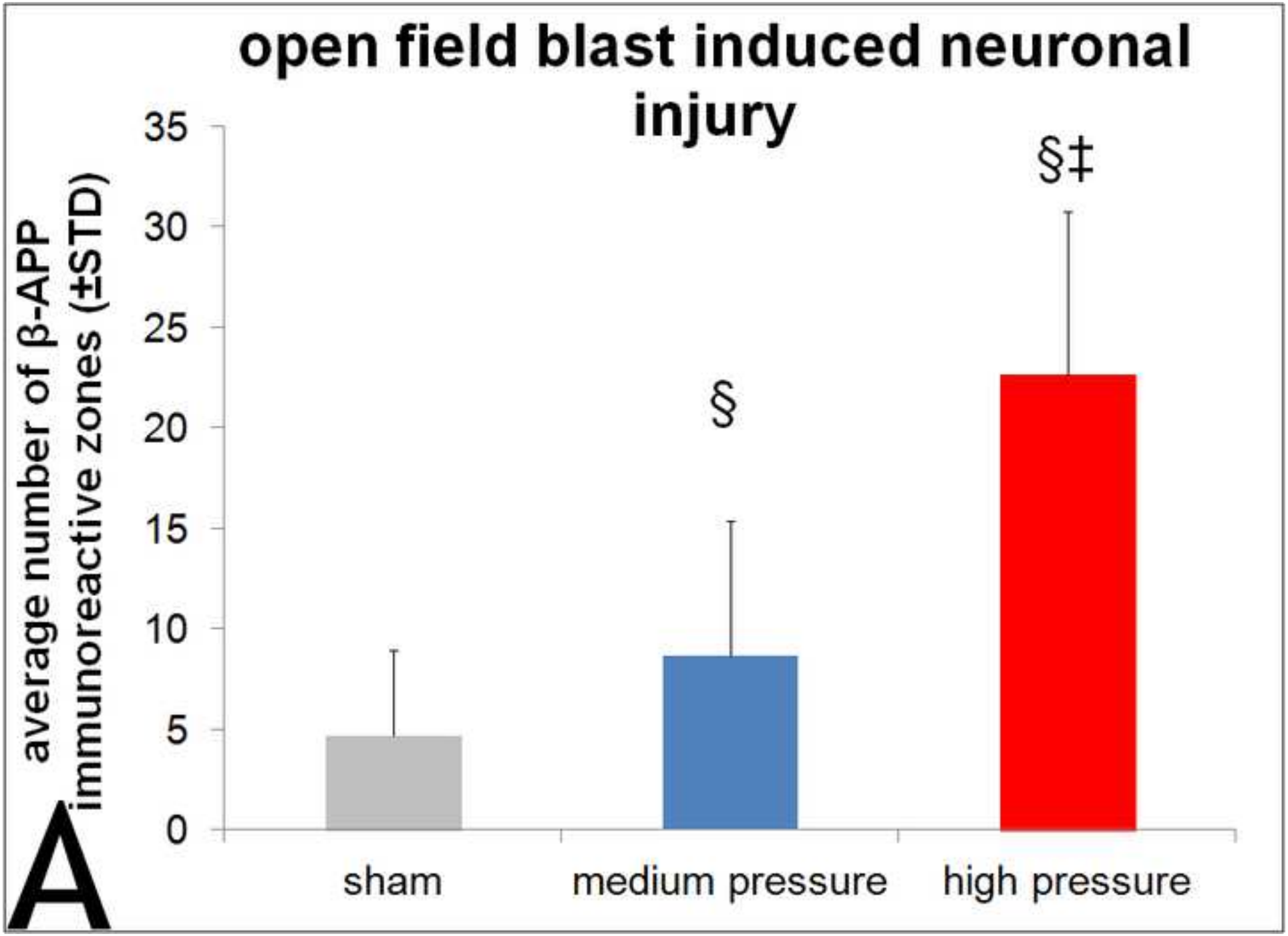

Figure1

Click here to download Figure Fig_1B.tif

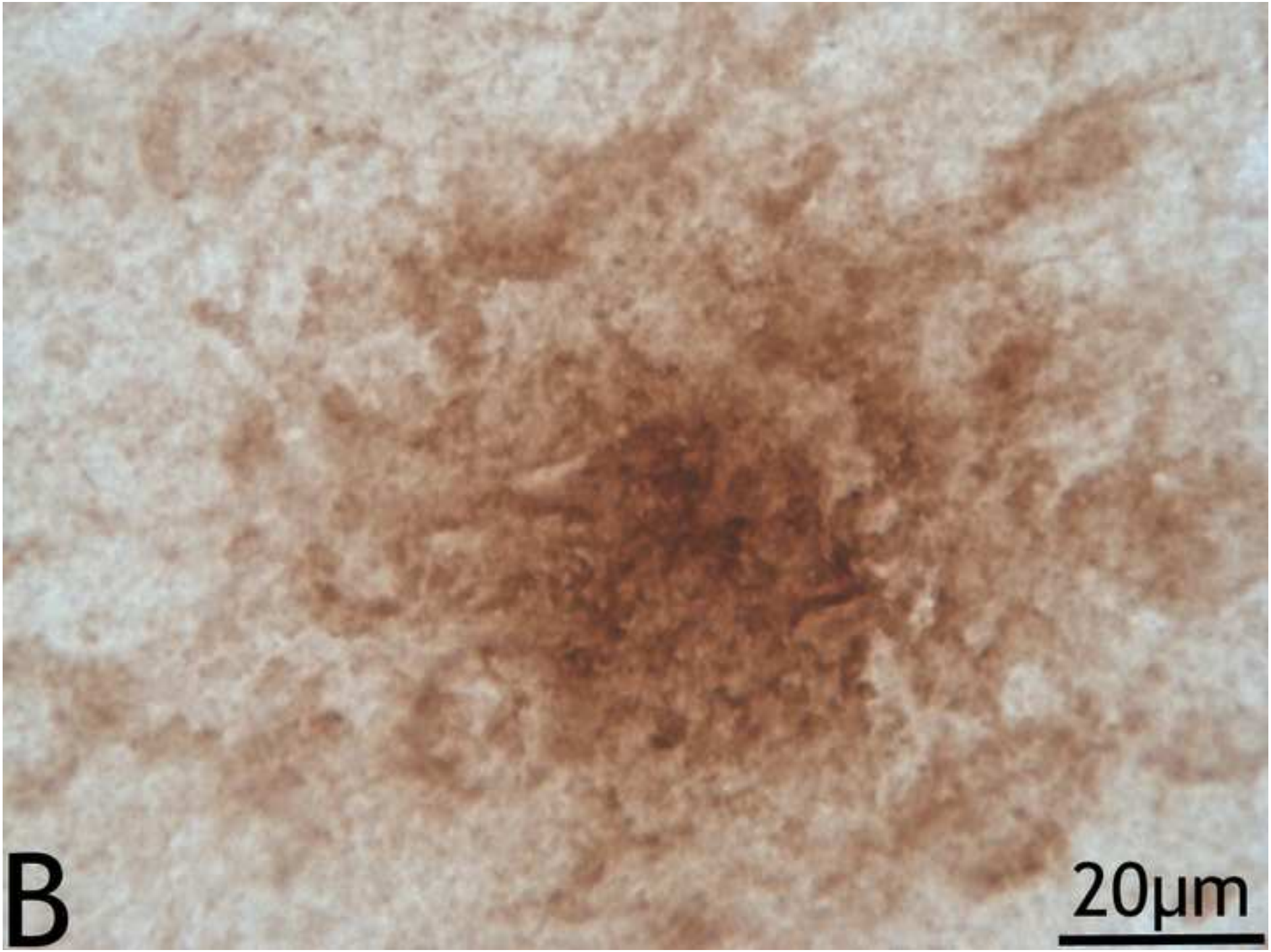

Figure1

Click here to download Figure Fig_1C.tif

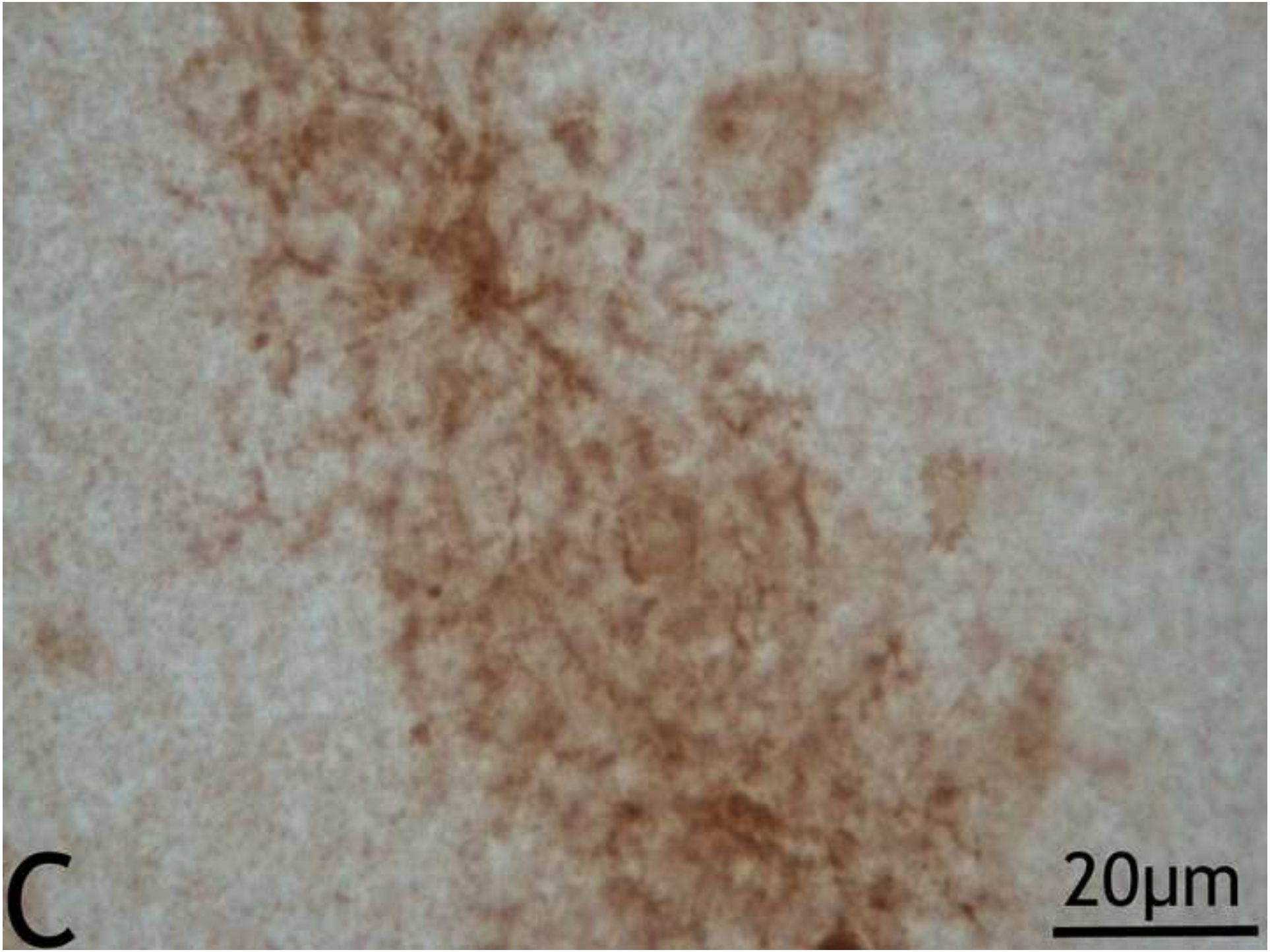

Figure1

Click here to download Figure Fig_1D.tif

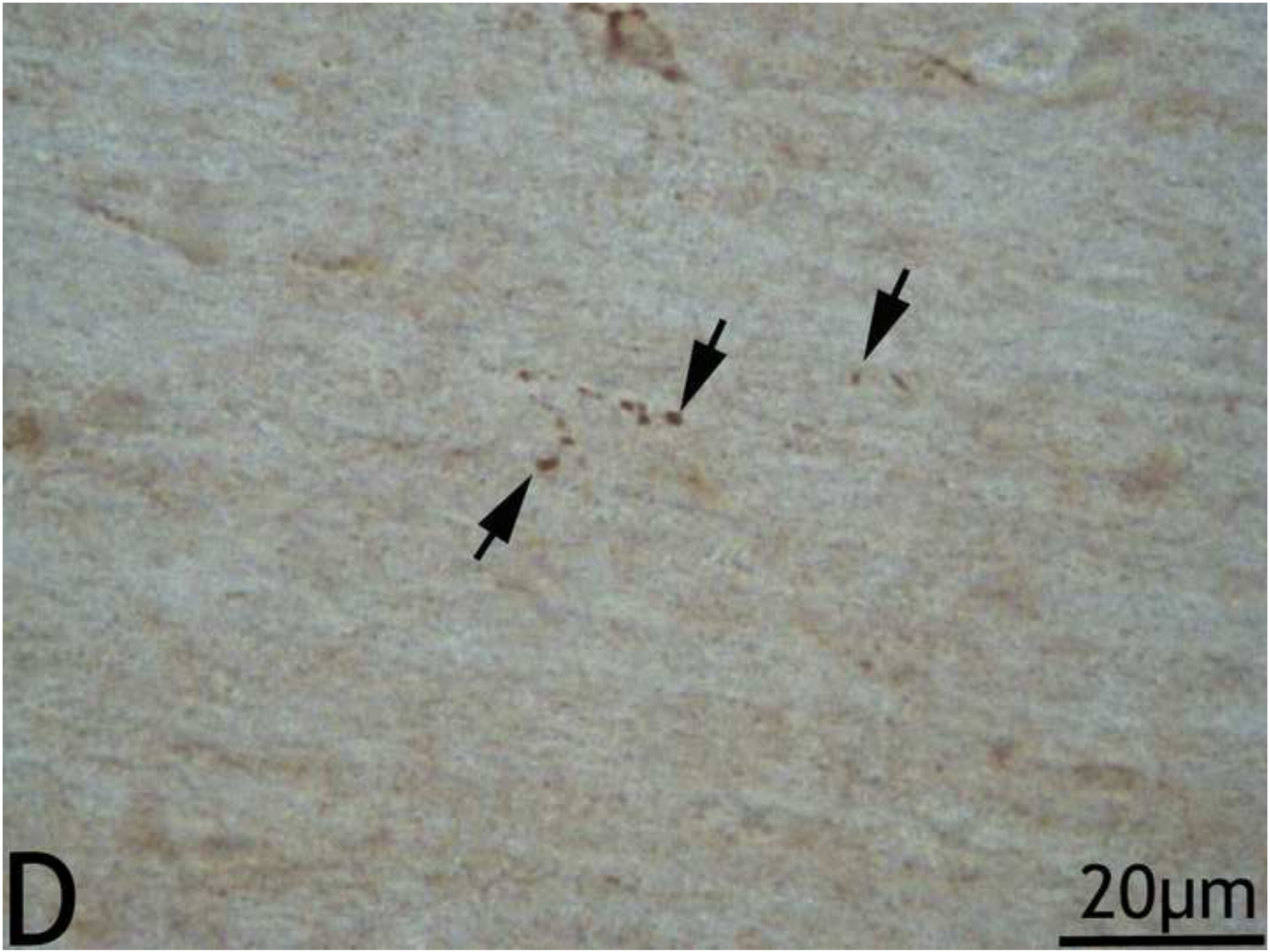

Figure1

Click here to download Figure Fig_1E.tif

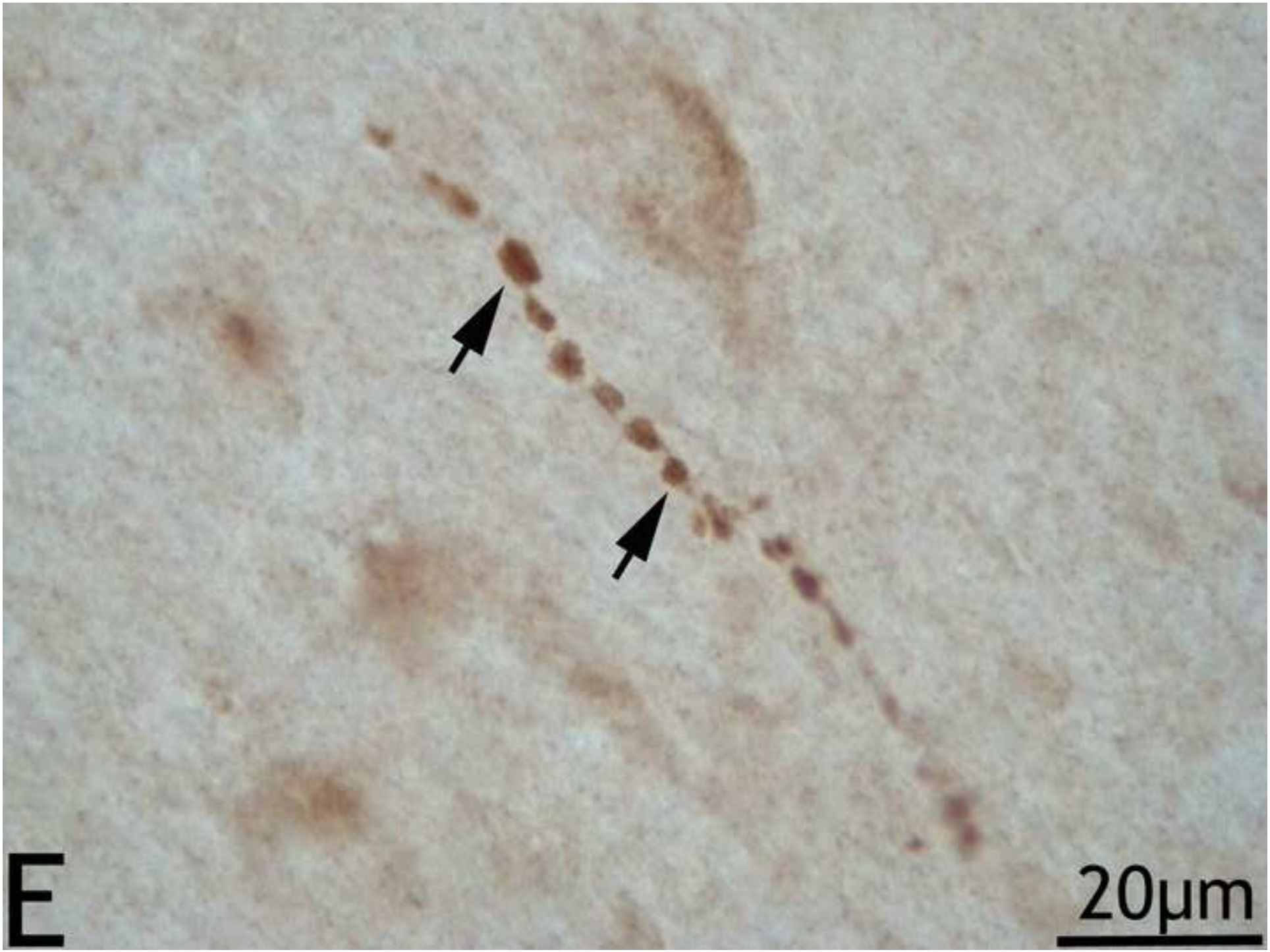

Figure2

Click here to download Figure Fig_2A.tif

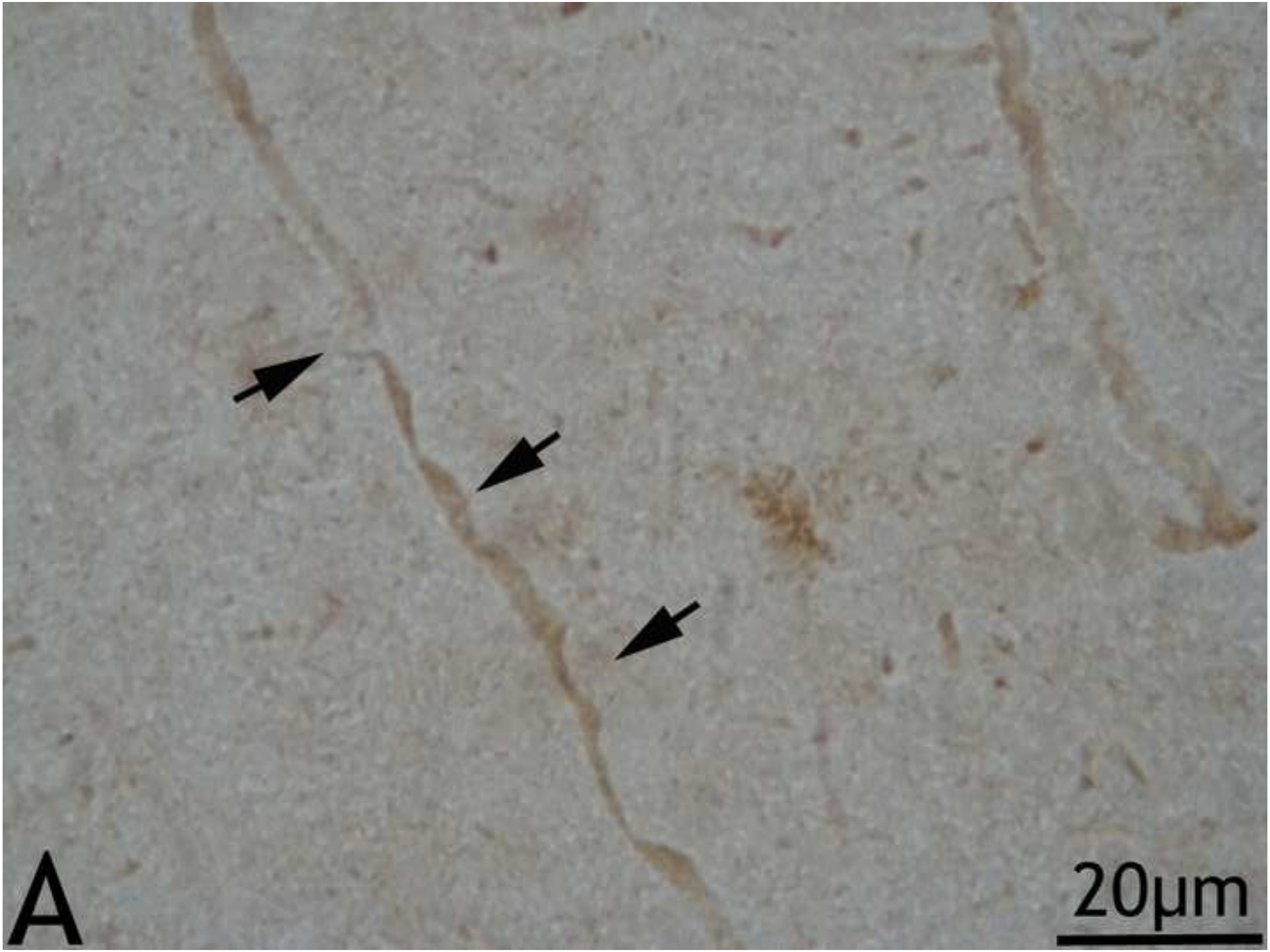

Figure2

Click here to download Figure Fig_2B.tif

Figure2

Click here to download Figure Fig_2C.tif

Figure2

Click here to download Figure Fig_2D.tif

Figure 3

Click here to download Figure Fig_3A.tif

Figure 3

Click here to download Figure Fig_3B.tif

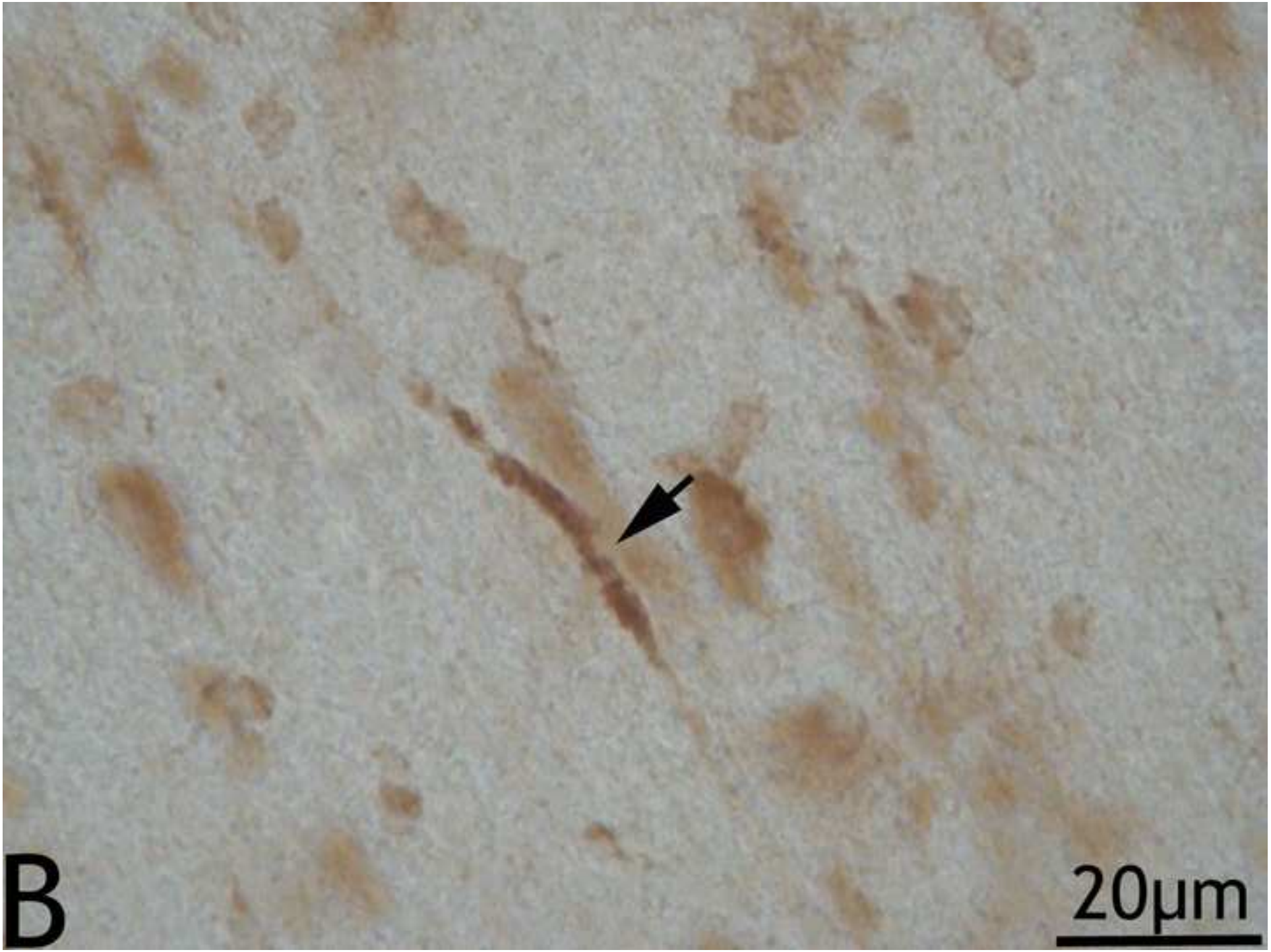

Figure 3

Click here to download Figure Fig_3C.tif

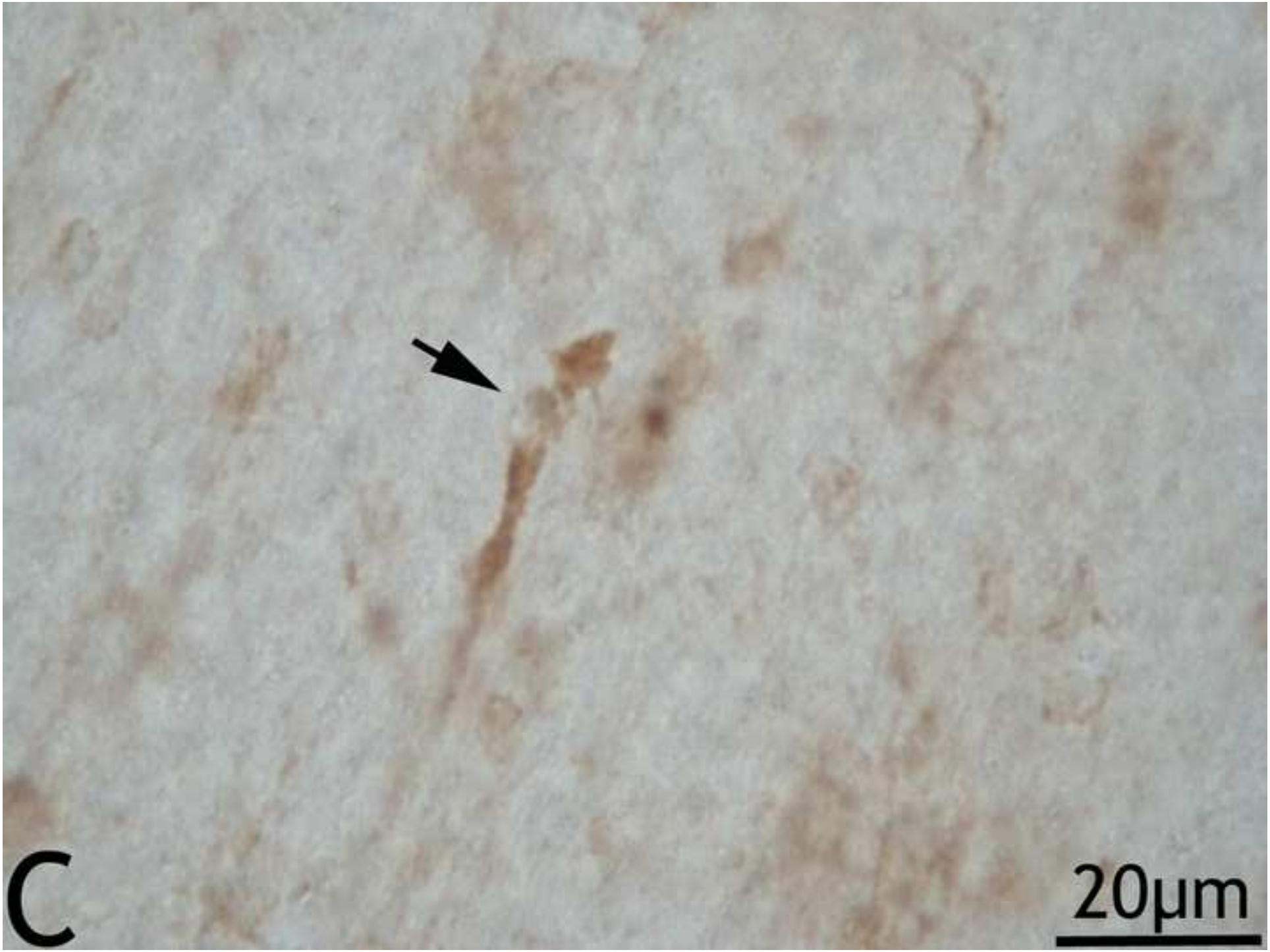

Figure 4

Click here to download Figure Fig_4A.tif

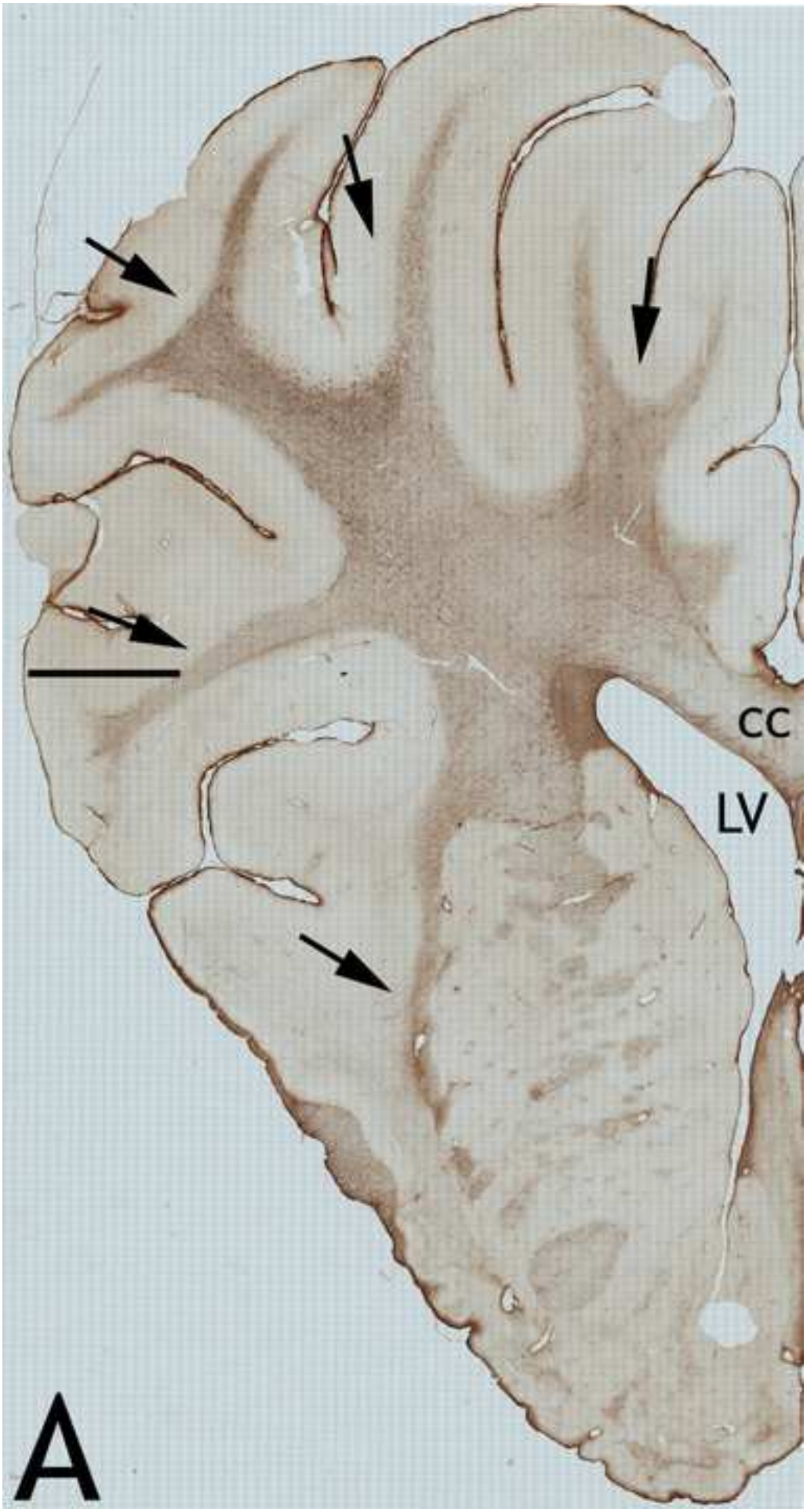

Figure 4

Click here to download Figure Fig_4B.tif

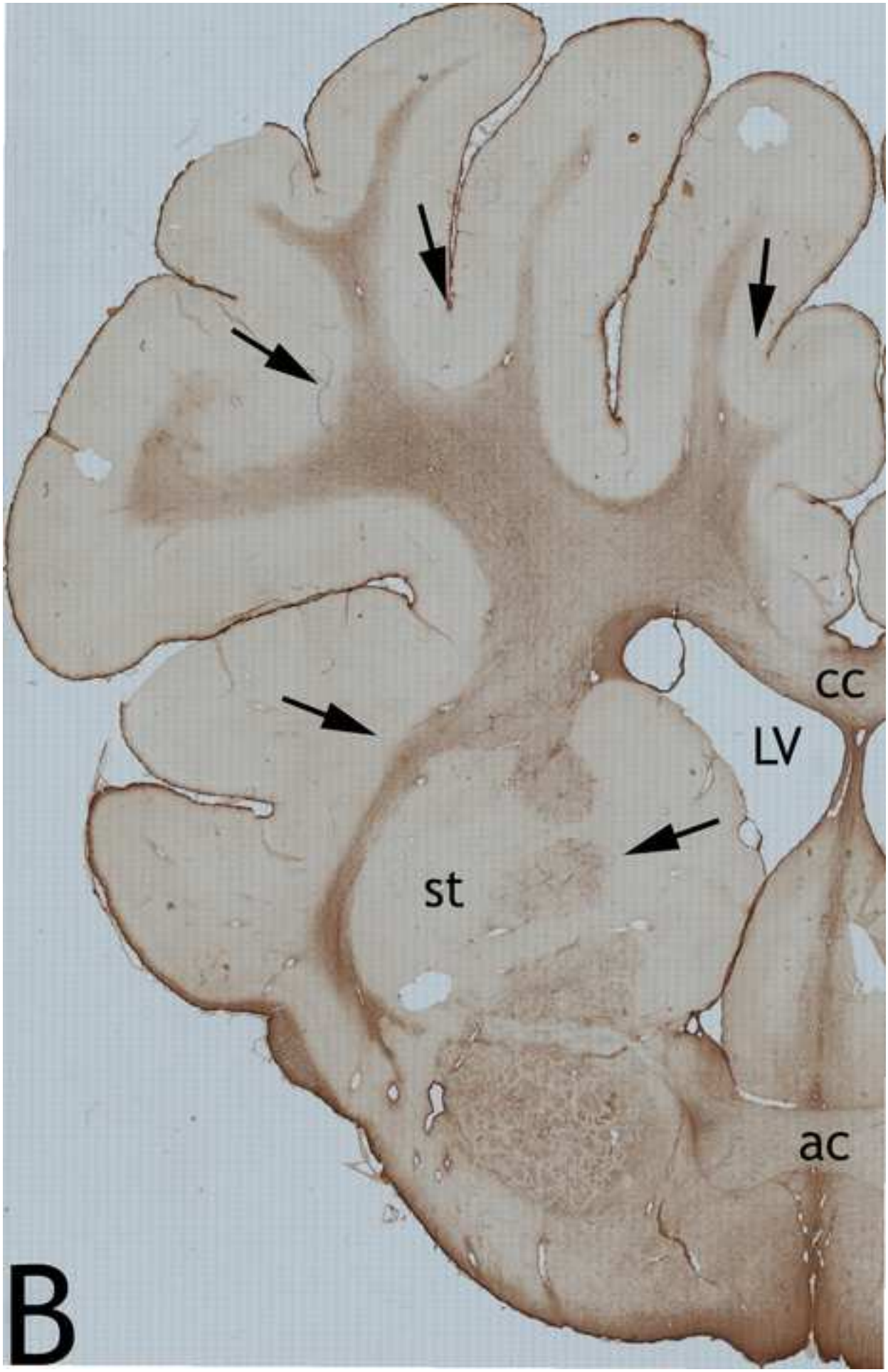

Figure 4

Click here to download Figure Fig_4C.tif

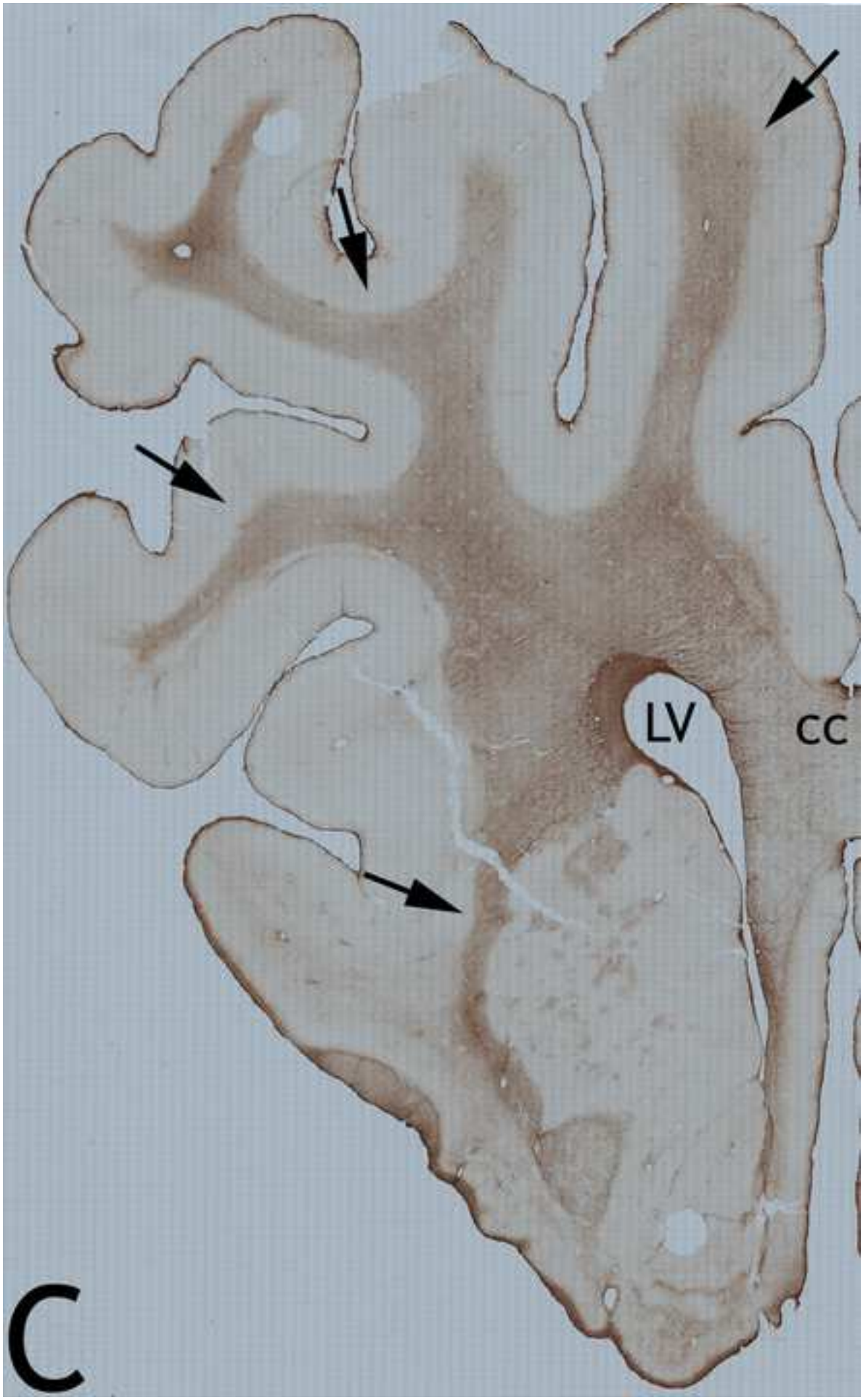

Figure 5

Click here to download Figure Fig_5A.tif

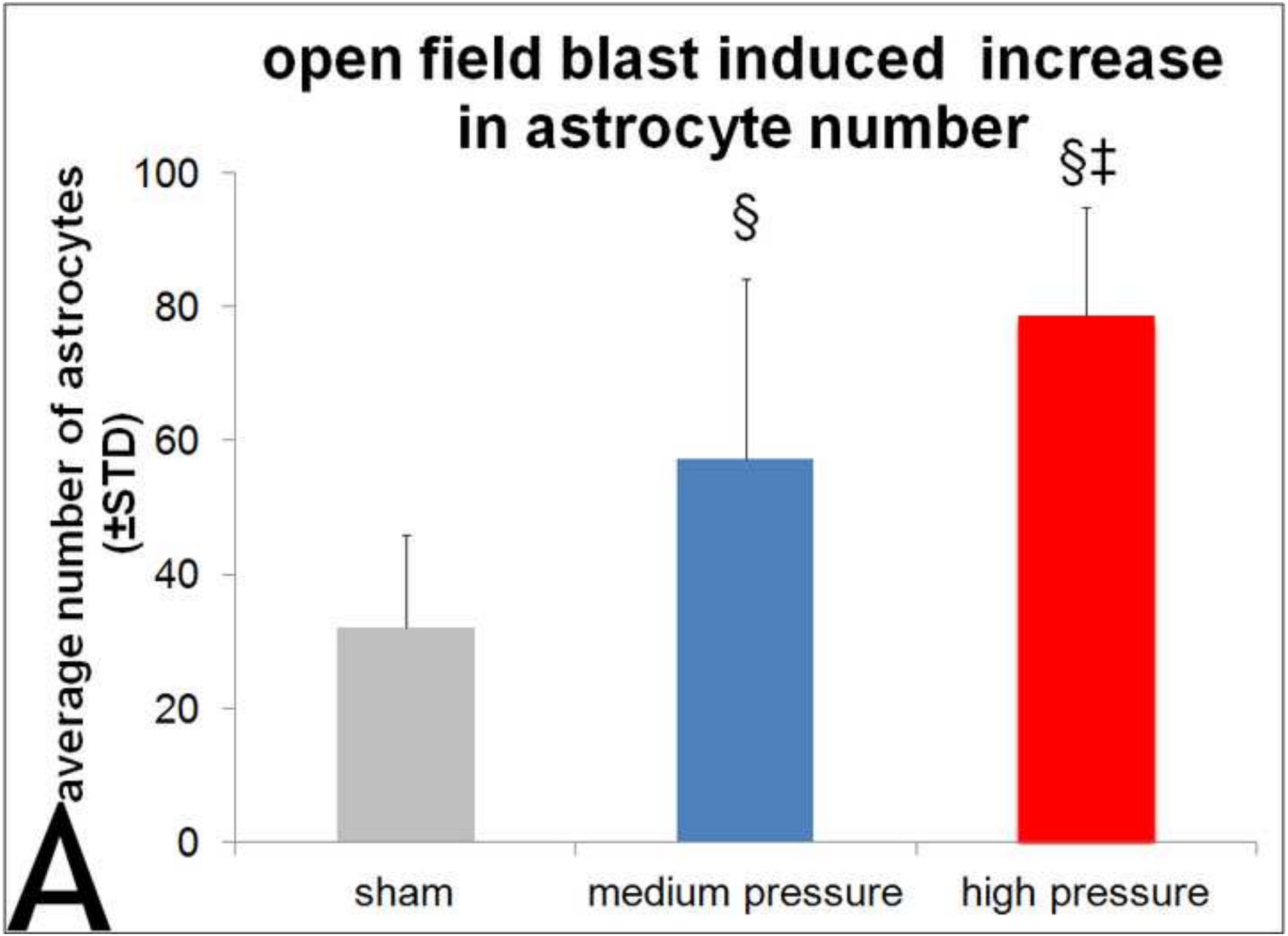

Figure 5

Click here to download Figure Fig_5B.tif

Figure 5

Click here to download Figure Fig_5C.tif

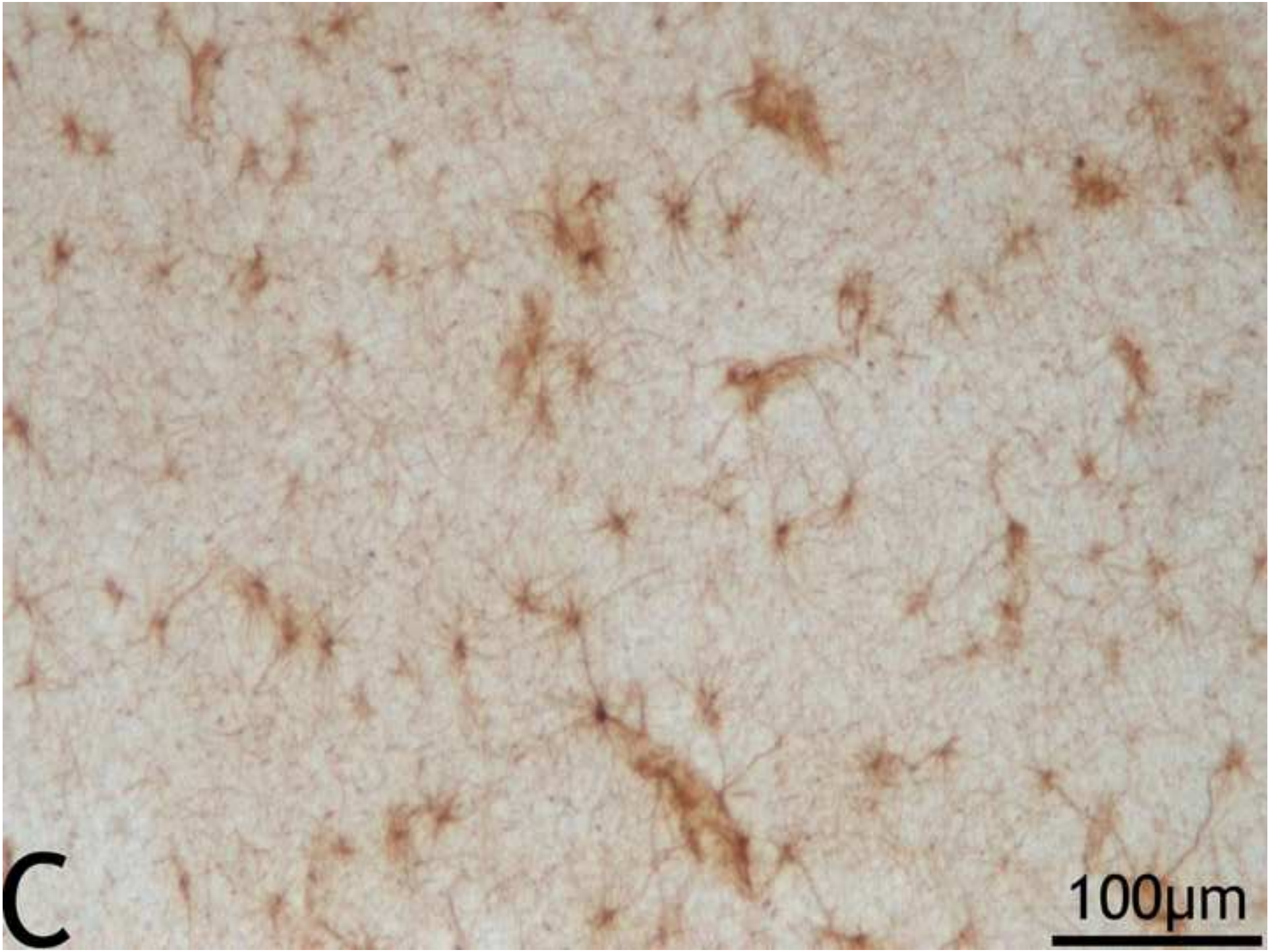

Figure 5

Click here to download Figure Fig_5D.tif

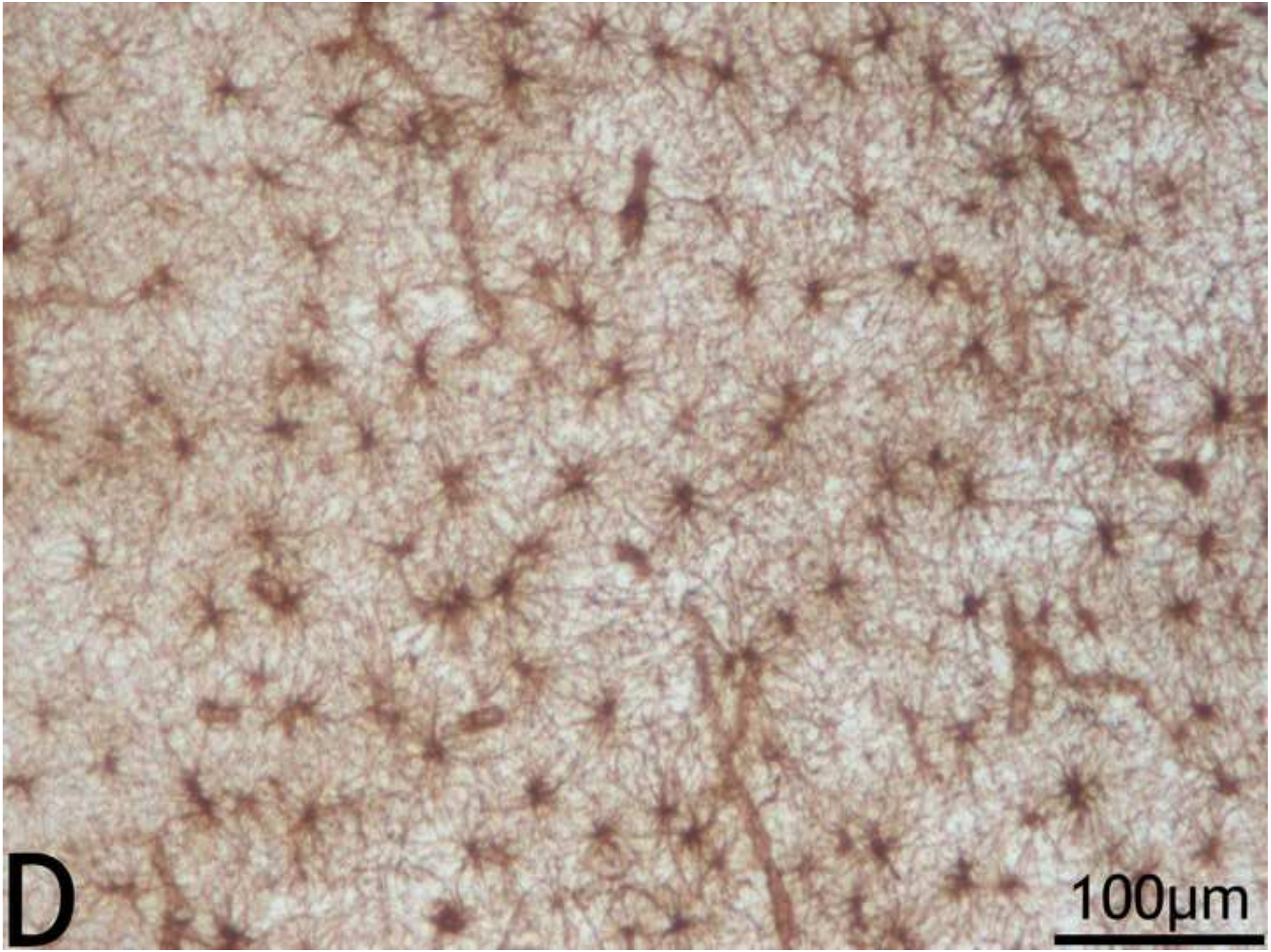

Figure 6

Click here to download Figure Fig_6A.tif

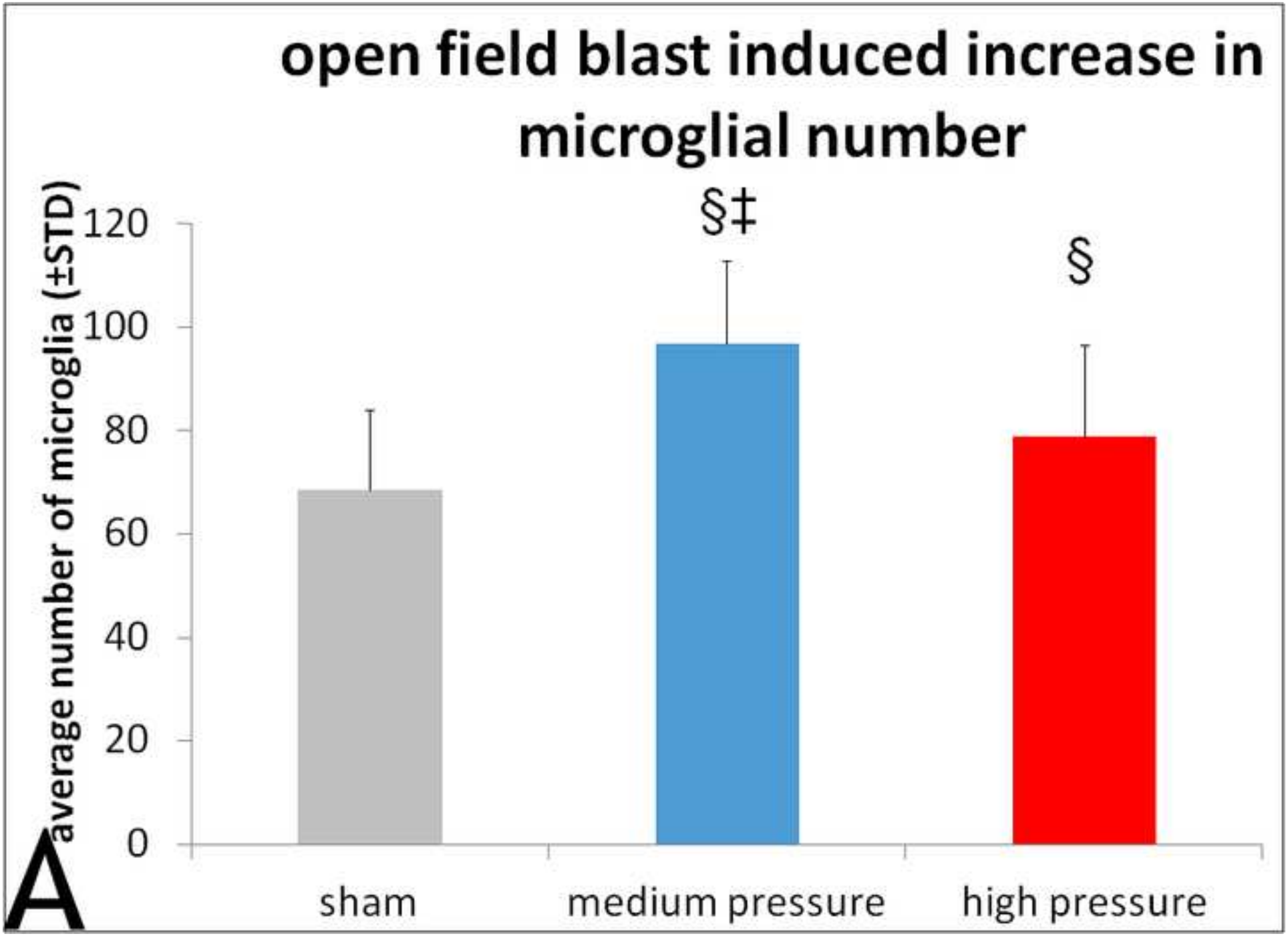

Figure 6

Click here to download Figure Fig_6B.tif

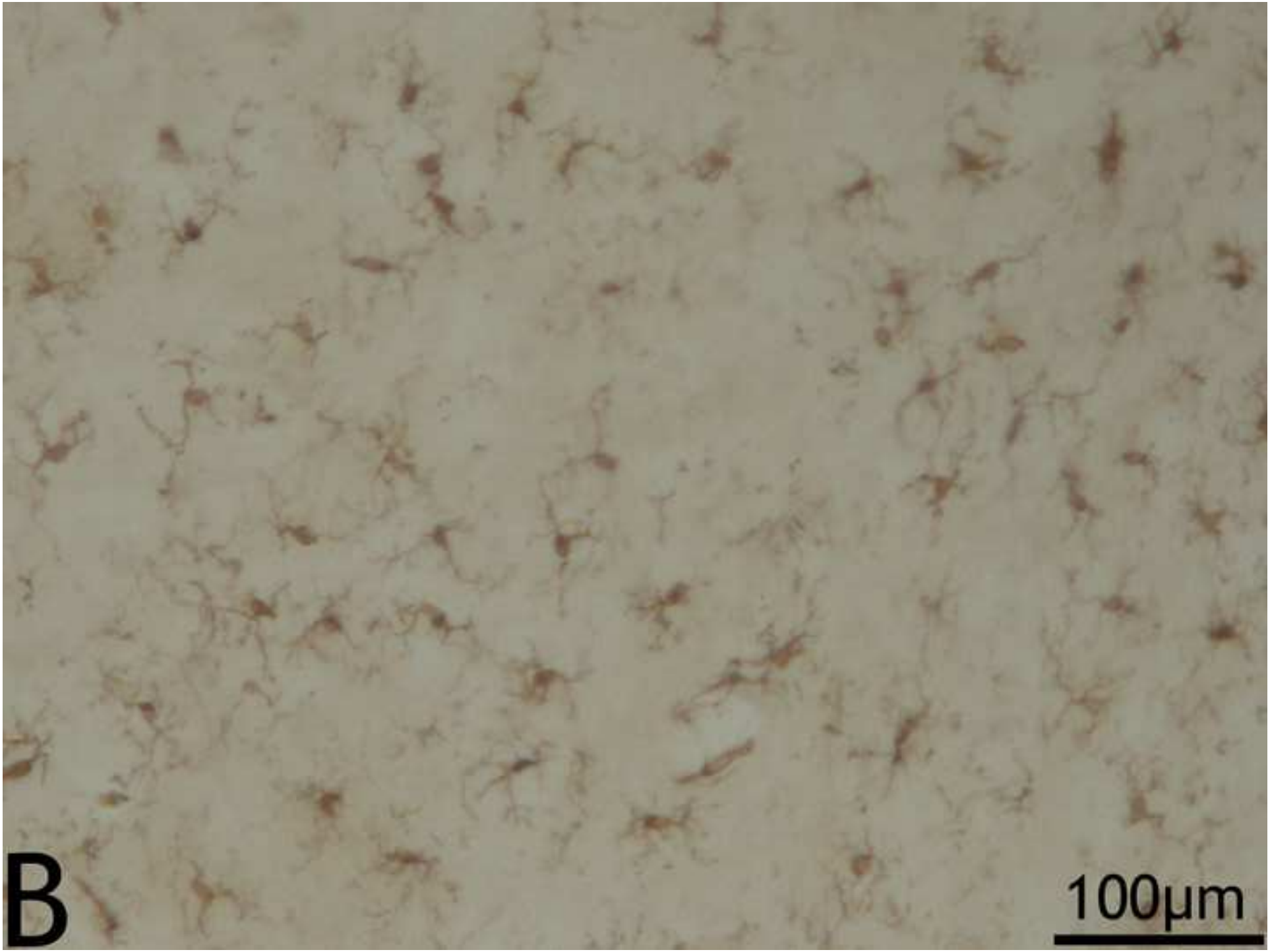

Figure 6

Click here to download Figure Fig_6C.tif

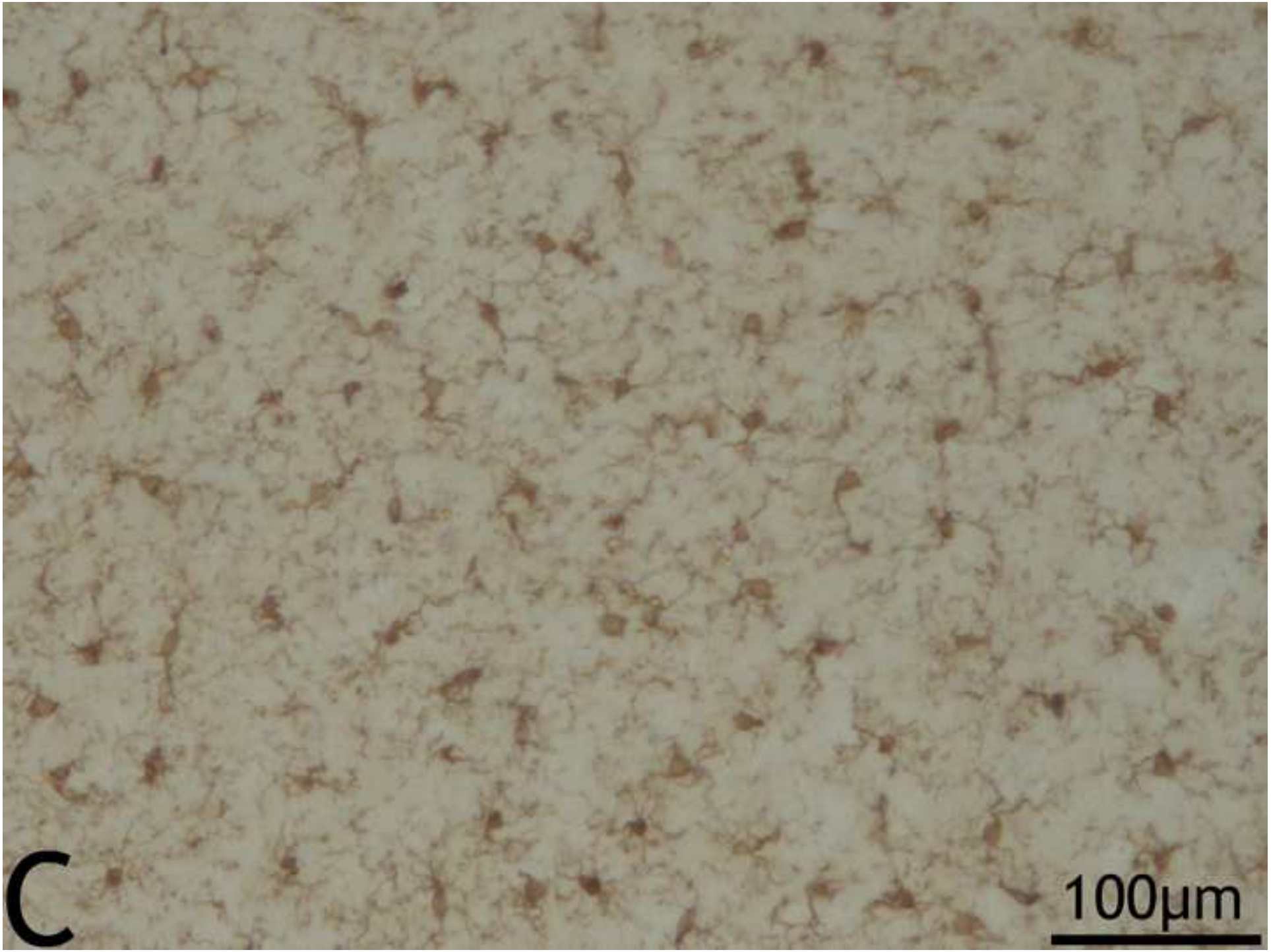

Figure 6

Click here to download Figure Fig_6D.tif

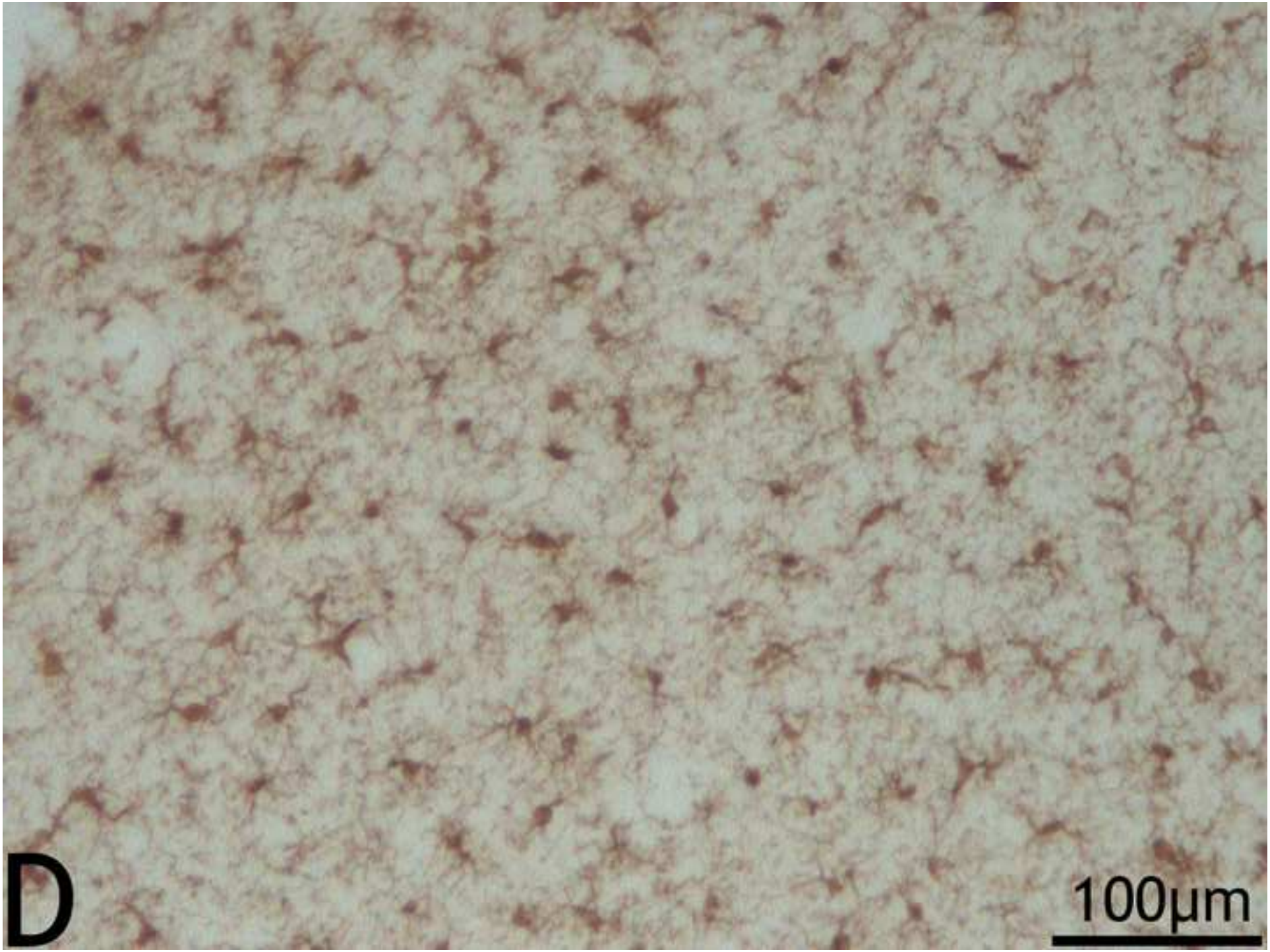

Appendix 3

Test data from Task 2 – Third PMHS test

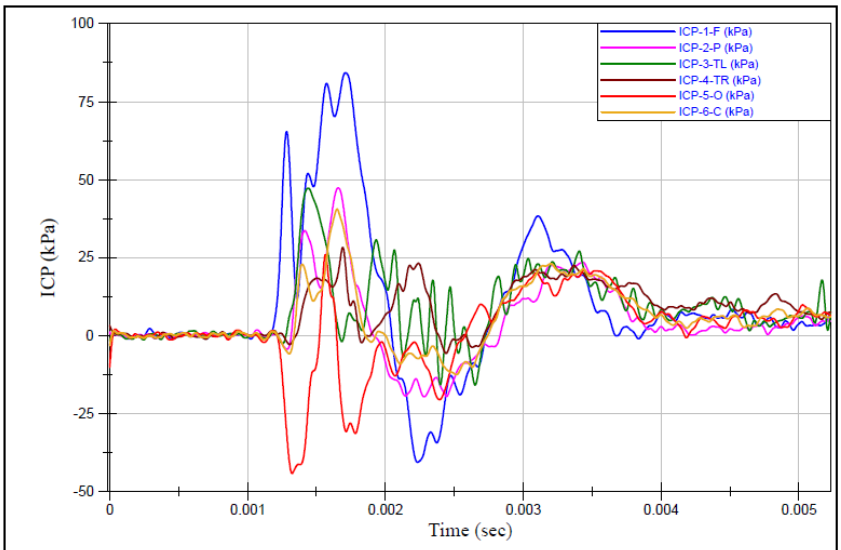

ICP-1-F	ICP-2-P	ICP-3-TL	ICP-4-TR	ICP-5-O	ICP-6-C
-0.4	0.2	-0.2	0.5	-1.5	-0.5
-0.4	0.1	-0.2	0.4	-1.4	-0.4

Figure A1. Intracranial pressure data – Test #1

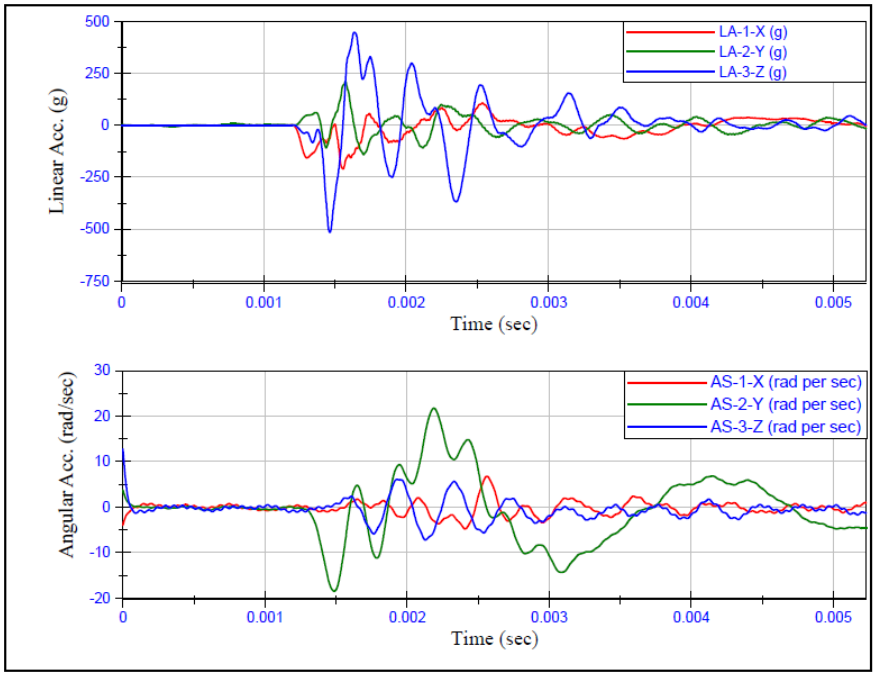

Figure A2 Head linear acceleration and angular velocity data – Test #1

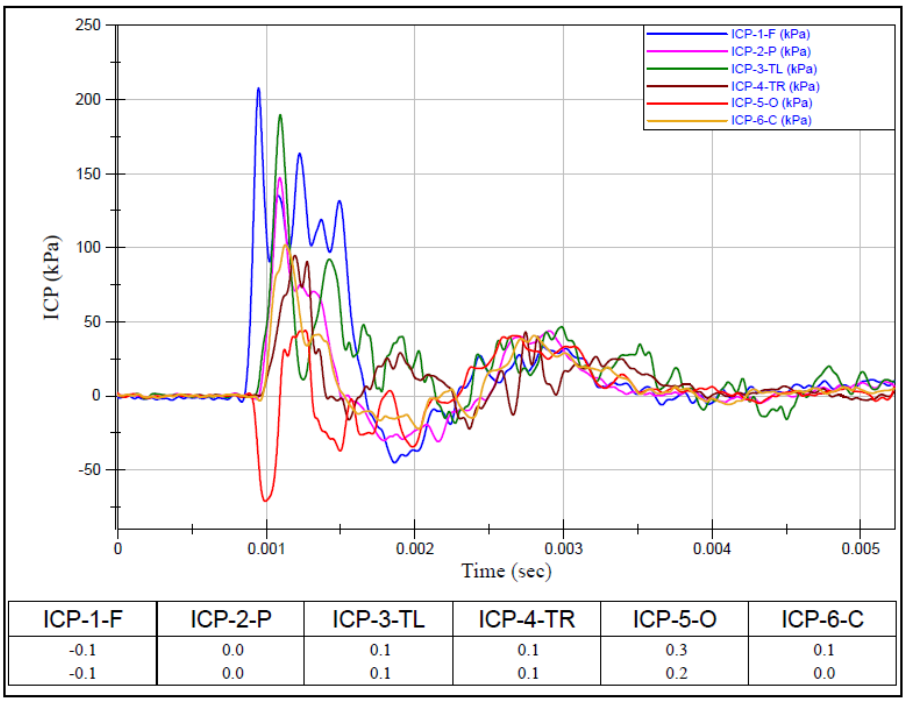

ICP-1-F	ICP-2-P	ICP-3-TL	ICP-4-TR	ICP-5-O	ICP-6-C
-0.1	0.0	0.1	0.1	0.3	0.1
-0.1	0.0	0.1	0.1	0.2	0.0

Figure A3. Intracranial pressure data – Test #2

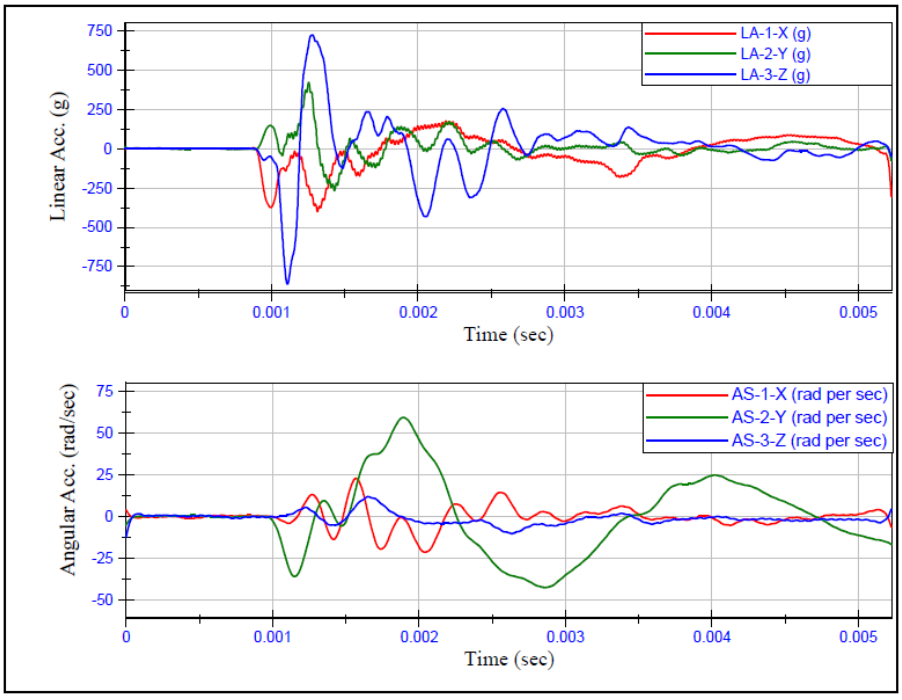

Figure A4. Head linear acceleration and angular velocity data – Test #2

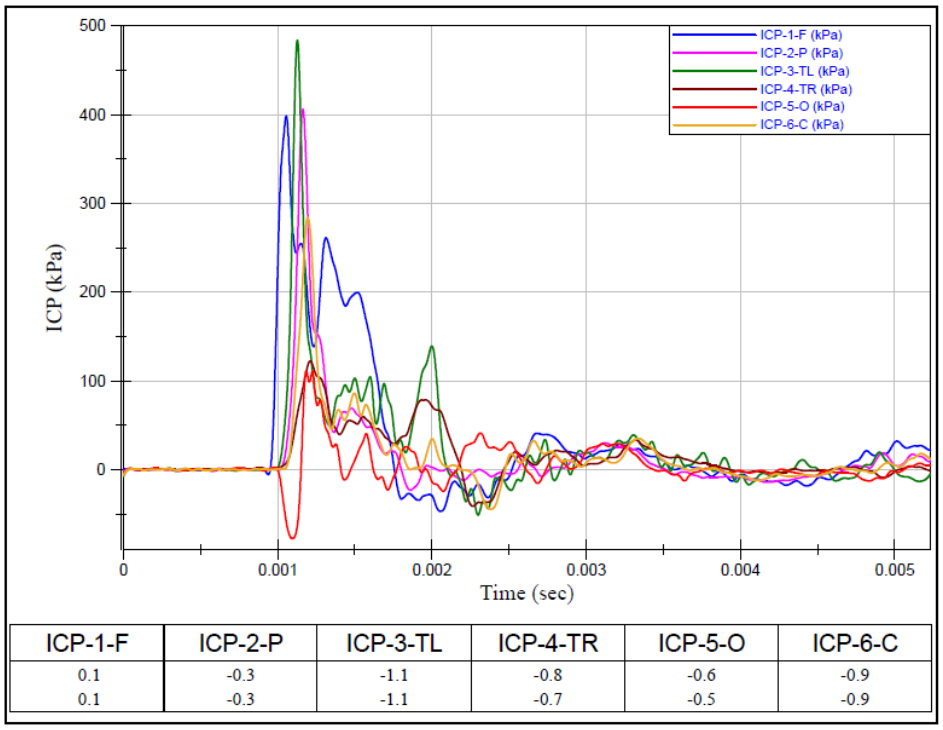

ICP-1-F	ICP-2-P	ICP-3-TL	ICP-4-TR	ICP-5-O	ICP-6-C
0.1	-0.3	-1.1	-0.8	-0.6	-0.9
0.1	-0.3	-1.1	-0.7	-0.5	-0.9

Figure A5. Intracranial pressure data – Test #3

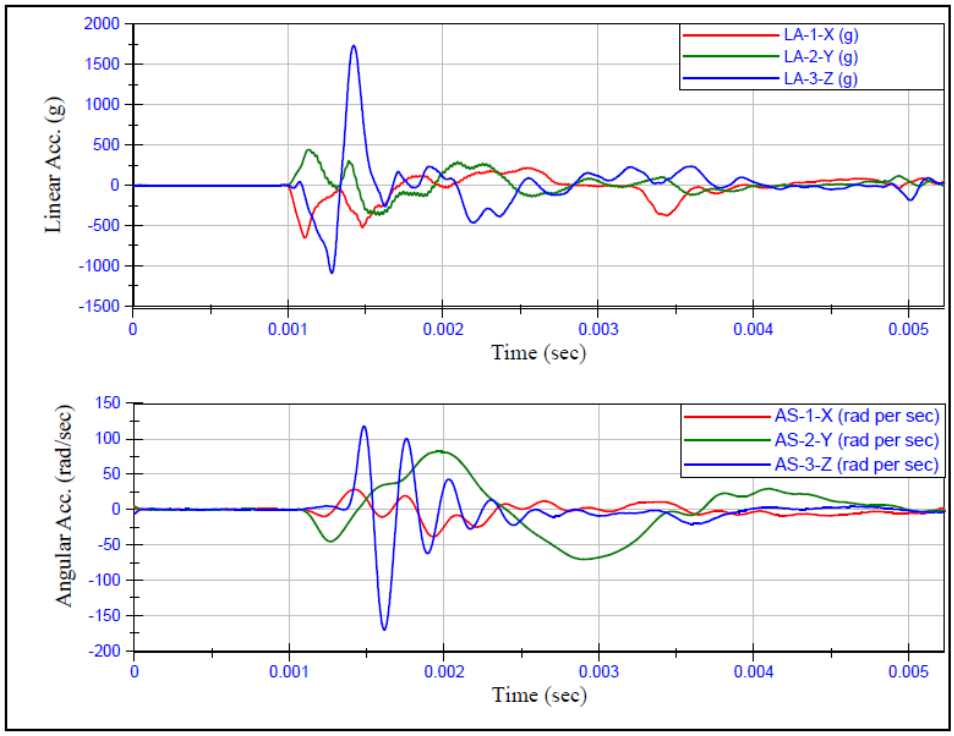

Figure A6. Head linear acceleration and angular velocity data – Test #3

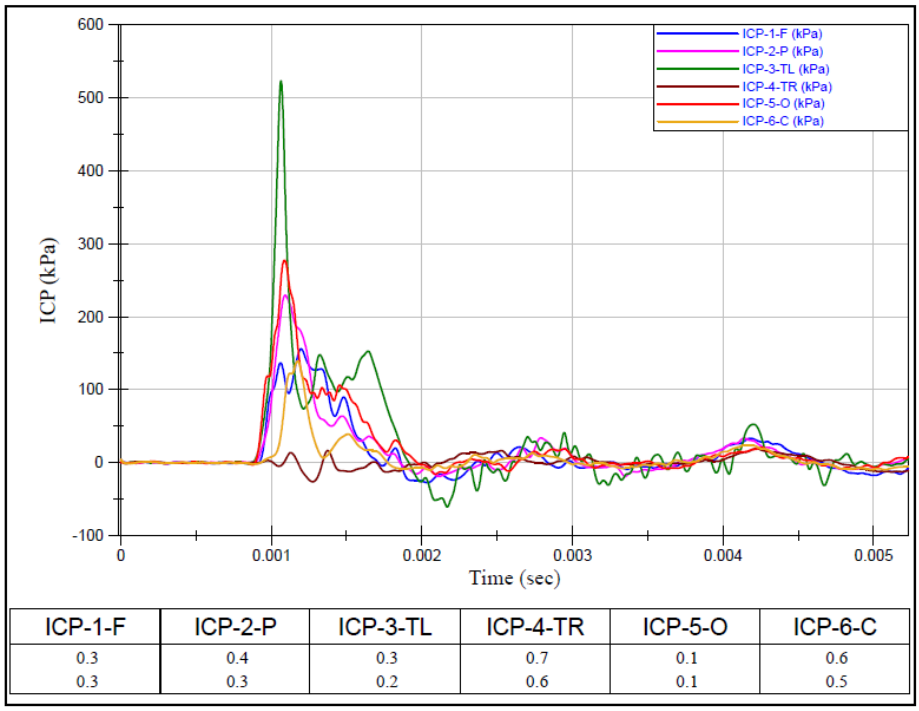

ICP-1-F	ICP-2-P	ICP-3-TL	ICP-4-TR	ICP-5-O	ICP-6-C
0.3	0.4	0.3	0.7	0.1	0.6
0.3	0.3	0.2	0.6	0.1	0.5

Figure A7. Intracranial pressure data – Test #5 (No data were acquired for Test #4 due to trigger failure)

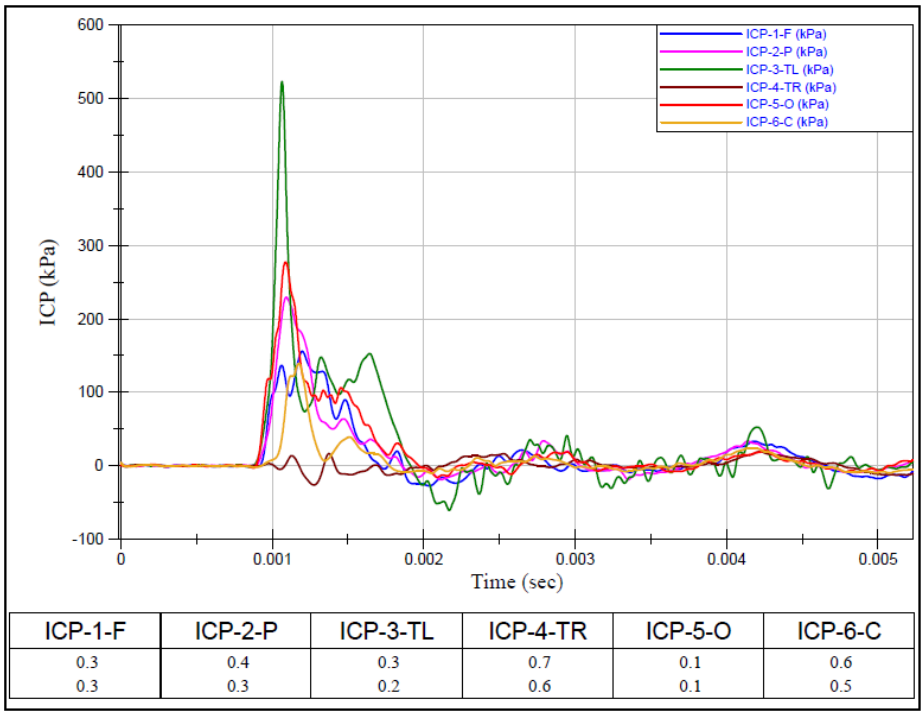

ICP-1-F	ICP-2-P	ICP-3-TL	ICP-4-TR	ICP-5-O	ICP-6-C
0.3	0.4	0.3	0.7	0.1	0.6
0.3	0.3	0.2	0.6	0.1	0.5

Figure A8. Head linear acceleration and angular velocity data – Test #5 (No data were acquired for Test #4 due to trigger failure)

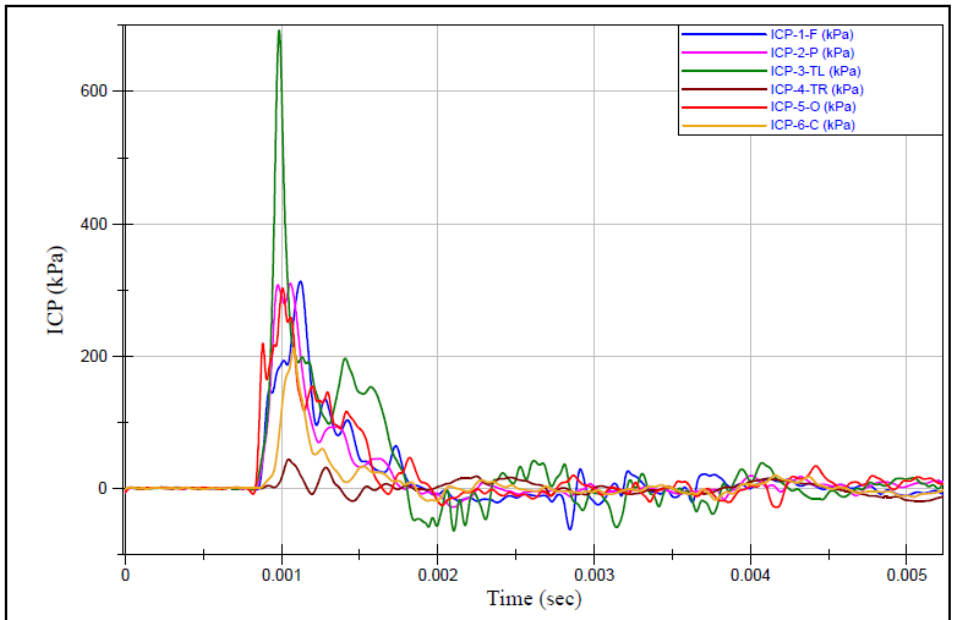

ICP-1-F	ICP-2-P	ICP-3-TL	ICP-4-TR	ICP-5-O	ICP-6-C
-0.4	-0.9	-0.4	-0.5	-1.0	-0.1
-0.4	-0.9	-0.4	-0.4	-0.9	-0.1

Figure A9. Intracranial pressure data – Test #6

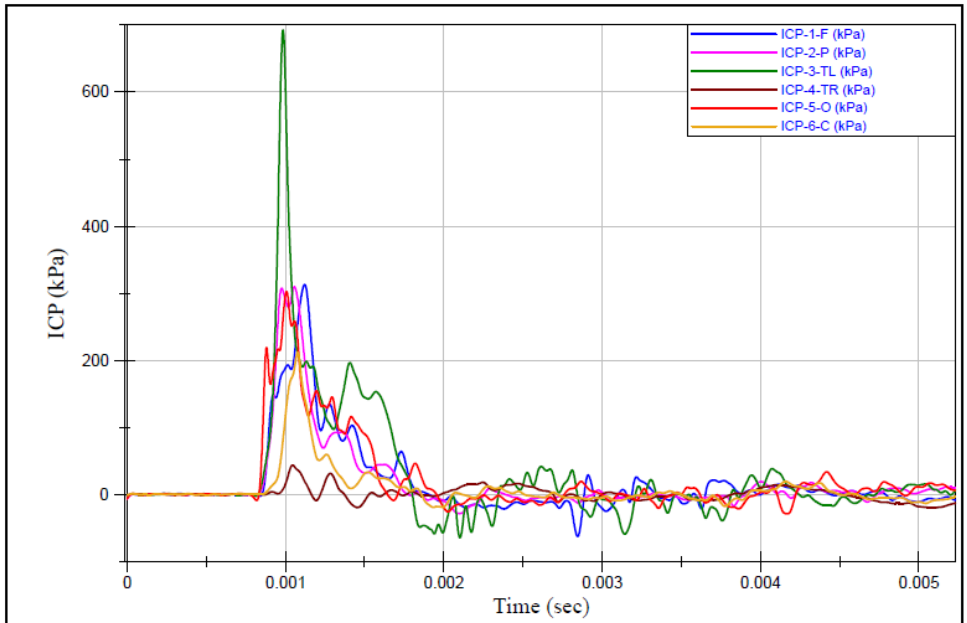

ICP-1-F	ICP-2-P	ICP-3-TL	ICP-4-TR	ICP-5-O	ICP-6-C
-0.4	-0.9	-0.4	-0.5	-1.0	-0.1
-0.4	-0.9	-0.4	-0.4	-0.9	-0.1

Figure A10. Head linear acceleration and angular velocity data – Test #6

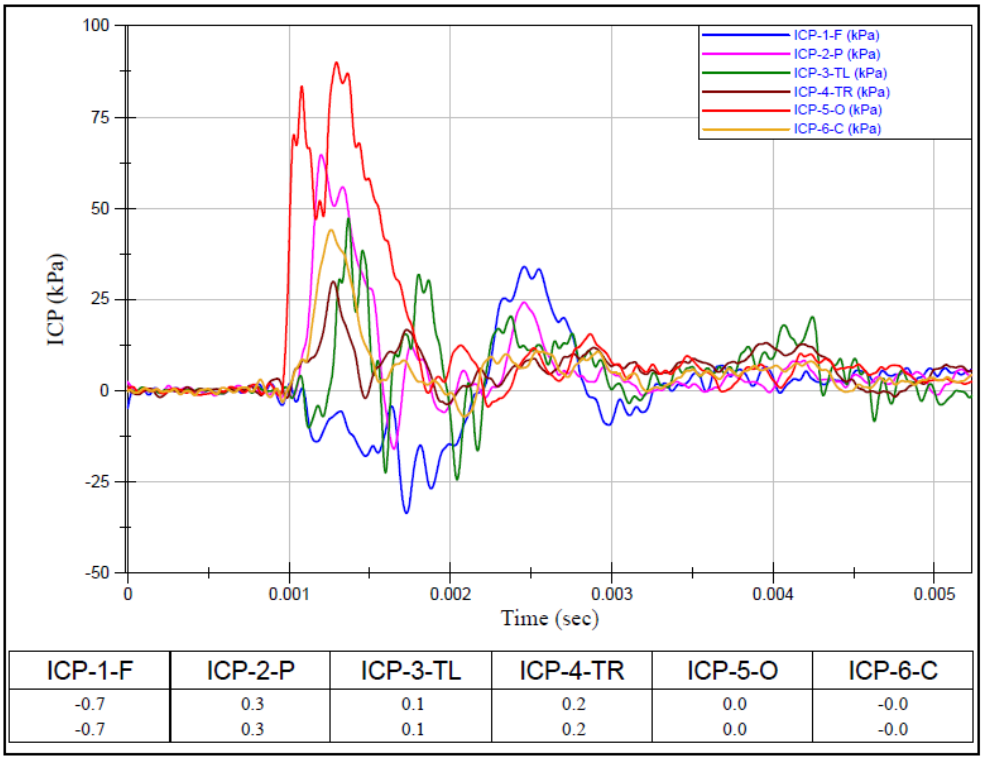

ICP-1-F	ICP-2-P	ICP-3-TL	ICP-4-TR	ICP-5-O	ICP-6-C
-0.7	0.3	0.1	0.2	0.0	-0.0
-0.7	0.3	0.1	0.2	0.0	-0.0

Figure A11. Intracranial pressure data – Test #7

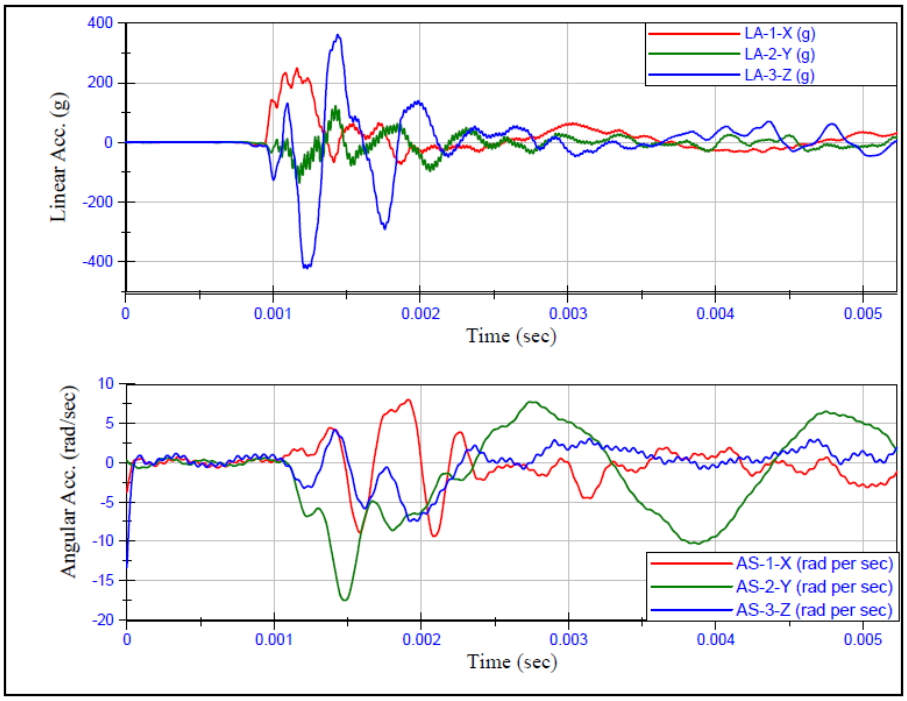

Figure A12. Head linear acceleration and angular velocity data – Test #7

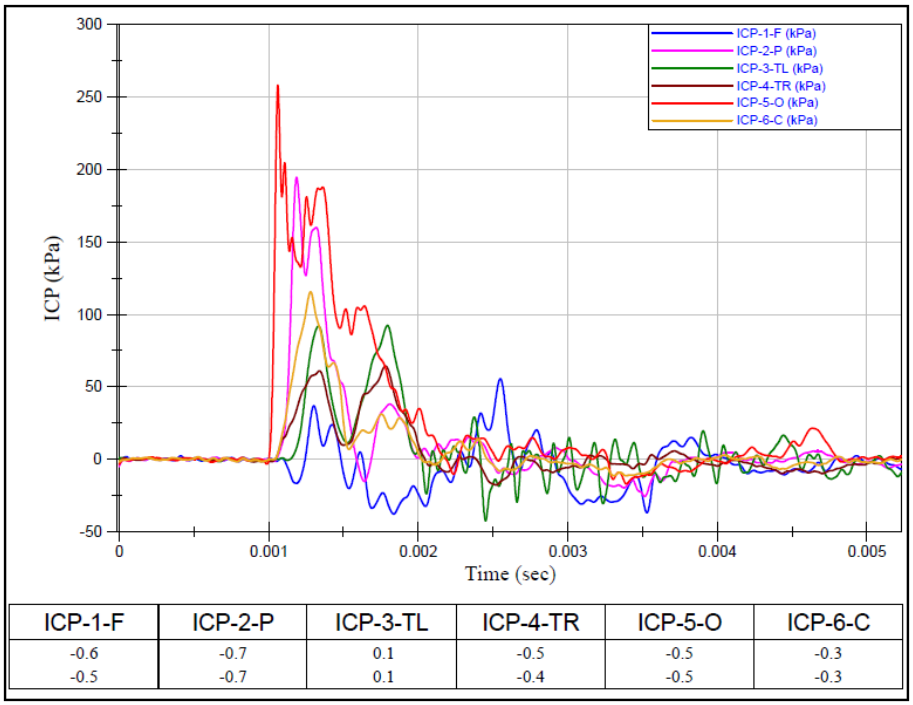

ICP-1-F	ICP-2-P	ICP-3-TL	ICP-4-TR	ICP-5-O	ICP-6-C
-0.6	-0.7	0.1	-0.5	-0.5	-0.3
-0.5	-0.7	0.1	-0.4	-0.5	-0.3

Figure A13. Intracranial pressure data – Test #8

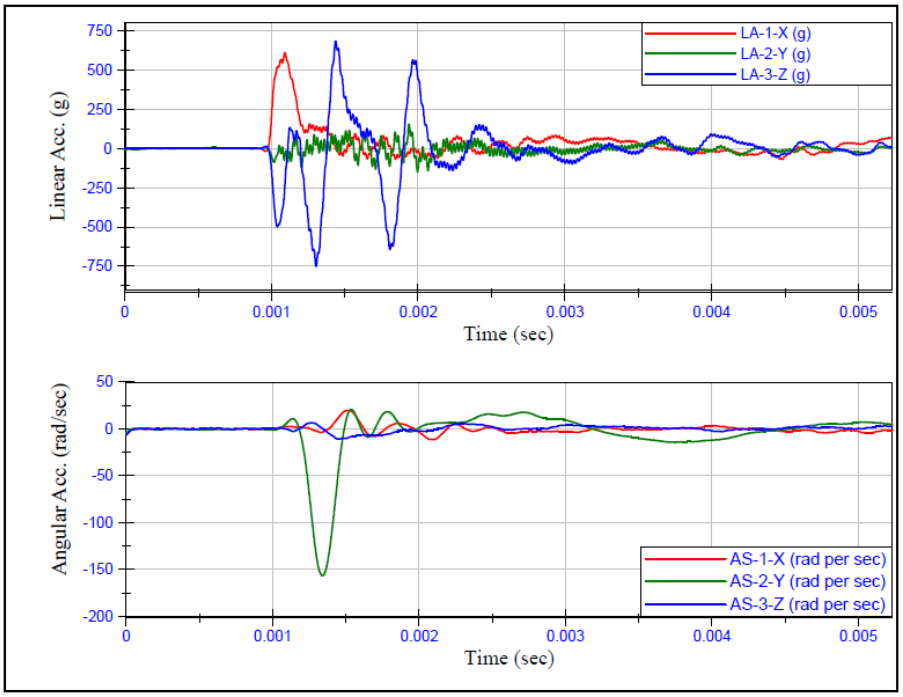

Figure A14. Head linear acceleration and angular velocity data – Test #8

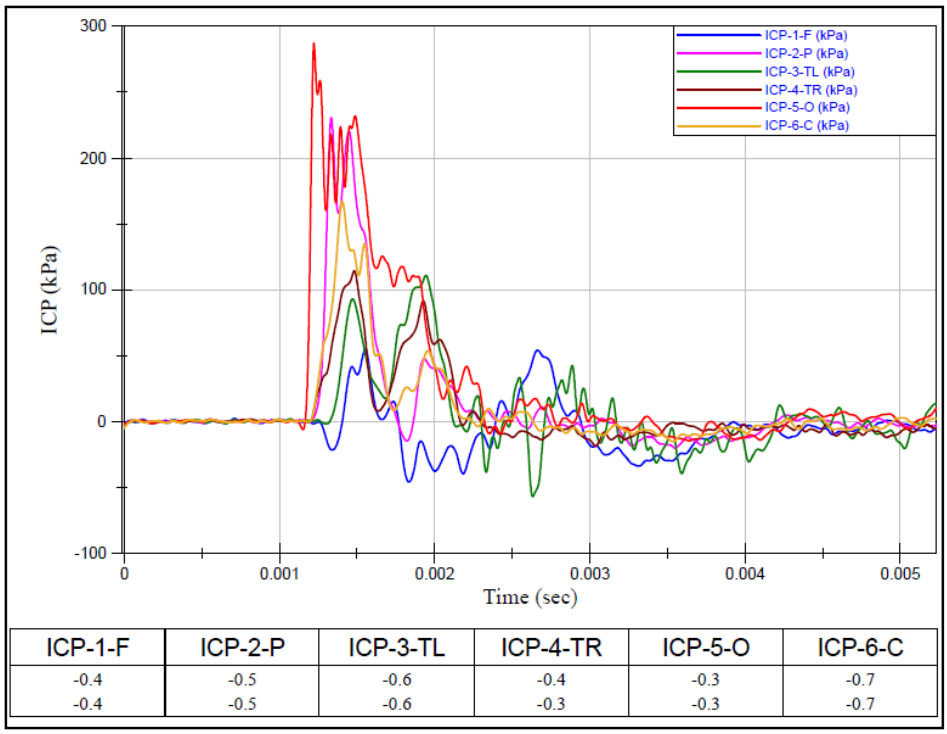

ICP-1-F	ICP-2-P	ICP-3-TL	ICP-4-TR	ICP-5-O	ICP-6-C
-0.4	-0.5	-0.6	-0.4	-0.3	-0.7
-0.4	-0.5	-0.6	-0.3	-0.3	-0.7

Figure A15. Intracranial pressure data – Test #9

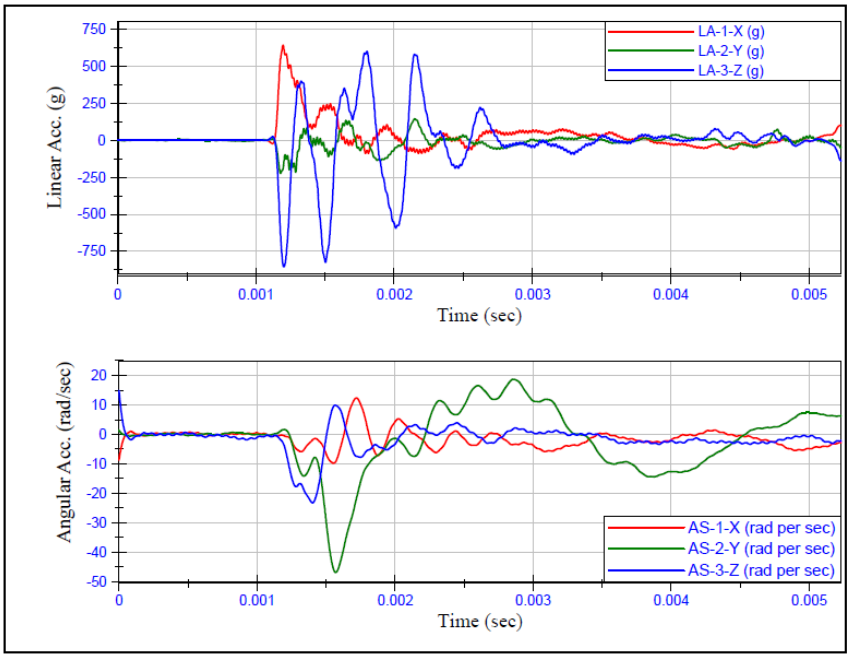

Figure A16. Head linear acceleration and angular velocity data – Test #9